Ascertaining the late Holocene sea-level and climate variability from the mudflats of Kori creek

Avinesh Kumar

A dissertation submitted for the partial fulfilment of

BS-MS dual degree in science.

Indian Institute of Science Education and Research Mohali

April 2019

Certificate of Examination

This is to certify that the dissertation titled "**Ascertaining the late Holocene sea level and climate variability from mudflat of Kori creek**" submitted by **Avinesh kumar (Reg. No. MS14031)** for the partial fulfilment of BS-MS dual degree programme of the Institute, has been examined by the thesis committee duly appointed by the Institute. The committee finds the work done by the candidate satisfactory and recommends that the report be accepted.

Dr. Anoop Ambili Dr. Sharmila Bhattacharya Dr. Shubhra Sharma
(Supervisor)

Dated: April 15, 2019

Declaration

The work presented in this dissertation has been carried out by me under the guidance of Dr. Shubhra Sharma at the Indian Institute of Science Education and Research Mohali.

This work has not been submitted in part or in full for a degree, a diploma, or a fellowship to any other university or institute. Whenever contributions of others are involved, every effort is made to indicate this clearly, with due acknowledgement of collaborative research and discussions. This thesis is a bonafide record of original work done by me and all sources listed within have been detailed in the bibliography.

Avinesh kumar

(Candidate)

Dated: April 15, 2019

In my capacity as the supervisor of the candidate's project work, I certify that the above statements by the candidate are true to the best of my knowledge.

Dr. Shubhra Sharma

(Supervisor)

Acknowledgement

My first and foremost thanks is to my thesis supervisor Dr. Shubhra Sharma. It was a great experience to work under her guidance on a nice challenging problem. I very much appreciate her unique way of handling a student's doubt by providing him/her the correct line of thought and then allowing one to figure out by oneself, as it helped me learning many new things during the process. Along with her significant inputs, she also provided me enough freedom to approach the problem differently by encouraging new ideas.

I am extremely thankful to Dr. Falguni Bhattacharya, Scientist B, Institute of Seismological Research (ISR), Gandhinagar, Dr. Gaurav Chauhan, Assistant professor, K.S.K.V. Kachchh University, Bhuj, his students Abhishek Lakhote and Anil Chavan for their valuable help and timely sampling in the field. I am also grateful to Dr. Anil D. Shukla, Scientist SF, and Dr. Ravi Bhusan, Scientist SG, Physical Research Laboratory (PRL) Ahmedabad, Gujarat, India, for allowing me to complete the sample analysis under their valuable guidance.

I am also thankful to Romi Nambiar, Nirmal Kumar, Ankur J. Dhabi, Harsh Raj and Rahul for their help during sample analysis at Physical Research Laboratory (PRL) Ahemdabad.

I am thankful to Dr. Navin Juyal, Honorary Scientist, Physical Research Laboratory (PRL) Ahmedabad, Gujarat, India for his valuable suggestions and guidance.

I thank my friends Sreenath. S.S, Pardeep Kumar, Neetu, Indrajeet Tambe, Aviansh Kumar, Ravi Kumar , Shubham Bhojane and Apoorav Alawada for always being there for me and supporting me through up's and downs of my life.

I would like to sincerely acknowledge DST, Government of India for providing me INSPIRE fellowship. I am much thankful to IISER Mohali for providing me infrastructure and all technical support.

No acknowledgement would ever adequately express my gratitude to my family. Their

moral support has always boosted my confidence and motivated me to achieve goals in my life. It is their love and affection which gives me a reason to succeed.

Avinesh Kumar

Dated: April 15, 2019

List of Figures **PageNo.**

List of Tables **Page No.**

Notation

- **LGM : Last glacial maximum**
- **LKP : Lakhpat**
- **Wt.% : Weight percentage.**
- **C/N : Ratio of weight percent carbon to nitrogen.**
- **TOC : Total organic carbon.**
- **TN : Total nitrogen.**

Contents

Abstract

Holocene sea-level change representing the recent most change in the sea curve post-LGM is a challenging task as besides the eustatic changes, the estimates are affected by hydro-isostatic changes, modulations in ocean and land topography, tectonics and geoidal changes. Therefore local estimates and curves must be generated for a region which accounts for these factors. From the Gulf of Kutch there are a few studies estimating early-late Holocene sea level changes. However, the estimates are varied and there is need for more robust data points to generate a regional picture.

The present study was made in this direction to understand the late-Holocene sea level changes from the relict mud-flats preserved at the distal end of Kori Creek and to also understand the relationship with climate variability. The 1m deep core section of a partially active mudflat from Lakhpat in the Kori creek region was investigated using geochemical and Carbon/Nitrogen elemental analysis. To chronologically restrain the core Pb-210, Cs-137 and AMS C-14 radiocarbon dating was employed. On the basis of selected geochemical proxies the study reveals three phases of sea-level change from bottom of the core. The first phase shows a high sea-level stand followed by relatively low stand and then marginally high stand with fluctuations. The higher tendency of the sea coincides with wetter climate in the region which seems to have dominating role in controlling the fluctuations. However, the phases could not be chronologically constrained. The Pb-210 and Cs-137 results show the sediments to be older than 150-200 years while the AMS ages were not consistent and could not be used.

The upliftment of the sediments after 1819 earthquake as it lies proximal to the Sunda high region is expected which explains the absence of modern sedimentation. However, the C-14 AMS ages are older than expected and give an unrealistically low sedimentation rate (0.3 mm/yr) to the 1 m core. The incorporation of dead carbon from the catchment rocks is suspected. Hence, due to the lack of robust data on chronology the detailed correlation of the sea-level with the climate is not attempted. Nevertheless, the absence of mudflat sedimentation in the last 150-200 years suggest the low the sea-level in the recent times, while a relatively higher sea level during suspected late- Holocene period with fluctuations. The provenance of the sediments was suggested to be dominantly from Indus delta as the sediments are supplied via longshore current with some contribution from the proximal Thar desert. For future research it is hypothesised that the sea-level changes in the region are dominantly controlled by the climate with tectonic over printing which needs to be corrected for. Also, an alternative

chronological technique like optical stimulated dating technique may be explored to chronologically restrain the core.

Chapter 1
Introduction

The Quaternary period is marked by cyclic eustatic sea-level changes which are suggested to be governed by melting or expansion of ice sheets and are therefore known as the glacio-eustatic changes (Lowe and Walker, 2014). Holocene sea-level change represents the recent most change in the sea curve post-LGM when sea-level fell eustatically by 120±20 m (Pirazzoli, 1991). Until the 1960s the Holocene sea level estimates were suggested to be eustatic but the large discrepancy in the estimates given by various studies led to the launching of UNESCO and International Union of Geological Sciences (IUGS) sponsored program – Project 61 and Project 200 in which it was suggested that for Holocene unlike the post-LGM sea-level change the Holocene sea-level was not uniform globally due to hydro-isostatic effects (Bloom, 1967, 1971). The hydro-isostatic effect is defined as the differences in load caused on the sea floor by melting of the ice sheets – a concept that was first given by Daly, (1934). By 1980s it was clear that (1) Holocene sea level was affected by modulations in ocean topography causing difference in relative sea level histories; (2) the sea-level histories across the globe were varied considerably especially for the late Holocene and; (3) sea-level estimates followed a regional trend governed by isostasy (Pirazoli, 1976, 1977; Bloom, 1977; Clark et al., 1978; Peltier et al., 1978). Therefore a global model of Holocene sea-level is illusory and misleading. This is highlighted by the more than 4000 radiocarbon ages compiled globally since last 16 ka which suggest a variation of 200 m to -160 m below the datum for Holocene level as the tectonic and geoidal changes become more important (Fig 1.1); Marcus and Newman, 1983; Newman et al., 1986; 1987). Subsequent studies also supported these suggestions world-wide (Gehrels et al., 2006). Instead, relative sea level where the change in sea level takes place through movement in land or sea is more realistic for Holocene, and therefore local relative sea level (RSL) curves must be generated for the regions (Pirazoli et al., 1992; Lowe and Walker, 2014). Holocene sea level was modulated by a combination of factors that perturbed the land-sea configuration (Engelhart et al., 2015; Lambeck et al., 2014; Milne et al., 2005; Shennan and Horton, 2002; Vacchi et al., 2014). In Holocene especially the biggest challenge remains to separate the effect of glacio-static and isostatic (tectonic) changes in sea level as no part of the land is "stable" to remain unaffected by the tectonic movements (Lowe and Walker, 2014).

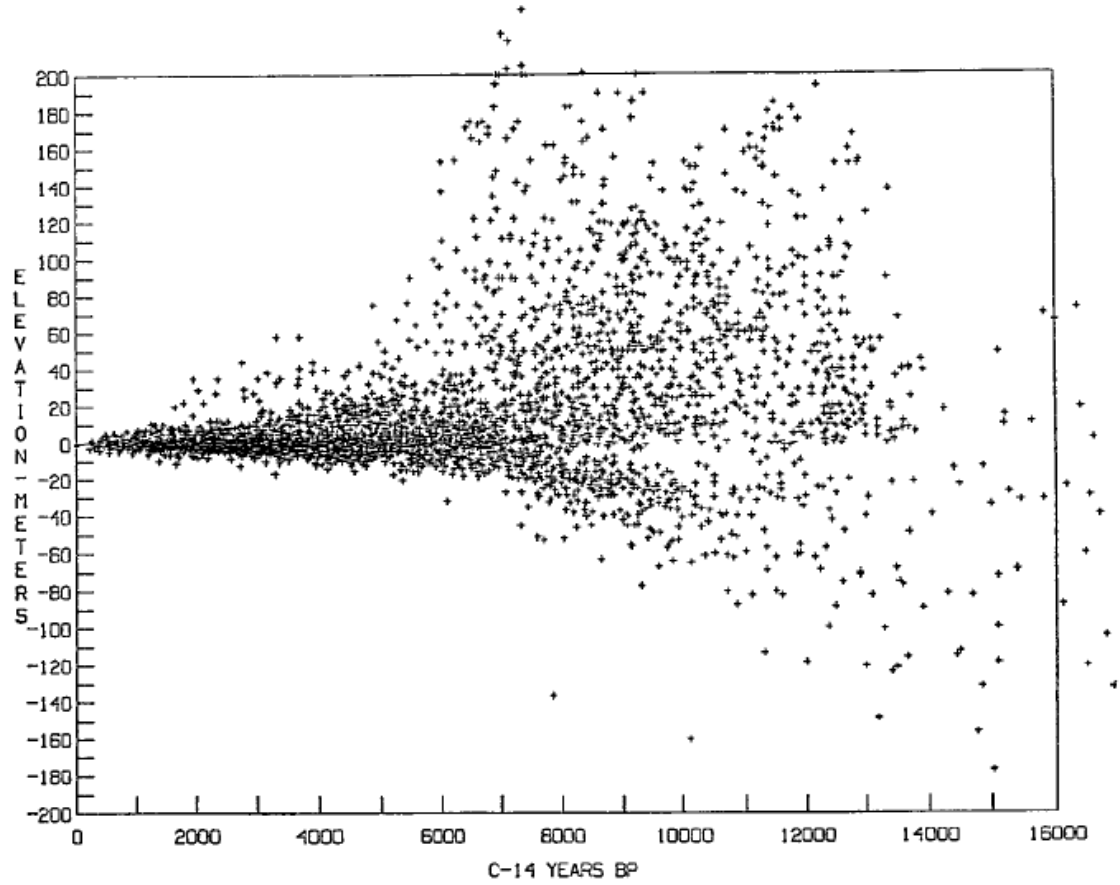

Figure 1.1 : Plot of relative sea- level change with respect to radiocarbon age (Pirazzoli 1991).

The glacio-isostatic rebound effect post Last Glacial Maximum (LGM) in the higher latitude (Shennan and Horton, 2002) was particularly demonstrated to be significant in the compilation of global Holocene sea level data by Newman, (1986). Second major challenge is to account for the irregularities introduced in the earth surface due to gravitational deformities and internal changes in the earth's density (geoidal isostasy); transfer of mass from the equator to higher latitudes as the ice sheets grow and vice-versa (glacio-isostasy) and loading effect of oceans on crust (hydro-isostasy). The site-specific estimates of sea-level, however, are independent of the geoidal isostasy (Lowe and Walker, 2014) but glacio-isostasy and hydro-isostasy are known to affect the areas far away from the ice-sheets (Vink et al., 2007; Long et al., 2009). During the Holocene, a more gradual postglacial rebound and residual rebound is more important than the restrained rebound which is defined as the rapid crustal adjustment after the ice sheet recession. The post-glacial rebound is more gradual that follows restrained rebound continues till present. The residual rebound refers to the small uplift required to re-establish the crustal equilibrium

(Lowe and walker, 2014). Another major challenge is deconvoluting the effect of hydro-isostasy because of difference in crustal density and ocean siphoning. Ocean siphoning refers to the encroachment of land by sea water ingression as the forebulge in front of the melting ice sheets collapses and continental shelves tilt toward the ocean. The tilting is due to the increase in the mass of ocean water as well as continental isostatic recovery. Also, the subsiding forebulges in the higher latitudes lead to equatorial ocean siphoning when ocean water from the low latitudes as in the Indian Ocean (Kench et al., 2009; Woodroffe et al., 1990) moves toward the poles causing relative sea level (RSL) fall especially in late Holocene (Mitrovicaand Milne, 2002). Thus, considering the complex response of the Holocene sea-level changes to various geological and geophysical processes (mentioned above), more studies need to be carried out on RSL changes from localities which are either unaffected by major tectonic and glacial isostasy (Lambeck et al., 2002; 2010) or where the tectonic contributions can be accounted for.

The limited chronologically constrained studies from the Indian coast estimates indicate that sea level fluctuated significantly during the mid to late Holocene (Benerjee, 1993; 2000; Benerjee et al., 2015; Bhatt and Bhonde, 2005; Das et al., 2017; Juyal et al., 1995; Kunte and Wagle, 2005; Pant and Juyal, 1993). The fluctuation is not only due to the glacio-eustacy but are the cumulative expression of tectonically induced changes (Banerjee et al., 2015; Juyal et al., 1995; Pant and Juyal, 1993), coastal configuration modifications and bulking by the sediments dispersed through alongshore current (Ferrier et al., 2015). For example, the Indus delta region which is located in the vicinity of the study area is known to receive enormous sediment flux from the hinterland. Such huge sediment flux transferred over millennial timescales can produce meter-scale changes in sea level near the delta (Ferrier et al., 2015). Relatively there is number of studies form the eastern coast and from the Saurashtra Peninsula (western coast) of India. From the tectonically stable eastern coast Benerjee (2000) dated the Holocene sea level to suggest ~3 m high sea level at ~7 ka; and ~1 m high sea level between 5.2 and 4.2 ka. On the other hand from the tectonically active Saurashtra peninsula, the raised oyster beds were dated to indicate sea level between 2 and 3 m during 8.6 to 2.5 ka (Juyal et al., 1995; Pant and Juyal, 1993). Recently Benerjee et al., (2015) refined the estimate from the Saurashtra peninsula after accounting for the tectonic component and suggested that the mid-Holocene sea level was ~1 m higher than the present which is similar to the observation was made by Brückner

(1989) who suggested ~1 m high sea level than present between 6 and 5 ka. The Holocene sea level studies from the tectonically active Kutch coastline (Bhattacharya et al., 2014 and reference therein) are limited and provide different estimates on Holocene sea level. For example, in the Little Rann, Gupta (1975) initially suggested ~4 m deep sea level ~2 ka while marine sedimentation was suggested to continue in the Great Rann till ~500 years (Khonde et al., 2011). On the contrary Tyagi et al., (2012) suggested tidal flat sedimentation between 5.5 to 2 ka in the western Great Rann. While more recently, Das et al. (2017) postulated ~2 m high sea level between 6 and 3 ka. Therefore, needless to say, more chronologically robust estimates are required to understand the land-sea interaction and nature of sedimentation in the western Kutch.

1.1 Measuring sea level change and associated challenges

Sea level is affected by a number of factors like tides, the density of water, currents, atmospheric forcing, astronomical and meteorological influences on gravity, removal/addition of ice sheets, volcanic debris, sedimentation, and erosion, etc. Eustatic sea level largely depends on variation in the volume of ocean basins and mass/density of ocean water (steric changes). While relative sea level change may be caused by regional uplift/subsidence of land and changes in gravitation, rotation, atmospheric pressure, winds, ocean currents, etc. A large number of disciplines and variety of data from archaeology, geomorphology, geology, geophysics, oceanography, geochemistry, ecology, etc. have contributed to understanding the sea-level changes. Among the geomorphic indicators marine like benches, rock platforms, notches, raised littoral, tidal and estuarine platforms, caves, coral reefs, and submerged river valleys are useful for defining former sea level positions. For example, especially in tectonically stable areas, coral reefs which grow only in narrow intertidal zones can be dated precisely by U-series dating to give an estimate of sea-level (Lowe and Walker, 2014). Similarly, estuarine, tidal, and marine deposits with encrusted marine organisms collected in growth position and mangroves offer more continuous records than the fragmentary terrestrial erosional landforms (Pirazoli, 1991; Tyagi et al., 2012). Being in the transitional zone of riverine freshwater flux and marine brackish water, the tidal and estuarine environments are the most useful in recording the minor fluctuations in sea level changes as these often protected from the erosional processes and have shallow waters which preserve alternating terrestrial, tidal and marine sequences (Lowe and Walker, 2014). The sea-level is usually measured in relation to a present-day

reference which may be level inhabited by the living counterpart of a fossil or present-day local tidal datum level based on non-biological indicators like sea-drifted material, flat tidal surface etc. (Jardine, 1986; Pirazoli et al., 1991). The accuracy of the sea-level curve generated depends upon the error associated with the chronology, instrumental surveying error, interpretation of the index points taken to demarcate sea level, temporal scale of the study where the local factors are becoming significant at centennial scale.

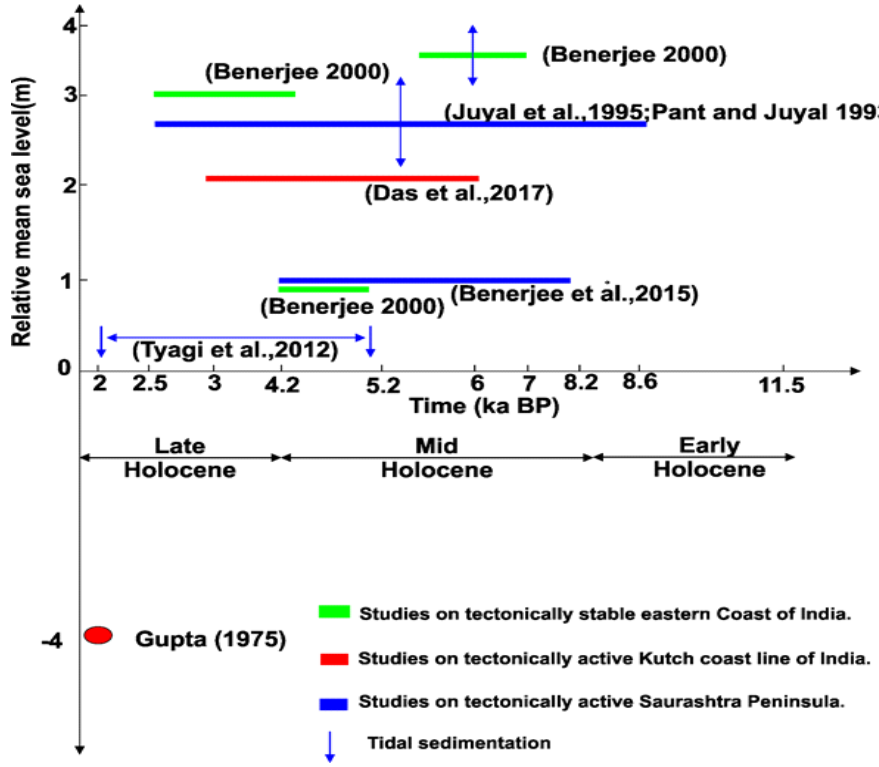

Figure 1.2: Schematic representation of various sea- level study estimates in India.

1.2 Importance of sea-level studies

Global sea-level has been rising at an alarming rate of 0.31 cm/year mainly because of enhanced temperature that has led to the melting of ice sheets and glaciers and thermal expansion of ocean water. Higher sea level implies great inland ingression of the sea during storms, enhanced erosion, and submergence of coastal areas. However, the sea-level change is not uniform globally and varies with some regions more prone to the effect of sea-level rise than others (NOAA, 2018). The Fourth Assessment Report (AR4) of the IPCC on Climate Change projected that global sea level would rise by up to ~60 cm by 2100 in response to global warming to ocean warming and glaciers melting. However, the recently

identified accelerated decline of polar ice sheet mass raises the possibility of future sea-level rise (SLR) of 1 m or more by 2100. Today, low-elevation coastal zones below 10-m elevation contain ~10% of the world population. Here, non–climate related anthropogenic processes (such as ground subsidence due to oil and groundwater extraction, or reduced sediment supply to river deltas caused by dam building) often amplify local vulnerability associated with climate-related SLR. In view of this, it is important to understand the recent to sub-recent changes in the sea-levels at the local scale in order to evolve scientifically viable mitigation strategies. Towards this, the sediments deposited in the mud-flats (active and partially active) provides a good archive that can be exploited to understand the recent and sub-recent changes in the land-sea interaction. Thus, sea-level studies are important as:

1. Mapping and elevation measurement of past sea levels help in identifying the positions of former coastlines and establish a vertical range of sea-level variations for a region. By understanding the effect of glacial ice melt, change in ocean water properties and isostasy on past sea-levels, futuristic predictions become more accurate regionally and globally (Church et al., 2001; Lowe and Walker, 2014).
2. Past sea-level changes help us calculate the average rate of sea-level rise/fall over a period of time with respect to natural climate and hence facilitate the comparison with natural and anthropogenic causes of sea-level rise.
3. Often tectonics leaves a dominant imprint on the sea-level fluctuations, particularly during the Holocene times which can be understood by geological studies (Church et al., 2001).

1.3 Importance of tidal flats

(1) Tidal flats particularly are important as they act as buffer zones for sea-level rise and are useful for land reclamation. (2) Due to low energy conditions, the tidal flats preserve a continuous history of sea level changes (3) Additionally present day facies are important to understand as these facilitate comparison with the geological facies where coarser tidal flats house petroleum and fine-grained tidal flat contain coal (Daidu, 2013).

The present study is undertaken to the east of the Indus delta in the mud-flat environment of Kori Creek. Although inconclusive but there are suggestions that during the mid-Holocene and till around the 8th century AD, the Indus delta was close to the Kori Creek near Lakhpat (Snelgrove, 1979; Flam, 1993) and its westward shift (to the present

position) is attributed to the historical earthquakes (Rajendran and Rajendran, 2002). Tectonic influence is known to be one of the most defining control in the sea-level studies (Essat et al., 1999; Classens et al., 2009). The mud-flat sequence at the site is investigated using the multiproxy data (sedimentology, major and trace elements, and organic geochemistry) supported by Pb-210, Cs-137 and AMS radiocarbon dating.

Objective

The objective of the thesis is to ascertain the magnitude and the cause of the late-Holocene sea level changes with climate variability.

References

Atlas of Sea-level Curves: IGCP Project 61. International Geological Correlation Program, 1977.

Banerjee, P.K., 1993. Imprints of late quaternary climatic and sea level changes on East and South Indian coast. *Geo-marine letters*, *13*(1), pp.56-60.

Banerjee, P.K., 2000. Holocene and Late Pleistocene relative sea level fluctuations along the east coast of India. *Marine Geology*, *167*(3-4), pp.243-260.

Banerji, U.S., Pandey, S., Bhushan, R. and Juyal, N., 2015. Mid-Holocene climate and land–sea interaction along the southern coast of Saurashtra, western India. *Journal of Asian Earth Sciences*, *111*, pp.428-439.

Bloom, A.L., 1967. Pleistocene shorelines: a new test of isostasy. Geological Society of America Bulletin, 78(12), pp.1477-1494.

Bloom, A.L., 1971. Glacial-eustatic and isostatic controls of sea level since the last glaciation. *Late Cenozoic glacial ages*, pp.355-379.

Clark, J.A., Farrell, W.E. and Peltier, W.R., 1978. Global Changes in Postglacial Sea Level: A Numerical Calculation 1. *Quaternary Research*, *9*(3), pp.265-287.

Das, A., Prizomwala, S.P., Makwana, N. and Thakkar, M.G., 2017. Late Pleistocene-Holocene climate and sea level changes inferred based on the tidal terrace sequence, Kutch, Western India. *Palaeogeography, Palaeoclimatology, Palaeoecology*, *473*, pp.82-93.

Engelhart, S.E., Vacchi, M., Horton, B.P., Nelson, A.R. and Kopp, R.E., 2015. A sea-level database for the Pacific coast of central North America. *Quaternary Science Reviews*, *113*, pp.78-92.

Ferrier, K.L., Mitrovica, J.X., Giosan, L. and Clift, P.D., 2015. Sea-level responses to erosion and deposition of sediment in the Indus River basin and the Arabian Sea. *Earth and Planetary Science Letters*, *416*, pp.12-20.

Gehrels, W.R., Marshall, W.A., Gehrels, M.J., Larsen, G., Kirby, J.R., Eiríksson, J., Heinemeier, J. and Shimmield, T., 2006. Rapid sea-level rise in the North Atlantic Ocean since the first half of the nineteenth century. The Holocene, 16(7), pp.949-965.

Juyal, N., Pant, R.K., Bhushan, R. and Somayajulu, B.L.K., 1996. Radiometric dating of Late Quaternary sea levels of the Saurashtra coast, western India: an experiment with Oyster and Clam shells. *Oceanographic Literature Review*, *6*(43), p.563.

Kench, P.S., Smithers, S.G., McLean, R.F. and Nichol, S.L., 2009. Holocene reef growth in the Maldives: Evidence of a mid-Holocene sea-level highstand in the central Indian Ocean. *Geology*, *37*(5), pp.455-458.

Kunte, P.D. and Wagle, B.G., 2005. The beach ridges of India: A review. *Journal of Coastal Research*, pp.174-183.

Lambeck, K., Esat, T.M. and Potter, E.K., 2002. Links between climate and sea levels for the past three million years. *Nature*, *419*(6903), p.199.

Lambeck, K., Rouby, H., Purcell, A., Sun, Y. and Sambridge, M., 2014. Sea level and global ice volumes from the Last Glacial Maximum to the Holocene. *Proceedings of the National Academy of Sciences*, *111*(43), pp.15296-15303.

Lambeck, K., Woodroffe, C.D., Antonioli, F., Anzidei, M., Gehrels, W.R., Laborel, J. and Wright, A.J., 2010. Paleoenvironmental records, geophysical modelling, and reconstruction of sea level trends and variability on centennial and longer timescales. *Understanding sea level rise and variability*, pp.61-121.

Lowe, J.J. and Walker, M.J., 2014. *Reconstructing quaternary environments*. Routledge.

Marcus, L.F. and Newman, W.S., 1983. Hominid migrations and the eustatic sea-level paradigm: a critque: p. 63–85 in: PM Masters and NC Flemming, eds., Quaternary Coastlines and Marine Archaeology.

Milne, G.A., Long, A.J. and Bassett, S.E., 2005. Modelling Holocene relative sea-level observations from the Caribbean and South America. *Quaternary Science Reviews*, *24*(10-11), pp.1183-1202.

Mitrovica, J.X. and Milne, G.A., 2002. On the origin of late Holocene sea-level highstands within equatorial ocean basins. *Quaternary Science Reviews*, *21*(20-22), pp.2179-2190.

Newman, W.S. and Baeteman, C., 1987. Holocene excursions of the Northwest European geoid. *Progress in Oceanography*, *18*(1-4), pp.287-322.

Newman, W.S., 1986. Paleogeodesy data bank and paleogeodesy. In *Technical report. IGCP Project 200 Newsletter and Annual Report*. Univ. of Durham.

Pant, R.K. and Juyal, N., 1993. Late Quaternary coastal instability and sea level changes: New evidences from Saurashtra coast, Western India. *Zeitschrift fur Geomorphologie*, *37*, pp.29-29.

Peltier, W.R., Farrell, W.E. and Clark, J.A., 1978. Glacial isostasy and relative sea level: a global finite element model. *Tectonophysics*, *50*(2-3), pp.81-110.

Shennan, I. and Horton, B., 2002. Holocene land-and sea-level changes in Great Britain. *Journal of Quaternary Science: Published for the Quaternary Research Association*, *17*(5-6), pp.511-526.

Vacchi, M., Rovere, A., Chatzipetros, A., Zouros, N. and Firpo, M., 2014. An updated database of Holocene relative sea level changes in NE Aegean Sea. *Quaternary international*, *328*, pp.301-310.

Vink, A., Steffen, H., Reinhardt, L. and Kaufmann, G., 2007. Holocene relative sea-level change, isostatic subsidence and the radial viscosity structure of the mantle of northwest Europe (Belgium, the Netherlands, Germany, southern North Sea). *Quaternary Science Reviews*, *26*(25-28), pp.3249-3275.

Woodroffe, C. and McLean, R., 1990. Microatolls and recent sea level change on coral atolls. *Nature*, *344*(6266), p.531.

Woodroffe, C.D., 1990. The impact of sea-level rise on mangrove shorelines. *Progress in Physical Geography*, *14*(4), pp.483-520.

Chapter 2
Tidal Flats
Geomorphic indicator of relative sea level change

Tidal flat is almost horizontal, negligibly sloping coastal areas commonly found on the coastlines and on the shores of lagoons and estuary which are inundated during the high tide and are exposed during the low tide. The tides are marked with a rhythm (Daidu, 2003). They are the interacting surfaces for marine, river and land environments and conserve coastal wetland bio-diversity acting as a buffer to accommodate rising sea level. (MacKinnon et al., 2012; IUCN, 2013). Often the tidal surfaces are barren or marshy and consist of unconsolidated sediments (Jackson, 1997). These are different from high energy sandy beaches which are steeper and are dominated by waves (Semeniuk V. 2005). Tidal flats are deposited under low energy conditions with relatively limited biota and have less physical reworking which is favorable for the development of a profuse coastal history and sedimentological features like cross-lamination and ripple-lamination in sand, lenticular and flaser bedding, ripple-laminated silt in clay, and tidal runoff on low gradient slopes to form meandering tidal creeks (Daidu 2003). Meso-tidal conditions favor the development of extensive tidal flats.

2.1 Classification of tidal flats

There are several criteria based on which tidal flats can be characterized. These include geomorphic settings, tidal range, sediment size, and composition etc. Below each classification is discussed in detail (Daidu, 2003; Church et al., 2001):

1. *Geomorphic classification*

Tidal flats often form part of large coastal systems like deltas, estuaries, lagoons, gulfs, bays, straits, rias, sounds, creeks, and cuspate forelands. Alternatively, these could also develop along an open coast, broad embayments or in the leeward side of lagoons. Tidal flats form after the waves dissipate quickly on the shore and the tidal water penetrate lagoons, estuaries and delta systems many kilometers (tens to hundreds) inland (Daidu, 2003). These flats are largely a result of sediment accretion along a prograded shore; however, these may also comprise of thin veneers of modern sediments deposited in the tidal cut surfaces (Church et al., 2001). Tidal flats sequences finer sediments along the open

coast and margins of tidal embayments, estuaries and creeks (Allen, 2000).

Depending on the magnitude of exposure to waves and depositional environment tidal flats are classified into three major types: (1) back-barrier settings, (2) tide-dominated estuaries, and (3) deltas and adjacent chenier plains (Daidu, 2003).

1) Back-barrier tidal flats

These occupy the landward side of barrier islands, spits, and bars, where waves are either low or absent. Tides travel landward through tidal inlets with rapidly decreasing velocity. Either the tidal occupy the entire back area as in lagoons and wave-dominated estuaries (Fig. 2.1 (a)), or may be completely filled with the tidal channel and flat system. Such geomorphic setting receives limited sediment input from land.

2) Tide-dominated estuaries

The exposure of waves is varied in these estuaries. In the innermost part of an estuary or a delta or for the gourd-shaped estuaries there is no direct exposure of the waves while the open mouth estuaries or deltas are more subjected to wave erosion. Small flats that develop near the mouth of small rivers and are sandy while flats in the downstream of a mega-river delta are filled with fine sediments which are transported by longshore currents from the delta. For example tidal flats developed in the Kori creek.

3) Open coast tidal flats

These flats are in direct contact with the open sea and lie adjacent to chenier plains. These are characterized by multiple long-term alterations of deposition and erosion which are governed by the waves, river sediment discharge or shifting of the main channel. Large rivers are having wider chenier plains foster the growth of muddy open sea tidal flats while small rivers are composed of sand and are associated with erosional features and rocky cliffs. E.g., Flats near Amazon River delta.

2. Tidal range and tides classification

Tides are long-period waves created by the gravitational pull of the moon and the sun on the earth surface. The ocean water fluctuates back and forth as these bodies interact with the earth in their monthly and yearly orbits (NOAA, 2018). Spring tides are formed when the sun, moon, and earth are aligned resulting in cumulative gravitational pull on the

ocean waters, and therefore the tides are higher than the average.

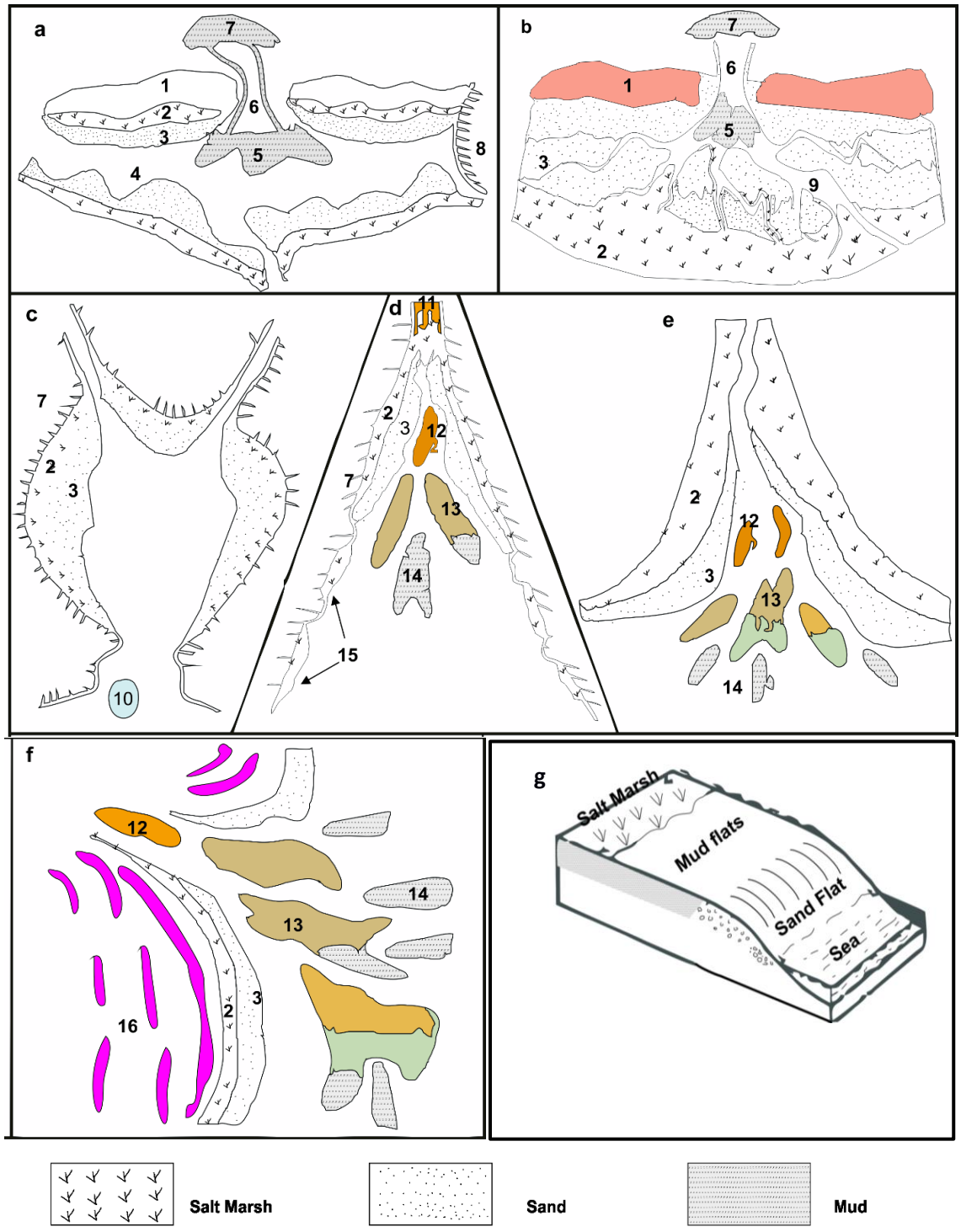

Figure 2.1: Schematic plot of tidal flats in the different coastal environments with varying sediments input a: Back barrier tide; b: Tide dominated estuary; c: poorly filled gourd shape estuary d: Partly filled open mouth estuary; e: highly filled open mouth estuary f: Tide dominated delta; g: Open coast tidal flat. 1-Barrier island, 2-Saltmarsh, 3-Bare intertidal flat, 4-Lagoon, 5-Flood tidal delta, 6-Tidal inlet, 7-Ebb-tidal delta, 8-Rocky coast, 9-Tidal

channel/creek, 10-Rocky island, 11-Bay-head delta, 12~13-Tidal sand bar/island, 14-Subtidal sand bar/ridge, 15-Gravel/sand beach,16-Chenier ridge. (Modified after Daidu 2013 and Boyed et al., 1992).

The neap tides occur after seven days of spring tide when the sun, moon, and earth are at right angle to each other resulting in lower than average tidal depth. Both types of tides occur twice a month. Tides influencing the flats can vary in range globally from ~1 to 15 m and may be diurnal (one tide a day), semi-diurnal (2 tides a day) or mixed (2 tides daily with variable maxima and minima across the day). There are two main tides that are higher or lower than average. They occur twice monthly and are called neap and spring tides.

Based on the range of tides a tidal flat may be classified as microtidal (<2m), meso-tidal (2-4 m), and macrotidal (>4 m). The extreme macro-tidal range is >8 m and common in open coast flats (Church et al., 2001; Diadu, 2003).

C) Zonal classification

Various levels within a tidal flat can be divided into different zones based on biological or sedimentological factors:

1) *Low/bare tidal flats* – are sandy and vegetation free. These are exposed during the mean and extreme low spring tides.

i. *Middle Tidal Flats* – have a low gradient and are centered on mean sea level. These are influenced by neap tides and maybe vegetated by mangrove in tropical latitudes in their upper parts.

ii. *High tidal flats* - flats are inundated only during mean and extreme high spring tides. These are dominated by mud, are salt-encrusted plains in arid zones while are vegetated by salt marshes/mangroves in a humid climate (Semeniuk V. 2005).

2) *Classification based on grain size and sediment composition*

Based on the dominant particle size these may be classified as muddy, sandy, or gravelly tidal flats.

Based on sediment composition these are mainly categorized into two groups and exhibit two extremes in their setting.

Siliciclastic tidal flats- are the supply abundant tidal flats in deltas and estuaries which are mainly composed of fluvial delivered terrigenous sediments such as quartz sand, quartz silt, and phyllosilicate clay (kaolinite and illite). In the semi-arid and arid climate, the upper part of siliciclastic tidal flats may develop carbonate nodules or gypsum crystals or maybe salt encrusted, due to increase upslope in pore water salinity. The grain size variation across the siliciclastic tidal flat is generally governed by climate setting, biogeography, and sediment type ,where sand is found in low tidal zone and mud in high tidal zone with specific biogenic contribution in particular tidal zone hence the sedimentary structure of siliciclastic tidal flat is the result of various physical and biological processes.

Carbonate tidal flats - are generally found in mid to low latitude warm climates, and these are composed of carbonate silt and clay, various sand-size carbonate grains and the products of cementation (e.g., crusts, breccias, interclasts) and are associated with petroleum reservoirs potential. These tidal flats have little or no terrigenous flux from the terrestrial sources to dilute the carbonate accumulation contributed by local biogenic and abiotic sources, hence these tidal flats are carbonate-rich .Carbonate tidal flats have a plethora of diagenetic and sedimentary products such as cemented layers and crust development, progressing to surface mounding, a formation of compressional polygon and tepees, and then leading to fragmentation, brecciation, and formation of interclasts. Carbonate tidal flats in more arid climates also develop evaporite minerals suites such as beds of gypsum nodules, gypsum platey crystals, gypsum mud, and halite crust (Semeniuk V. 2005).

Although no tidal flat is entirely composed of single type of sediments like, siliciclastic tidal flats may sometimes have minor to moderate carbonate components of shell gravel, shell grit and skeletal sand like shell fragments, foraminifera which is mainly find in carbonate tidal flats (Semeniuk V. 2005). Similarly in carbonate tidal flat, there may be siliciclastic sand, mud or gravel from oceanic, aeolian or due to local erosional sources.

C) Morphological classification

Based on the morphological zones a tidal flat may be classified into different types:

i. *Sub-tidal zone* – that zone of the coast that is permanently inundated under the low water line and has gentle relief. Often the exposed intertidal flats gradually grade into subtidal flats without perceptible relief. The coarsest sediment fraction occurs at the boundary of inter-sub tidal flats, and there is a gradual fining trend both towards the sea and towards the inter-tidal zone. Seaward fining happens because the hydrodynamic energy decreases with increasing water depth while towards the inter-tidal zone water velocity slackens (Daidu 2003, Li et al., 1992).

ii. *Intertidal zone* – the part of the coast that is exposed/submerged during low/high tide. It consists of bare flats and salt marshes and may be further divided into the upper, middle, and lower subzones based on grain-size, vegetation, tidal level, etc. the upper part of the zone is characterized by extremely fine sediments.

iii. *Supratidal zone* – the zone that is inundated only during extreme high tides and is well above the highest tide level. There may be mangroves, scanty vegetation, salt marshes or salt pans in this zone depending upon the climate. The boundary between inter-tidal and supra-tidal zone is generally marked by an erosional cm to m thick escarpment where grain size becomes coarser if it is a recessional tidal flat and vice versa.

2.2 Geomorphic processes on tidal flats

Tidal flats are gently inclined to flat surfaces experiencing interactive and interrelated exogenous and endogenetic process and agents of fluvial, marine, atmospheric, climatic and biological origin. These processes have physiochemical gradients and operate on a variety of grain size from mud to gravel. Various processes operating on tidal flats are (Semeniuk V. 2005) -

i. *Oceanographic:* These processes involves erosion, deposition and, transport of sediments facilitated by tidal currents, wave action, storms and, cyclone.Tidal currents transport mud in suspension and sand by traction.

The transport of sand is affected during the flooding period when tidal currents are progressing or regressing from their maximum velocities. While the deposition of mud is affected during the low current velocity and slack water, mud deposit is also affected by

fluctuation in water temperature, since cold water and warm water have different viscosities, which led to the variation in mud particle settling velocities (Krogel and Flemming 1998). As the tidal currents systematically increase and decrease across the tidal cycle which results in the development of ripples, then mega ripples and again ripples and formation of various bedding features like laminated mud, lenticular bedding and flaser bedding (Semeniuk V. 2005).

ii. *Fluvial processes:* These involve delivery of sediments and fresh water to the shore in estuaries and deltas.

iii. *Meteorological/atmospheric processes:* These involve the evaporation, wind erosion, transport and deposition, rain, ice-crystallization and water temperature fluctuation. Wind transport, erode and deposit sand into tidal flats as fallout and form adhesion ripples.

iv. *Hydrologic and Hydro chemical processes:* These involves the rise and fall of water table under the tidal flat, dissolution, and precipitation of carbonate minerals, evaporate minerals and iron minerals and many redox reactions. The groundwater hydrology of tidal flats is important because it affects the interstitial pore water salinity gradients and moisture gradients which influences the precipitation of evaporate minerals.

v. *Biological processes:* These includes the accumulation of beds of biogenic materials like shell beds, bio stromal reefs, and plant materials, bio mediated of precipitation of minerals like iron sulfide, burrow structuring root structuring of sediments. The biota present in tidal flats like mangroves, modify the tidal currents and induces sedimentation by trapping and binding of sediments by vegetation and algal mats (Semeniuk V. 2005).

Sedimentary structures in tidal flats

Tidal flats may develop in all coastal settings except the wave-dominated beaches, and the bedding type associated with intertidal flats generally transits landward into salt marshes or mangroves. The availability of coarse sediments and landward decreasing of hydrodynamic energy, surface sediments are usually finer. The upward fining succession of sediment pattern is deposited in the lower energy phase or during storm

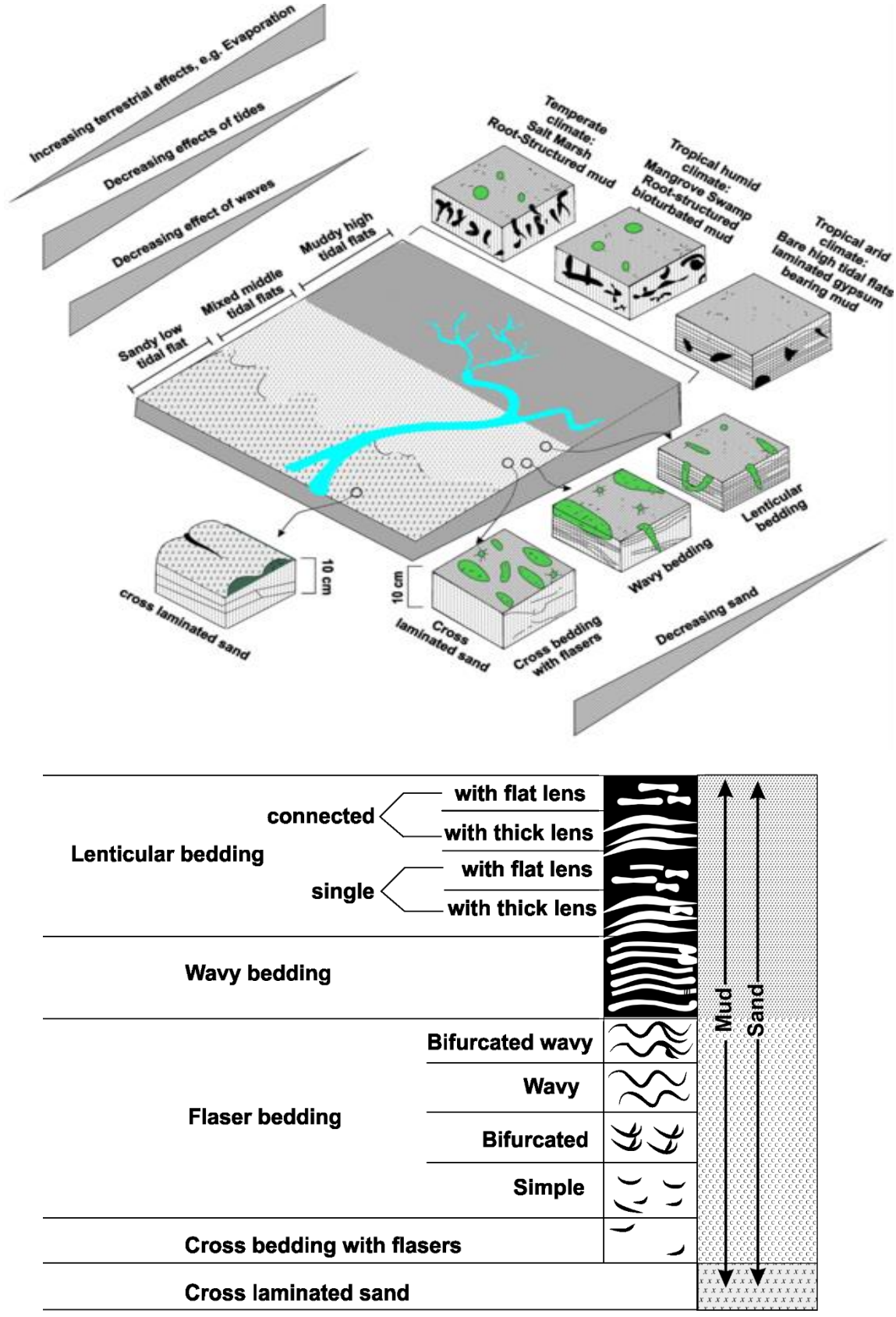

Figure 2.2: Schematic of morphological classification of tidal flat (Modified after Reineck and Singh 1980).

waning phase. Therefore the grouping pair of sand dominated layers and mud dominated layers is the product of seasonal variation of wave climates on muddy exposed tidal flats (Fan et al., 2004).

The sediment type on the tidal flat is related to their positioning with respect to the slope on the tidal flat as a result of the interplay of tidal action and wave processes. This lead to partitioning based on the particle size like sand in low tidal flat, mixed sand and mud on mid tidal flat and mud on the high tidal flat and in absence of intense biogenic activity the sediments got separated in layers and laminate to develop Flaser bedding , lenticular bedding , wavy bedding or interlaminated sand and mud.

Flaser bedding forms when sediments are exposed to intermittent flows and results in the formation of alternate mud and sand layers. These types of bedding mainly have sand particles in their layers (Semeniuk V. 2005).

Lenticular bedding forms during the period of slack water. The mud suspended in the water got deposited over the sand when water velocity gets zero; these types of bedding mainly contain silt and clay particles. The sand formations within the bed look like lens. Hence this bedding gets the name lenticular. These bedding are used to infer tidal rhythm, tidal current and tidal slack in a tidal flat environment (Semeniuk V. 2005).

Wavy bedding forms if the amount of mud and sand in sediments are equal then wavy bedding is formed, it is formed when mud is deposited over rippled or cross stratified sand, it follows the alternating concave and convex nature of ripples, which give it a wavy appearance, it usually makes the boundary between flaser and lenticular bedding (Semeniuk V. 2005).

Cyclic tidal rhythmites or laminations which represent neap-spring tide cyclicity by variations in (sandy) bed/lamina thickness. These are formed in the subtidal channel settings and are not common in modern or ancient tidal-flat environments. Their development requires wave protection, high sediment supply, and enough accommodation space availability over the short term (Semeniuk V. 2005).

For the inter-tidal environments, there is no unique bedding. Flaser, wavy and lenticular bedding is a gradational spectrum of heterolithic deposits where laminae of sand

and mud alternate. The finer fraction in the bedding is deposited by the slackening of tides although coarser sediments may also represent episodic flooding on the alluvial plains, or weak storms in the offshore environments. If it is pro-gradational tidal flat, it will comprise of upward fining sequence with well-developed flaser bedding at the base, followed by wavy bedding and lenticular bedding and overlapped by saltmarsh deposits. Whereas, thicker upward fining coarser sequence with hummocky cross-stratification may represent a storm event (Daidu, 2003).

2.3 Biota of tidal flats

The biota of any tidal flat is decided by biogeography and climate, substrate and hydrochemistry of the tidal flats. The most common biota of tidal flat includes mangroves, salt marsh, algal mat and stromatolites, polychaetes, molluscs, crustacea, resident fish and invading nektonic fishes and avifuna. The abundance and zonation of these species in a tidal flat are determined by physiochemical and biological conditions. Mangroves occur in tropical tidal flats in mid to upper tidal flat whereas in temperate tidal flat these mangroves are replaced by salt marsh (Samphire and Spartina). Primary production within a tidal flat is driven by mangroves and salt marshes. These macrophytes fix nutrients and carbon in the tidal flat and support the local resident fauna, and the export of the detritus support benthic biota of polychaetes, molluscs, and crustacea. With an increase in salinity, the upper tidal flat may be inhabited by algal mats and stromatolites in mid-upper tidal zones of tidal flats (Ginsburg and Hardie 1975). The molluscs, polychaetes, and crustacea are the primary and secondary invertebrates consumers generally present on all tidal flats, although their species diversity may decrease in temperate regions (Semeniuk V. 2005)

Tidal flats are biologically zoned like benthic groups species show zonation across the tidal flat related to the frequency of inundation, substrate, pore water salinity and interspecies competition, etc. similarly macrophytes also exhibit zonation which is related to groundwater salinity, substrate and elevation of habitat above mean sea level, and many of the benthos are burrowing forms, and the macrophytes have diagnostic root structures hence therefore these zonation of biota result in facies and a signature of specific tidal level across the tidal flats like, Arenicola burrows are the diagnostic of mid to low tidal sand flats, coarse root structured substrates and associated faunal burrows are the diagnostics of

mangrove vegetated high tidal flat, whereas the fine root structured substrates are diagnostic of salt marsh vegetated high tidal flats (Semeniuk V. 2005).

References

Alexander, C.R., Davis, R.A. and Henry, V.J. eds., 1998. Tidalites: Processes & Products (Vol. 61). SEPM (Society for Sedimentary Geology).

Church, J.A., Gregory, J.M., Huybrechts, P., Kuhn, M., Lambeck, K., Nhuan, M.T., Qin, D. and Woodworth, P.L., 2001. Changes in sea level. In , in: JT Houghton, Y. Ding, DJ Griggs, M. Noguer, PJ Van der Linden, X. Dai, K. Maskell, and CA Johnson (eds.): Climate Change 2001: The Scientific Basis: Contribution of Working Group I to the Third Assessment Report of the Intergovernmental Panel (pp. 639-694).

Daidu, F., Yuan, W. and Min, L., 2013. Classifications, sedimentary features and facies associations of tidal flats. Journal of Palaeogeography, 2(1), pp.66-80.

DALRYMPLE, R.W., 1992. Tidal depositional systems. Facies models, response to sea level change, pp.195-218.

Davies, J.L., 1972. Geographical variation in coastal development. Oliver and Boyd.

Fan, D., Li, C., Wang, D., Wang, P., Archer, A.W. and Greb, S.F., 2004. Morphology and sedimentation on open-coast intertidal flats of the Changjiang Delta, China. Journal of Coastal Research, pp.23-35.

Ginsburg, R.N. ed., 2012. Tidal deposits: a casebook of recent examples and fossil counterparts. Springer Science & Business Media.

Klein, G.D. ed., 1976. Holocene tidal sedimentation (Vol. 30). Dowden, Hutchinson & Ross.

Ping, L.C.H.C.W., 1992. Depositional Sequences and Storm Deposition on Low-energy Coast of China [J]. ActaSedimentologicaSinica, 4, p.014.

Semeniuk V. (2005) Tidal Flats. In: Schwartz M.L. (eds) Encyclopedia of Coastal Science. Encyclopedia of Earth Science Series. Springer, Dordrecht.

Wiltshire, K.H., Tollhurst, T., Paterson, D.M., Davidson, I. and Gust, G., 1998. of Book: Sedimentary Processes in the Intertidal Zone (Vol. 139). Geological Society.

Chapter 3
Study area

3.1 Geological evolution of Kutch since Mesozoic

The Kutch, Cambay and Narmada basins are the three pericontinental major marginal rift basins in the western margin of Indian craton formed by rifting along Precambrian tectonic trends at different times during Mesozoic era with varying thickness of Mesozoic sediments and hence considered as the essential Mesozoic marginal marine basin which are bounded by intersecting sets of faults (Biswas 1982).

The Kutch rifting had initiated since the Mesozoic period (~250 Ma) when India was drifting towards north after the breakup from Gondwana land (Nortan and Sclater 1979), which is interpreted as Extensional tectonics regime. During this extensional regime, the origin of multiple Horsts and Graben has happened along the series of normal faults (Biswas 1987). These graben provided the place for marine and continental deposition of sediments during the Mesozoic and Quaternary period.

During the Tertiary period (~66 Ma) there was a reversal in the stress regime, the extension tectonic regime changed into compressional tectonic regime due to the collision of the Indian plate with the Eurasian plate. Due to this collision, the volcanic eruption happened, and the flow of basaltic lava made the Deccan Traps. The genesis of modern-day Rann of Kutch and Banni Grassland is associated with Reverse fault during compressional tectonic regime (Biswas 1987; Talwani and Gangopadhyay 2001; Biswas and Khattri 2002).

The Kutch basin exposes thick accumulation of clay-silt and conglomerates deposits of Mesozoic to Quaternary period. In Mesozoic, during the regressive cycle, the continental flux dominated the marine flux and the deposition of conglomerates and sandstones, or deltaic clastic sediments has happened whereas when the marine flux were

deposited dominates the continental flux during transgressive cycle carbonates, shales and clay-silt were deposited (Biswas 1981).

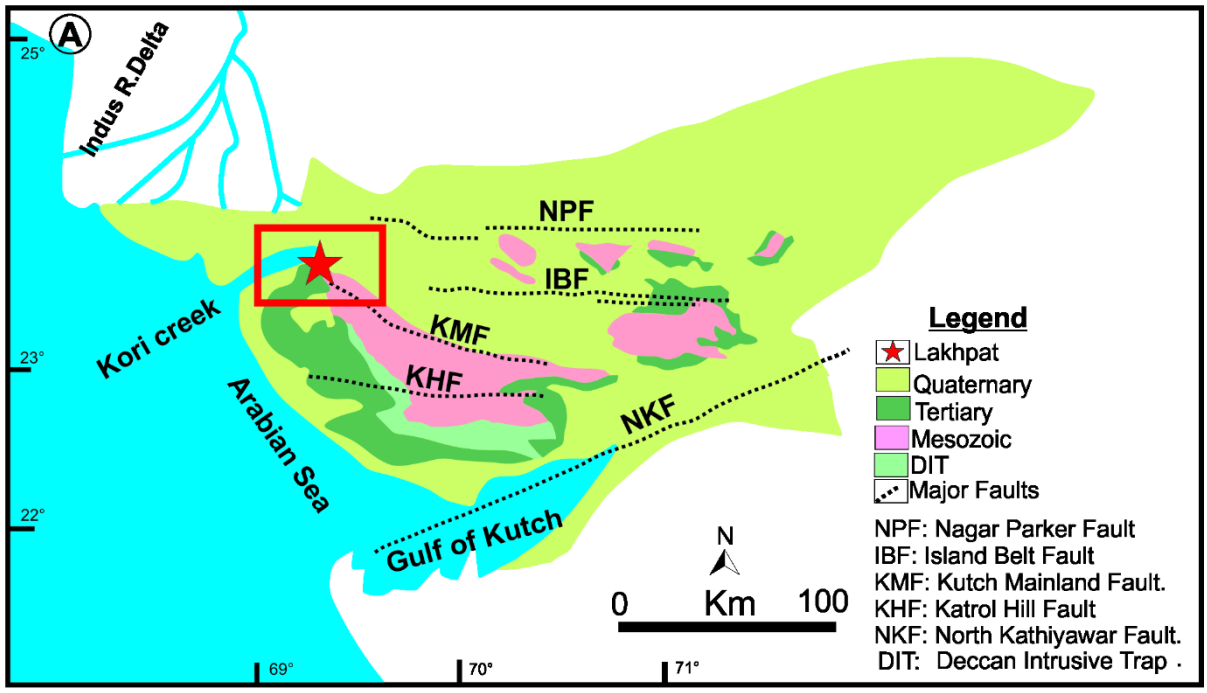

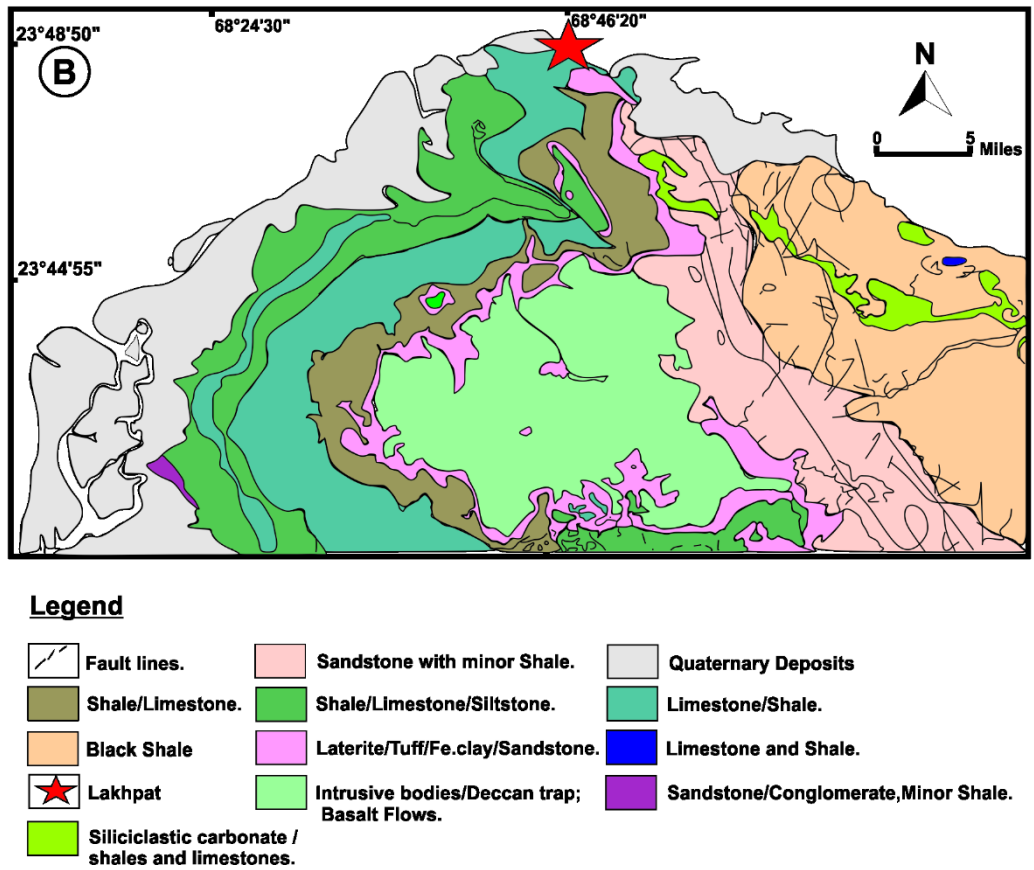

(Modified after Bhattacharya 2015; Biswas 1987; Biswas and Deshpande 1973)

Figure 3.1: (A) Geological map of the region showing major lithology and faults. The coring site near Lakhpat is marked with red star. The detailed lithology of the region within red rectangle is shown in (B)

3.2 Geomorphology

The areas which are in the proximity of the continental margin, Climate, Tectonics, and Sea level changes played a vital role in the landscape evolution. Mostly then, the climate, Tectonics and Sea level changes would have been the major crucial responsible factor for the landscape evolution of The Rann of Kutch during the Quaternary time (Glennie and Evans 1976).

Rann of Kutch

Kutch, also spelled as Cutch, is the phonetic rendering of the Persian word whose nearest translation into Roman letters is Kutch, meaning "alluvium brought down by the rivers" and the words Rann of Kutch mean a "marsh of alluvium" or wasteland.

The geomorphic setup of Kutch is dominated by prominent fault bound uplifts, the Mainland Kutch, Wagad highland and the island belt consisting of Pachchham, Khadir, Bela and Chorar islands (Biswas, 1974). The Kutch is divisible into two parts The Great Rann of Kutch and The Little Rann of Kutch. These cover almost 45,000 km^2 area and comprise a flat, barren landscape that occurs about 2-6 m a.m.s.l.The Rann together marks a significant site of continuous Quaternary sedimentation which is not yet adequately understood.

The *Rann of Kutch* (rann = ephemeral playa lake) is broadly divided into two parts,

a.) The Great Rann of Kutch,

b.) The Little Rann of Kutch

The Great Rann of Kutch encompasses an area of ~ 16,000 km^2 and is bounded by Arabian sea and Indus Delta in the south and west, the Thar Desert in North, the Aravalli Ranges in the east and in the south there is the Kutch upland, whereas in compression of this the Little Rann of Kutch has a spread over an area of ~ 4,100 km^2 and is located in the southeast of the Great Rann of Kutch connected to the Great Rann by narrow saline stretch in north. It is bounded by the mainland from three sides and opens into the Gulf of Kutch in the southwest.

According to the study done by Biswas in 1987, the present configuration of the Kutch basin is due to the differential movement along Nagar Parker Fault (NPF), Kutch Mainland Fault (KMF) and Allah Bund Fault which resulted in the formation of series of horsts and graben. At present in response to the continually acting compressive stress on

the Indian plate the Kutch basin is going through the stress reversal phase with the uplift of large fault-bounded blocks.

During the last 2000 years, silting up of Rann along with tectonic uplift has turned the marine embayment into dry salt covered mud flats. Presently, the Great Rann lies marginally above the tidal range of the Arabian sea and is flooded annually by the seawater through the Kori creek in the south and Luni river in the east (Glennie and Evans 1976).

The major landforms of the Great Rann can be classified into two topographic units i.e.

i. The uplifted rocky island
ii. The low lying salt encrusted Rann surface.

The uplifted rocky island are four east-west trending islands commonly known as Island belt. From west to east, these are: The Pachham, Khadir, Bela, and Chorar made up of Mesozoic and Neogene marine rocks (Biswas 1987). These islands abruptly rise above the monotonous flat, salt-encrusted Rann surface, whose origin is understood as the surficial manifestation of tectonically active east-west trending Island Belt Fault (IBF) These islands have some peculiar geomorphological features like slope is south tilted, north facing escarpment at the northern margin of each island, raised intertidal flats, notches and marine erosional features indicates towards the mid-late Holocene uplift of the islands along the IBF (Chowskey et al., 2010). During Monsoon when the Great Rann of Kutch is submerged under floodwater, the island belt stands out and marks the geomorphic feature in the region.

The low lying salt encrusted rann surface is a large part of the Rann, which is saline but surficial expressions of the salt encrustation are much more evident as well as the variability in the landforms, and geomorphic processes are much more prominent in relatively low lying area. Based on the surface assemblage and flooding pattern, geomorphologically the low lying Rann is divided into four east-west trending zones (Roy and Merh 1982).

a. Bet Zone
b. Linear Trench Zone
c. Banni Plain
d. Great Barren Zone

a.) Bet Zone

The meaning of Bet is "raised land."Bets are the slightly elevated islands covered with grass. These bets are composed of fine mica and sand.

The origin of these bets is supposed to be associated with the remnants of abandoned river channels or the leftover of an ancient delta formed by the Indus River (Snelgrove 1979; Roy and Merh 1982 and Juyal 2014).

The distribution and arrangement of the islands are significant, and two distinct belts of the island are distinguished, one is Outer (southern) and Inner (Northen).
Outer comprises Keshmari bet, Bhangarwa bet, Ratadiya bet and Saheblana bet islands, whereas the inner one counts for the Mardak bet, Khijadiya bet, Wasra bet and others. The innermost of the Little Rann to the north of the inner island is dotted by several islands of varied size and shape (Pung bet, Shedwa bet, Nanda bet and other) known as the Island Zone of the Little Rann of Kutch.

The formation of these bets is supposed to happen in the fluvial depositional environment because of the presence of parallel laminated sand horizons instead of cross-laminated. Additionally, as these Bets are primarily consisted of Mica, which is a detrital mineral. Hence stating that the Nara river which once flowed into Great Rann of Kutch might have been the primary source of micaceous sediments into the region which might have brought these fine micaceous sandy sediments. (Reineck and Singh 1980; Oldham 1926; Alizai et al., 2011 and Chauhan 1994).

b.) Linear Trench Zone

The Linear Trench Zone is a depression extending from the Kori Creek to Kuar Bet and lying between the Banni and the Allah Bund. This depressed terrain is feed by water through various sources like it is tidally inundated by tidal waters of Arabian sea through Kori creek and by direct precipitation as well as the water from neighboring mainland streams collects in this zone and stagnates there which on evaporation give rise to vast salt encrusted plain (Thakker & Solanki 2018).

c.) Banni Plain

The origin of the word "Banni" is from the Hindi word "Banai" meaning made. This land is formed by the sediments deposited by Indus and other rivers in the past course of time

before the 1819 earthquake. Banni plain is a vast salt-encrusted plain which is sparsely invaded by halophytic grasses and bushes that provide shelter to various species of animals and birds (Juyal 2014).Banni plains are tectonically active, and therefore the presence of gullies which is cutting down into the Quaternary alluvial deposits is the result of a recent tectonic activity which triggered the erosion in the region (Kar 2011).

d.) Great Barren Zone

The Great Barren Zone is transitional part of the Little Rann of Kutch. It is a shallow depressed region which is influenced by monsoon flooding. It is located to the eastern part of the Great Rann and touches the dunes of the Thar Desert in the northwest. The Great Barren Zone is bounded by the narrow uplifted area near Kaur bet limiting its reach from western Great Rann.

The Little Rann of Kutch

The Little rann is a triangular shaped, almost landlocked basin that opens up to the west into the Gulf of Kutch and the geographical position of the Little Rann is to the SE of Wagad uplift which shows a complex structural setting. The southern margin of Wagad is marked by various discrete EW trending faults, which is collectively known as South Wagad Fault System (SWFS). Whereas The Great Rann of Kutch is an EW trending sub-basin which is bounded by the Nagar Parker Fault (NPF) in the north and the Kutch Mainland Fault (KMF) in the Southand comprises almost half of the area of the seismically active Kutch palaeorift basin.

The flat landscape of Ranns is variously described as ‘intriguing’ to ‘unique’ to ‘without any counterpart in the world.’ (Burnes 1835, Roy & Merh 1981). The Ranns are believed to be uplifted floor of former gulfs (Merh 2005, Maurya et al., 2008). The great Rann was an EW trending gulf that joined up with the Arabian Sea in the west while the Little Rann is believed to mark the landward extension of the present day Gulf of Kutch. A study done by Oldham in 1926 suggests that the navigable sea existed at least up to ~ 2000 yr B.P.

Surficial preliminary studies of sediments have suggested that these are mostly clay-rich, which are in agreement with the known marine origin of the terrain (Srivastava 1971; Glennie & Evans 1976). Due to closeness to the sea and open area, the prevalence of strong wind is responsible for the wind-blown thin slit cover over the surface. The most striking

feature of the landscape is the presence of several islands, locally known as bets. These bets vary in area from several square meters to several square kilometers. Mostly they are flat sandy surfaces. However, a few exposes the Mesozoic rocks and display rugged hilly topography.

Earthquakes in Rann

In the recent times, one aspect of Rann that has received considerable attention from the contemporary workers is the repeated liquefaction of the Rann sediments due to large magnitude earthquakes occurred along the various EW trending faults of the Kutch basin. The Great Rann is tectonically active terrain and has experienced earthquakes of varying magnitude in the past. The earthquake of 893CE and 1668 CE which were located in the north and northwest of the Great Rann were severe. The 1819 Allah Bund earthquake (magnitude 7.5) brought a significant change in the geomorphology of the terrain it has produced ~ 90 km long scrap in the northern part of the Great Rann and widespread liquefaction in the Ranns (Oldham 1926, Bilham 1998, Rajendran & Rajendran 2001). Again in 1956 Anjar and 2001 Bhuj has faced the severe earthquake which resulted in widespread liquefaction in the rann sediments whereby the enormous amount of saline water and sandy sediments were ejected from the subsurface (Chung & Gao 1995, Turtle et al., 2002).

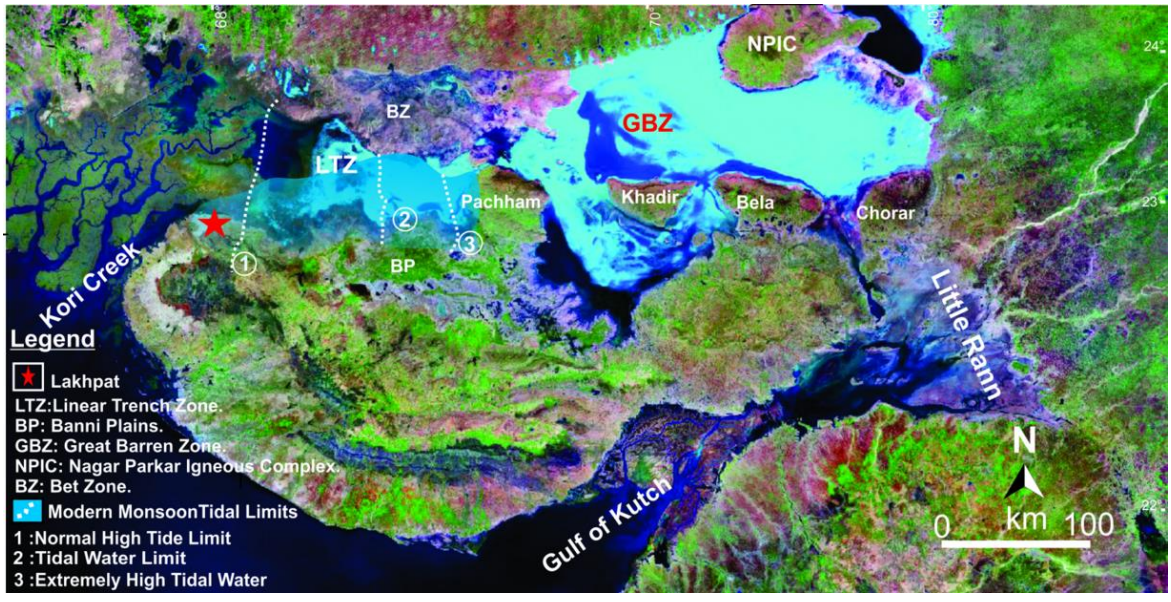

Figure 3.2: Major geomorphological zones are demarcated on LANDSAT (False Colour Composite). Note that the coring site near Lakhpat (red star) is inundated under the normal tide limit.

3.3 Climate Division

The climate of Kutch is arid to semi-arid with three distinct seasons, the cold season from December to February and from March to June region faced extreme hot summer season. In the month from June to September area faces southwestern Monsoon whereas the October and November constitute the post-monsoon transition period between the rainy and cold season.

The temperature of the Kutch region shows a considerable variation from location to location. It varies from 0°C in winters to 46° C during summer. During summer the day temperature is less in coastal areas compared to interior areas. After February temperature starts to rise rapidly till May and the daily maximum temperature during May is ~ 38° C. However, this sometimes reaches up to 48° C in the interior areas of the Kutch. During winters in January, the mean daily maximum temperature is ~ 26° C, and the minimum is 10° C.

During the onset of monsoon in mid-June, the day temperature starts to decline but the nights remain hot and humid. When monsoon withdraws in the middle of September the day temperature slightly increases till October, however night temperature decreases. The Humidity of Coastal region of Kutch remains high throughout the year, exceeding 60% on the average. During the months of southwest monsoon, the relative humidity exceeded by 80% in the coastal areas and by 65% in the interior areas. The rain fall in the Kutch is irregular, short but high in intensity varies from 420 mm to 261 mm; hence region is characterized by deficit rainfall pattern. The region received 95% of annual rainfall in the month of July in 15 effective rainy days hence based on the records of last eight decades collected at 15 rain gauge stations covering the entire region the average rainfall stands at 340 mm.

In the Kutch, winds are normally light to moderate but become strong during late summer and southwest monsoon seasons. The areas near to coast face stronger winds, especially during monsoon. The high temperature and wind speed lead to high evaporation losses in the area (Maurya et al., 2003).

Kori Creek

The Rann of Kutch was well inhabited around 4000 – 5000 years ago and was navigable by the Arabian Sea through Kori Creek in 325 B.C. (Dales 1966; Bist 1994;

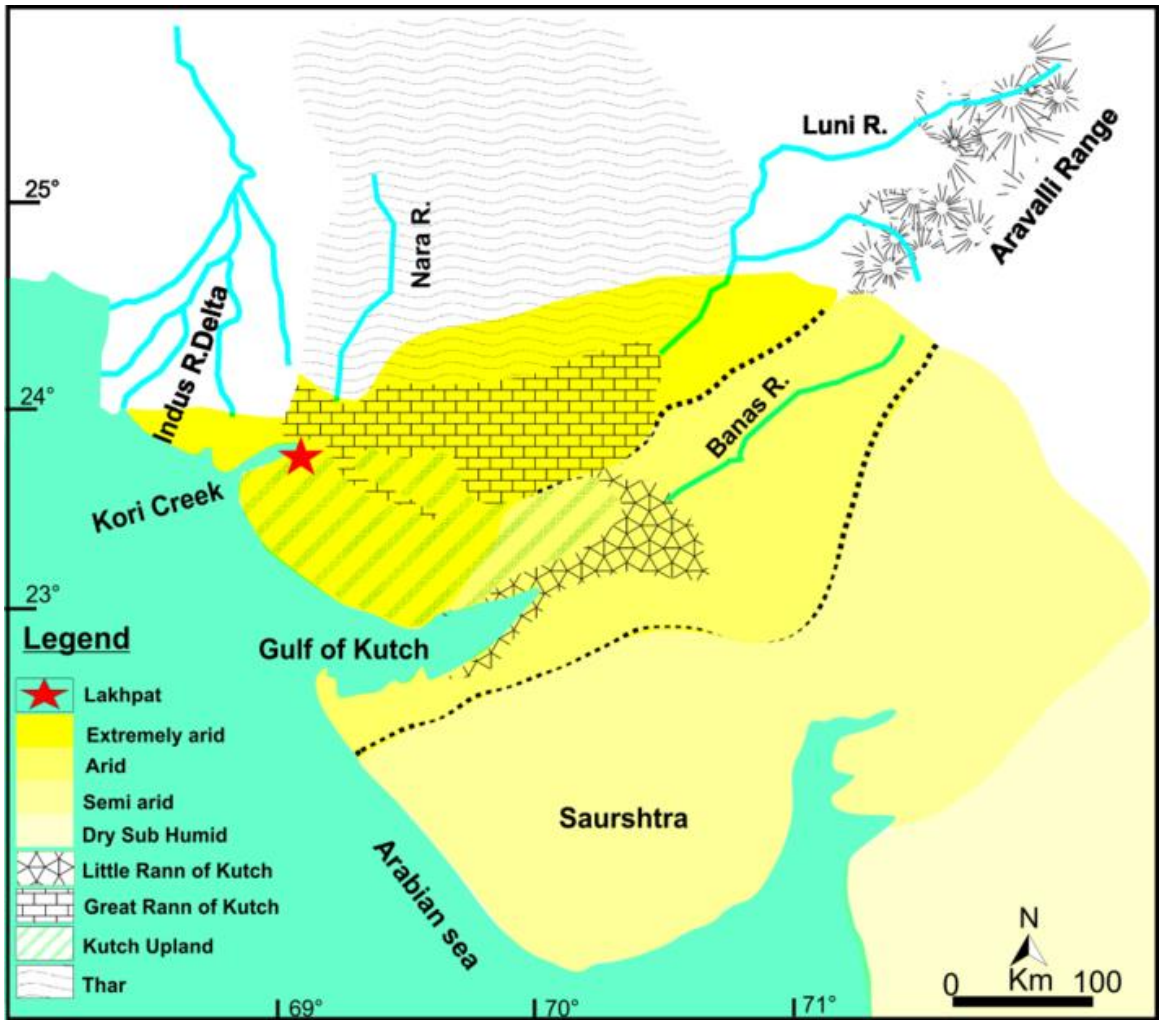

(Modified after Juyal 2014; Maurya et al., 2002; Glennie and Evans 1976)

Figure3.3: Map showing the major geomorphological and climate divisions of Gujarat. The core site near Lakhpat is marked with a red star.

and Siveright 1907). According to the historian about 712 A.D. Arab had invaded this region, and their chronicles contain reliable details on the growth of this delta.

Interestingly this well-inhabited area converted into a vast expanding saline dessert by 1361 A.D. So what could have happened between A.D. 712 and 1361 that transformed an inland sea into a marsh? According to the historians (e.g., Williams, 1958), a massive earthquake occurred on the northern shores of the Rann of Kutch within this interval (A.D. 1030) which pulverized the well-settled ancient civilization. During mid-eleventh century A.D., the Indus River had also changed its course to the far west, and the tectonic activity

of region raised the level of Rann, which makes its navigation through Kori creek difficult (Wilhelmy 1969).

Despite all these changes the Indus and its tributaries keep on feeding Nara river flowing through Kori Creek and falling in Arabian sea, until 16th century A.D. But the massive earthquake of 1819 uplifted the bed of Nara which destroyed all the settlement along its bank and the Nara has also abandoned that waterway (Oldham 1926). Among all the destroyed settlement Sindri Fort was the chief destruction, which can never be rebuilt because the earthquake caused the shoaling of the river, blocking access to the Arabian Sea.

The 1819 Earthquake generated a ~ 90km long uplifted region the salt-encrusted surface of the Rann. This Bund consists of thinly laminated alternating layers of dark brown silt and clay encrusted with salt and ferruginous tubules sediments. This is entirely different from land-derived fluvial bet sequences (Rajendran et al., 2001). Allah Bund means "mound of God" a long track of uplifted land bordered on the south by the salt-encrusted surface of the Ranns and a crucial coseismic feature came into existence after 1819 Rann of Kutch earthquake (M 7.5) in northwest India. (Burnes, 1835; Baker, 1846; Lyell, 1857), which has attracted many explorers to this area in the early part of the British colonial period. Large earthquakes with observable surface deformation are relatively rare in the cratonic area, and for this reason, the 1819 earthquake has fascinated geologists for a long time. The exploration of the Allah Bund, the first of its kind since the colonial period, provides new data on the morphology of the fault scarp and also documents evidence of past seismicity in the region (Rajendran et al., 1998; Rajendran, 2000).

Just seven years after the 1819 earthquake, a major flood in the Indus river burst all the artificial dams, submerging the entire area and finding a passage through the Bund (Burnes 1835; Lyell 1857). This brings a new feature to the scarp as the Indus river is eroding the scarp and depositing the sediments in the low –lying areas, significantly altering the earthquake-related topography. However, the steep southern face to be well preserved at many localities, conforming to the historical descriptions.

The Holocene stratigraphy of the region became mandatory to decipher the relationship between various prepositional sedimentary units within the trenches and also to isolate seismic signatures. This suggested that the sea level changes during 3-6 ka B.P might have influenced the sedimentary environment, resulting in the deposition of bluish

green clay with shells in the region. Following the withdrawal of the sea, distribution of deltaic deposits of fine sand and silt became more extensive. Due to tidal influence, brown to dark brown silty clays were laid over the deltaic sequence during the late Holocene (Rajendran et al., 1999).

Lakhpat Mudflats

Mudflats at Lakhpat are located in the mouth of tide-dominated gourd shaped estuary drained by Kori creek. Being in high inter-tidal zone, these are dominated by fine silts-clays and are protected from direct exposure of the waves and hence intense wave erosion. In the absence of any major drainage system the dominated supply of sediment is supplied via along-shore current that moves parallel to the Kutch coast (Tyagi et at., 2012). These mudflats are very gentle in slope and are inundated during the high tide limit during the monsoon. The outer edges of the flats are surrounded by flat salt marshes.

The core which is ~1 m thick is composed of thin laminae of clays and silt, which indicates that the deposition under low energy conditions as the velocity of the water slackened. During high tide, alongshore tidal currents surging through Kori creek brings the sediments flux and deposit these sediments in the various zones of tidal flats. When tides are swashing, they have very high energy and carry the most of the sediment flux, hence deposit coarser particles in supratidal zones of mudflats in the swashing phase. During back swash, the energy of tides lowers down significantly, and they can only carry fine grain clayey slit particle and deposit them in high intertidal zone as in Lakhpat mudflats. There is an absence of any type of lamination or bedding in the mudflats.

The significance of the present study

1. As discussed earlier it will help in generating a local estimate of relative sea-level change and land-sea interactions during the late Holocene and therefore enhance our understanding of the sea-level changes in the region.
2. Such studies serve as an input for the future sea-level projections and are therefore important for the refinement of predictions.
3. There are contradictory suggestions about sea-level governing the rise/decline of civilization in the study area as it affected the navigability (e.g., Das et al., 2017, Sharma et al., in press). The sea-level estimates along with climate variability will help in understanding if indeed there was any influence of sea-level on the civilization.

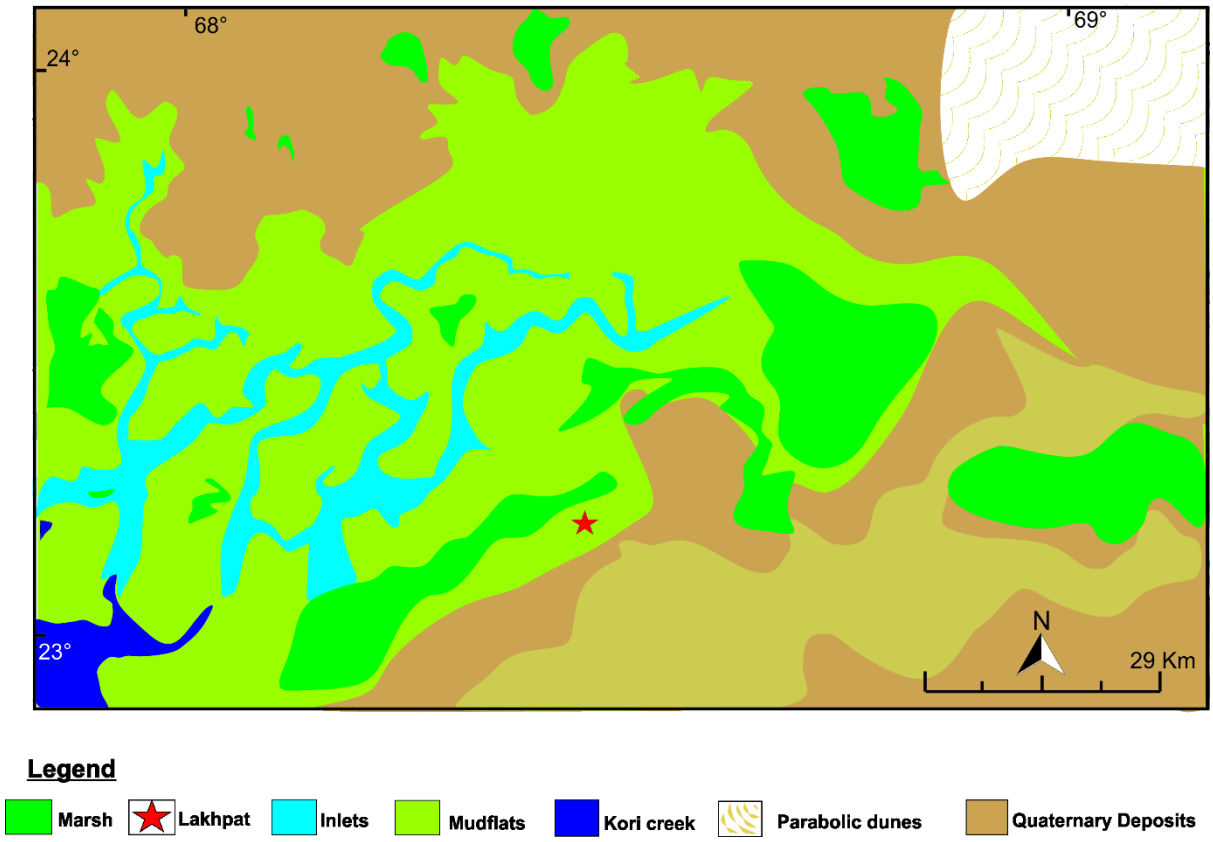

Figure 3.3: Detailed geomorphology of coring site and the surrounding region is traced from the Google Earth imagery that shows the dominance of tidal flat sediments.

Objective

The objective of the thesis is to reconstruct Holocene sea-level changes and climate variability from the mud flats of Kori creek. To achieve it geochemical proxies and C/N ratio along with chronology was employed.

References

Alizia, A., Carter, A., Clift, P.D., VanLaningham,S., Williams, J.C., Kumar, R., 2011.Sediment provenance , reworking and transport processes in the Indus River by U-Pb dating of detrital Zircon grains. Global and Planetary change 76, 33-55.

Baker, W.E. 1846. Remarks on the Allah Bund and on the drainage of the eastern part of the Sind basin, Transactions of the Bombay Geographical Society 7, 186-188.

Bilham, R.,1998. Slip parameter of Rann of Kutch, India, 16th July 1819, earthquake quantified from contemporary accounts in, Coastal tectonics, I.S. Stewart and C. Vita Finzi (Editors), Geological Society of London, Spec. Publ. 146, 295-319.

Bisht, R.S., 1994. Secrets of the water fort, Down to Earth 2, 25-31.

Biswas, S.K., & Khattri, K.N. 2002: A geological study of earthquakes in Kutch, Gujrat, India. - J. Geol. Soc. Of India 60:131-142.

Biswas, S.K., 1974. Landscape of Kutch A morphotectonic analysis.- Indian J. Earth Sci. 1: 177-190.

Biswas, S.K., 1981. Basin framework, Palaeoenvironment and depositional history of Mesozoic sediments of Kutch basin, Western India. Q.J. Geol. Min. Met. Soc. India, 53(1/2): 56-85.

Biswas, S.K., 1982. Rift basins in the western margin of India and their hydrocarbon prospects. Bull. Am. Assoc. Pet. Geol., 66(10): 1497-1513.

Biswas, S.K., 1987 Regional tectonics framework, structure and evolution of the western marginal basins of India. Tectonophysics 135:307-327.

Burnes, A., 1835. A memoir on the eastern Branch of the river Indus giving an account of the alterations produced by it by an earthquake in 1819, also a theory of the Rann , and some conjectures on the route of Alexander the Great, drawn up in the years 1827-28. Royal Asiatic Society 3, 550-588.

Chauhan, O.S., 1994. Influence of micro tidal environment on self-sedimentation. Gulf of Kutch, India. Continental Shelf Research 14, 1477-1493.

Chowsky, V., Maurya, D.M., Khonde, N., Chamyal, L.S., 2010. Tectonic geomorphology and evidence for active tilting of the Bela, Khadir and Bhanjada islands in the seismically active Kutch palaeorift graben, western India. Zeitschrift fur Geomorphogie 54, 467-490.

Chung, W.-P., and H.Goa, 1995. Source parameters of the Anjar earthquake of July 21, 1956, India and its seismotectonic implications for the Kutch rift basin, Tectonophysics 242,281-292.

Dales, G.F., 1966. The decline of Harappans, Scientific Am. 214, 92-100.

Glennie, K., Glennie, W.& Evans, G.(1976): A reconnaissance of the Great Rann of Kutch, India. – Sedimentology 23:625-647.

Gupta S.K. 1975: Silting of the Rann of Kutch during the Holocene.-Ind. Jour of Earth Sci. 2:163-175.

Juyal 2014. The Great Rann of Kutch: The largest Saline Marshland in India.

Kar A, 2011. Geomorphology of the arid lands of Kutch and its importance in land resource planning .In: Bandyopadhyay S et al (eds) Landform Processes & Environment Management. ACB Publications, Kolkota, pp 388-414.

Lyell, C. 1857. Principles of Geology, Eleventh Ed., Appleton & Co., New York, 834 pp.

Maurya, D.M., Thakkar, M.G., Patidar, A.K., Bhandari, S., Goyal, B., Chamyal, L.S., 2008.Late Quaternary geomorphic evolution of the coastal zone of Kutch, western India. Journal of Coastal Research 24, 746 – 758.

Merh, S.S., 2005.The Great Rann of Kutch: perceptions of a field geologist. Journal of the Geological Society of India65, 9-25.

Norton, I.O. and Sclater, J.G., 1979. A model for the evolution of the Indian Ocean and the breakup of Gondwanaland. J. Geophys. Res., 84(B12): 6803-6830.

Oldham, R.D., 1926. The Cutch (Kachh) earthquake of 16th June 1819 with a revision of the great earthquake of 12th June 1897.Memoir Geological Survey of India 46,71-147.

Oldham, R.D., 1926. The Cutch(Kachh) earthquake of 16th June, 1819 with revision of the great earthquake of 12th June 1897, India Geological survey Memoir 46, 71-147.

Rajendran, C.P., 2000. Using geological methods for earthquakes study: a perspective from perspective from peninsular India, Seismology 2000, Current Science: Special Section, K Rajendran and C.P. Rajendran (Editors), Indian Academy of Science Bangalore, India, 79, 1251-1258.

Rajendran, C.P., K. Rajendran, and B. John, 1998. Surface deformation related to the 1819 Kutch earthquake: evidence for recurrent activity, Current Sci. 75, no. 6, 623-626.

Rajendran, C.P., Rajendran, K., 2001. Characteristics of deformation and past seismicity associated with the 1819 Kutch earthquake, North Western India. Bulletin of Seismological Society of America 91, 407-426.

Rajendran, K., C.P. Rajendran, 1999. Seisomogenesis in the stable continental interior: an appraisal based on two examples from India, Tectonophysics 305, 355 -370.

Reineck, H.E., Singh, I.B., 1980.Depositional Sedimentary Environments .Springer-Verlag, Berlin.

Roy, B., Merh, S.S., 1982. The Great Rann of Kutch: An intriguing Quaternary terrain .Recent Research in Geology 29, 519-539.

Sivewright, R., 1907. Cutch and the Rann. The Geographical Journal 29, 518-535.

Snelgrove, A.K., 1979. Migrations of Indus River, Pakistan, In response to plate tectonic motion, J. Geol. Soc. India 20, 392-403.

Srivastava, P.K., 1971. Recent sediments in rann of Kutch, J. Geol. Soc. India 12, 392-395.

Thakker & Solanki, 2018.

Tuttle, M.P., Hengesh, J., Tucker, K.B., Lettis, W., Deaton, S.L., Frost, J.D. 2002: Observations and comparisons of liquefaction features and related effects induced by the Bhuj Earthquake Spectra 18: 79-100.

Tyagi, A.K., Shukla, A.D., Bhushan, R., Thakker, P.S., Thakkar, M.G. and Juyal, N., 2012. Mid-Holocene sedimentation and landscape evolution in the western Great Rann of Kachchh, India. *Geomorphology*, *151*, pp.89-98.

Wilhelmy, H. 1969. Das Urstromtal am Ostrand der indusebane und das Sarasvati Problem, Z. Geomorphol. (Supplements 6 and 8), 76-93(in German).

Williams, R. L.F., 1958. The black Hill Kutch in History and legend, Weindenfeld and Nicloson, London, 276 pp.

Chapter 4

Methodology

In order to achieve the objective of the thesis, geochemical analysis, and chronology was done on the core sediments. Details of the methods used are given below.

4.1 Core Extraction and Sampling

A core of 1 m was raised from relict mudflat near Lakhpat, Kutch, Gujarat, India (23°49'16'' N, 68°45'39" E). The area is inundated during high wind driven tidal surges during monsoon season and remains dry for the rest of the year (Fig. 4.1). A plastic pipe is having a diameter of 2.8 inches was gently pushed with light hammering into a mudflat. Care was taken that the pipe is kept straight (vertical) and sediments are not disturbed due to hammering. The samples (LKP-1 to LKP-51) were extracted from the core at 2cm interval for high-resolution data and the analysis was performed at Physical Research Laboratory (PRL) Ahmedabad, Gujarat, India.

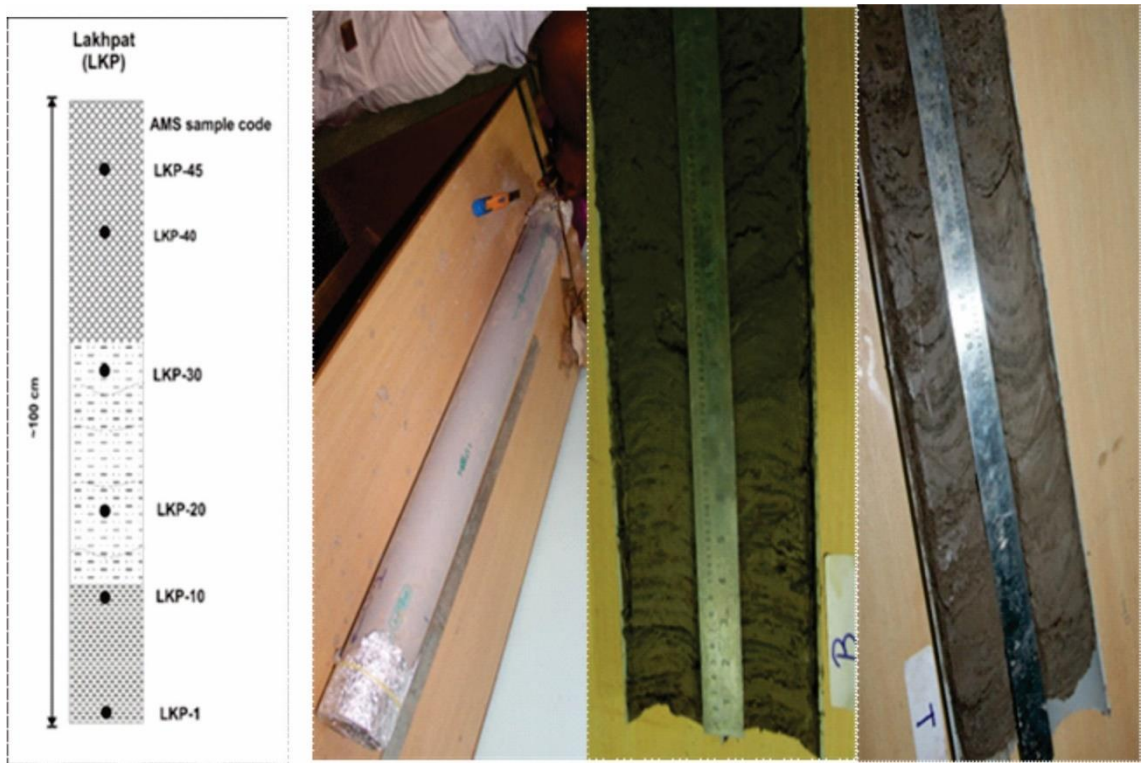

Figure 4.1: The Lithologic sequence of the core.

4.2 Geochemical Analysis

To infer the sea-level changes and climate variation 51 samples extracted from the core were analyzed for major element, trace element, and carbon/nitrogen ratio. Here is the list of the major metal oxides and some trace elements that were analyzed using XRF:

Al_2O_3, CaO, Fe_2O_3, K_2O, MgO, MnO, Na_2O, P_2O_5, SiO_2, TiO_2, Cr, Ni, Rb, Sr, V, and Zr.

Before analyses sample were prepared by the following procedure:

Sample preparation

In the laboratory, to get rid of excess sea salt (various halides of alkali metals), samples were placed in petri dishes and put in the oven for 12hrs at 115 ºC for drying, it will also enforce the salt re-crystallization. After drying the samples were washed with mille-Q water (18.56MΩ cm^{-1} resistivity) to remove the excess of salts followed by drying in the preheated oven at temperature 115 ºC for about 10 hours.

The dried and de-salted samples were ground into fine powder and treated with 0.7N HCl to get rid of in-situ carbonate salts (inorganic carbon present in the samples) followed by ultra-sonification at 80ºC, to break the dolomite bond and hence to neutralize the CO_3^{2-} present. After de-carbonation, samples were washed with mille-Q water to ensure that all of the excess 0.7N HCl was washed away (pH = 7.0). The samples were dried in the oven for about 12 hrs at 80 ºC to remove moisture present in the sample. Finally, this excess salt-free, de-carbonated (pH=7.0) and finely powdered samples were used for making pellets for X-ray fluorescence Spectrometry (XRF) for major and trace element analysis. For preparing the pellet 2.0 grams of de-carbonated powdered was mixed with 0.5 g of LicoWax (binder) and mechanical, hydraulic press machine was used for pellet making by exerting 15 Kilo-Newton pressure for approx. 2 minutes.

The X-ray Fluorescence (XRF) spectrometry (Axios, from Panalytical limited, Fig4.2) for major and trace elements, Flash 2000 CN element analyzer for C_{org}, N_{org} and C/N were used at Physical Research Laboratory (PRL), Ahmedabad, India.

(a) X-ray Fluorescence Spectrometry (XRF)

X-ray Fluorescence Spectrometry (XRF) is an analytical technique used for determining the chemical composition of various materials. XRF analyzers determine the

chemistry of a sample by measuring the fluorescent (or secondary) X-ray emitted from a sample when it is excited by a primary X-ray source. Each of the element produces a set of characteristic fluorescent X-rays ("a fingerprint") that is unique for that specific element, which is why XRF spectroscopy is an excellent technology for qualitative and quantitative analysis of material composition (Brouwer, P., 2006. Theory of XRF. Almelo, Netherlands: PANalytical BV).

These spectrometer systems can be Energy dispersive systems (ED-XRF) or Wave dispersive systems (WD-XRF). The elemental range for ED-XRF goes from sodium to Uranium whereas WD-XRF can detect even the broader range of elements like Beryllium to Uranium. ED-XRF spectrometers have a detector which measures the different energies of the characteristic radiation coming directly from the sample. In order to determine the abundance of elements, WDXRF spectrometers use an analyzing crystal which is kept at a specific angle with the sample. Only those X-rays that satisfy Bragg's law are reflected, and a single wavelength is passed on to the detector (Brouwer, P., 2006. Theory of XRF. Almelo, Netherlands: PANalytical BV).

Bragg's Law

When a beam of X-rays fall on the parallel planes (may be atoms in a crystal), for strong reflection from the surface, there is a specific relationship between the angle of incidence, the wavelength of the X-ray and the distance between the crystal planes, i.e.$sin\theta = \frac{n\lambda}{2d}$. where θ is the angle between the incident or reflected beam and crystal plane, λ is the X- ray wave length, d is the crystal plane separation and n is any integer (H. P. Myers 2002).

In the present study, Axios, Panalytical ltd. WD – XRF system was used to perform the analysis.The WD – XRF has the advantage of having a higher spectral resolution, low concentration detection and can detect elements below atomic number 10.

4.3 Carbon/Nitrogen Ratio

The Carbon to Nitrogen ratio (C/N or C: N ratio) is a proxy for paleoclimate provenance reconstruction. It is necessarily a ratio of the mass of carbon to the mass of nitrogen in sediment. This ratio act as an indicator to differentiate the total organic content

in the sediment based on its derivation from terrestrial source or marine source therefore, the C/N ratio serves as a tool for understanding the sources of sedimentary organic matter

Figure 4.2: XRF Spectrometer at Physical Research Laboratory (PRL), Ahmedabad and Various accessories used for preparing sample pellets.

which can lead to information about the ecology, climate, and ocean circulation at different times in Earth's history (Ishiwatari, R. and Uzaki, M., 1987).The continental plants are cellulose $\{(C_6H_{10}O_5)_n,\}$ rich and therefore have the high carbon content and thus, high C/N ratio (higher than 20) as compared to the marine plants which are characterized by low C/N ratio usually ranges from 4-10 (Gray, K.R., 1973; Stewart, K., 2006).

The Thermo Scientific FLASH 2000 Series Nitrogen and Carbon Analyser has been used to determine the amount of Nitrogen and Carbon in the samples. The FLASH 2000 Series works on the principle of Flash Dynamic Combustion method, where in the high-temperature reactor the sample is burned completely and get converted into the elemental gases, after which these produced gases are estimated accurately and precisely to determine the nitrogen and carbon content in the samples.

Sample preparation

For analyzing samples in the elemental analyser, decarbonated and powdered samples were packed manually in tin foils with the help of a pair of tweezers. These tin

foils are very delicate and can be torn apart while packing, so one has to be very careful while packing because a loosely packed or tore capsule may be lost some sample of it and give wrong data.

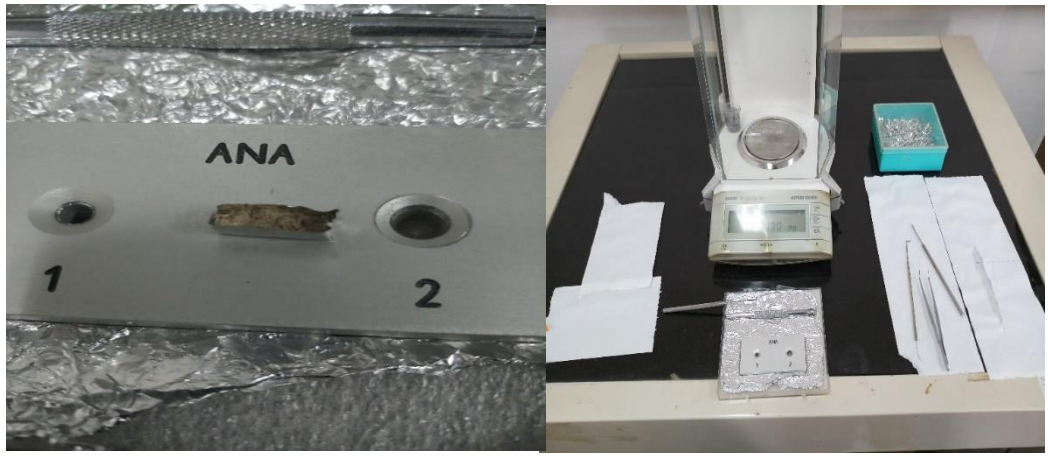

Figure 4.3: Various accessories used during sample packing for C/N analysis.

Functioning of FLASH 2000 Series C-N Analyser

The FLASH 2000 Series C-N Analyser has an oxidation and reduction reactor chamber where the complete conversion of sample into its corresponding gases takes place at very high temperature, a chromatography column is connected to a highly sensitive thermal conductivity detector, which has a wide detection range from 100 ppm to 100% for both Carbon and Nitrogen (Thermo Fisher Scientific 2008).

In the oxidizing chamber which is preheated at 900°C the complete combustion of the sample takes place at 1800°C in the presence of oxygen gas and helium gas, and it gets converted into gaseous form. All carbon present in the sample converted into CO and nitrogen gets converted into possible nitrogen oxides (NO_x). Here oxygen gas is used for combustion and helium gas is used as a carrier and also as reference gas (Thermo Fisher Scientific 2008).

In reducing chamber which is preheated to 600° C, gases (CO and NO_x) are passed, where NO_x gets reduced into N_2 gas in the presence of copper at 680°C, Further these gases are passed through a filter containing magnesium perchlorate which absorbs the moisture and then finally gases are passed through the gas chromatographic column where CO_2 and N_2 gas is separated and analyzed by Thermal conductivity Detector (TCD) (Thermo Fisher Scientific 2008).

Standard Calibration

For analysis of marine core sediment, calibration is done using standards: LOSS and HOSS, a calibration curve is plotted for area vs. concentration. Below in Table 4.1 standard values and accuracy and precision for the instrument is given in Table 4.2 (source: Physical Research Laboratory (PRL), Ahmedabad, Gujarat, India).

Table 4.1 Standard values of Loss and Hoss.

Element amount	Loss	Hoss
Carbon %	1.65	6.72
Nitrogen %	0.14	0.50

The calibration curve is used to determine the concentration of organic carbon and nitrogen.

Detector range for the instrument is as:

- C: 0.001 - 3.6 mgs
- N: 0.001 - 6.0 mgs

Table 4.2: Accuracy and precision for the instrument.

Mode	Accuracy (%)	Precision (%)
CHN	≤0.3	≤0.2
CHNS	≤0.3	≤0.2

4.4 Chronology

Two technique namely C-14 radioactive dating and ^{210}Pb along with ^{137}Caesium have been employed in the present study.

(A) The principle of C-14 Dating

The radiometric dating of C-14 provides objective age estimate for a carbon-based material; originated from any living organism on the planet. C-14 is a weakly radioactive isotope of carbon commonly known as radiocarbon and act as an isotopic chronometer. The

age of any sediment containing C-14 is estimated by measuring the amount of C-14 present in the sample and comparing this against known half-life of C-14 (Lowe and Walker 2014). C-14 or radiocarbon has the nuclear composition of 8 neutron and 6 protons and is an isotope of element carbon (C-12), it is unstable and weakly radioactive with a mean half-life of 5730 yrs. C-12 and C-13 are the naturally occurring stable isotopes of carbon.

The C-14 is produced due to continuous bombardment of cosmic ray neutrons in upper atmosphere knocks out proton from Nitrogen nucleus and in turn, produces C-14 in the lower stratosphere and upper troposphere (Lowe and Walker 2014).
The following nuclear reaction produces C-14

$$n + {}_7N^{14} \rightarrow {}_6C^{14} + p$$

n= neutrons, p= protons

The C-14 is rapidly oxidized in air and gets converted into CO_2. Plants and animals assimilate C-14 from carbon dioxide throughout their entire lifespan hence incorporate into the global carbon cycle on the death of an organism (Fig 4.4). This exchange of carbon with biosphere stops resulting in the decrease in the C-14 concentration at the rate which is determined by the law of radioactive decay (Fig. 4.5). Hence by estimating the amount of C-14 remained in the sample, the age of the organism can be predicted. It must be noted that though that radiocarbon dating results indicate when the organism was alive not when a material; from that organism was used (Lowe and Walker 2014).

The radioactive decay of C-14 follows the following nuclear disintegration reaction;

$$^{14}C_6 \rightarrow {}_7N^{14} + e^- + v_e^-$$

The law of radioactive decay is given by:

$$\frac{-\partial N}{\partial t} = \lambda N$$

Where N = number of atoms.

t = time constant.

λ = decay constant.

By emitting a beta particle (e^-) and an electron antineutrino (v_e^-) one of the neutrons in the C-14 nucleus get converted to a proton and the C-14 nucleus revert back to a stable non-radioactive isotope of N^{14} (Lowe and Walker 2014).

(a) Principal methods of Measuring Radiocarbon

Radiometric dating of C-14 conventionally done by three techniques –

1) Gas proportional counting
2) Liquid scintillation Counting
3) Accelerator mass spectrometry

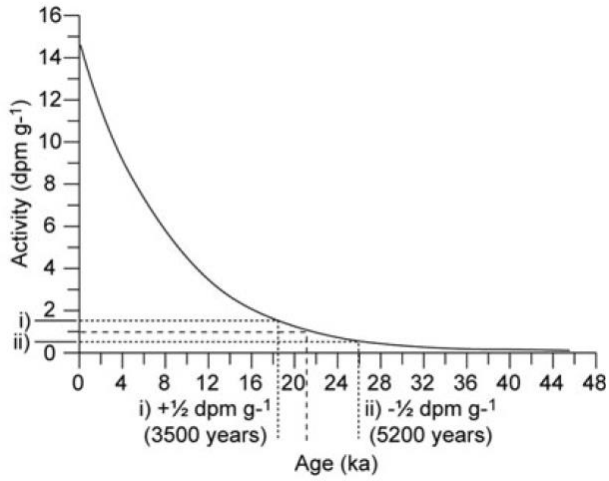

Figure 4.5: Radioactive decay curve (Lowe and Walker 2014).

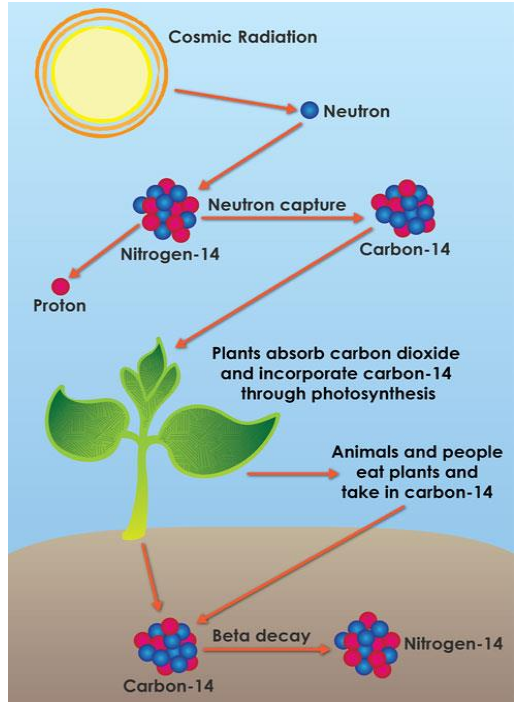

Figure 4.4: Incorporation of C-14 into food chain (science media group)

1) Gas proportional counting method is traditional radiometric dating technique that counts the beta particles emitted by a sample. In this method, first, the carbon in the sample is converted to CO_2, CH_4 or C_2H_4. These gases are further ionized by the radioactive decay, and a charged wire is present in the chamber counts the pulses of current passing through these gases. (Lowe and Walker 2014).

2) Liquid scintillation counting. In this technique, the sample is in liquid form, and a scintillator is added to it (a material that fluorescence when struck by a charged particle or high-energy photon). The added scintillator produces a flash of light when interacts with a beta particle which is detected by the photomultiplier (Lowe and Walker 2014).

3) Accelerator mass spectrometry (AMS) Accelerated Mass Spectrometer (AMS)(Fig. 4.7) is a technique for measuring isotopic ratios, combining mass spectrometry with an accelerator (Lowe and Walker 2014).

In the AMS carbon is converted to a single charged negative ion by bombardment with a Cesium ion beam in the ion source. This process is referred to as "sputtering." It is known that nitrogen does not form negative ions and so they are not produced in the process. In addition to C^- ions produced other negative ions are $^{13}CH^-$ and $^{12}CH_2^-$ which must be removed at different stages in the accelerator. Before acceleration, the ion beams corresponding to masses 12, 13, and 14 are separated, and higher and lower mass impurities are filtered with the help of injection magnet as they travel at different speeds. After this, first stage acceleration is given to the sample beam (1MV) and beam encounters a stripping canal where electrons are stripped out of the carbon ions. It has the effect of changing the potential of ions from negative to positive, which are then further accelerated away from the terminal due to the repulsion of the positively charged ion from the positive terminal voltage. These ions are further accelerated to a higher kinetic energy; order of millions of volts. This accelerated beam now passes through an analyzer magnet (A P McNichol et al. 2001). This separates the ions according to their masses following the principle that Lorentz force acts on the charged particle moving in a magnetic field (Fig. 4.6)

For an ion with charge q and momentum p in a homogeneous magnetic field with strength B oriented normally to the plane of motion, the radius of curvature of the trajectory r is proportional to:

$$r \propto \frac{p}{q.B}$$

As the trajectories of ions with different momentum over charge ratios (p/q) have different radii of curvature, the ions experience different deflections. An electrostatic analyzer is also present to remove the stray particles with the wrong energy and only particles with proper energy pass through it. The final isotope selection process occurs in a gas ionization chamber which gives the final results. The final result, or raw data, for each sample or standard consists of ^{14}C counts and ^{13}C, ^{12}C pulses (A P McNichol et al. 2001).

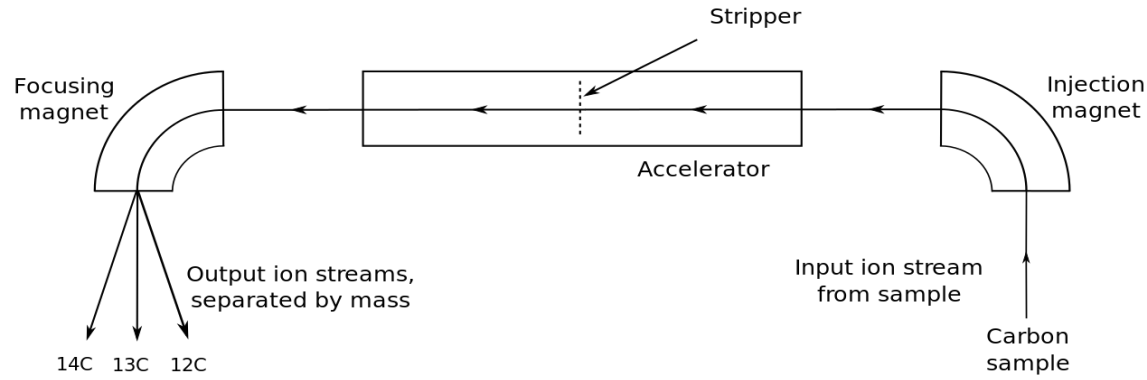

Figure 4.6: Simplified schematic layout of an accelerator mass spectrometer used for counting carbon isotopes for carbon dating. Based on a diagram in M.J. Aitken's Science-based Dating in Archaeology (1990); London: Longman; ISBN 0-582-49309-9; p. 83.

Figure 4.7: Accelerator Mass Spectrometer at, Physical Research Laboratory (PRL), Ahmedabad, India.

(b) Sources of error in radiocarbon dating

1. Temporal variations in C-14 production

A fundamental assumption in radiocarbon dating is that atmospheric C-14 concentrations have not varied significantly over time. Which is not true. Over forty years

ago, scientists working on tree-ring chronologies had found a clear discrepancy between ages of wood obtained by dendrochronological dating and those based on radiocarbon, and they found that the dendrochronological dates are older than the radiocarbon ages (Renfrew, 1973). The various causes of the long term variations in the Δ C-14 yet to be established but most particularly the variations in the strength of earth's geomagnetic field and changes in the intensity of solar activity affects the amount of cosmic rays entering into the earth's atmosphere hence it would lead to the variation in production of C-14 in the above atmosphere (Stuiver et al., 1991, van Geel et al., 2003).

Along with all natural variations the C-14 concentration in the atmosphere is also affected by anthropogenic activities. Over the past 200 years, the C-14 concentrations have been declined due to combustion of fossil fuels, which has released a large amount of inert C-12 into the atmosphere, which is also known as Industrial effect (Solomon et al., 2007).

1. Isotopic Fractionation

Natural samples incorporate ^{12}C, ^{13}C, ^{14}C into their systems with time while exchanging carbon with the atmosphere. However, the natural samples including plants and animals have a tendency of preferential incorporation of one isotope of carbon over the other. Due to this, the concentration of one isotope increases and other decreases. Specifically, plants incorporate more ^{12}C than ^{13}C than ^{14}C. As a result, abundances in the samples vary. This variation causes systematic errors in the radioactivity and age determination calculations (Lowe and Walker 2014).

To eliminate these errors, a $\delta^{13}C$ parameter was introduced which reflects the relative change in isotopic $^{13}C/^{12}C$ ratio introduced due to isotopic fractionation:

$$\delta^{13}C_{‰} = \frac{(^{13}C/^{12}C)_{sample.} - (^{13}C/^{12}C)_{std}}{(^{13}C/^{12}C)_{std}} \times 1000$$

The standard that is most widely used is carbon dioxide prepared from belemnites (Belemnitella americana) collected from the Peedee Formation (Cretaceous) of South Carolina is known as the PDB or referred as Vienna PDB or VPDB. Most of terrestrial samples have a negative δC-13 value compared to PDB standards. The normal value is taken to be -25 per mil (the mean isotopic composition of wood) (Lowe and Walker 2014).

2. Circulation of Marine carbon

The transport of C-14 from the atmosphere to ocean water is mostly limited to ocean surfaces because of the very slow mixing rate of surface and deep water. Hence the C-14 in deep water decays without being replenished. Therefore seawater has an apparent age also known as reservoir age (Kuzmin et al., 2001).

3. Contamination

In the organic sediments, the younger carbon or older carbon could be incorporated. The younger carbon can be added due to the root penetration through the profile or by the infiltration by younger humic acids through the soil horizons or sometimes may be due to bioturbation. This addition of younger carbon can give relatively younger age than the expected, if not account for correction (Lowe and Walker 2014).

Similarly, contamination by older carbon leads to the dilution of the C-14/C-12 ratio in the sample and hence the sediment could be wrongly dated to much older age (Lowe and Walker 2014).

C-14 dating measurements

A radiocarbon measurement is termed as a conventional radiocarbon age (CRA).

CRA convention includes –

- Usage of Libby half-life.
- Usage of oxalic acid or any appropriate secondary radiocarbon standard.
- Correction for sample isotopic fractionation to a normalized or base value of -25.0 per mille relative to the ratio of C-12/C-13 in the carbonated standard VPDB-Cretaceous belemnite formation at Peedee in South Carolina.
- Zero BP(Before Present) is defined as AD 1950, and
- The assumption that global radiocarbon levels are not considered. i.e., it remains constant.

Along with the date, estimated standard errors are also reported in radiocarbon dating result, hence" ±" values (Stuiver and Polach 1977).

Reporting Date

Till 2014 scientists use various format for reporting radiocarbon date, but as of 2014 the standard format required by journal RADIOCARBON is as follows.

The uncalibrated date should be reported as :{ C-14 yrs — ± standard deviation} BP.

- "C-14 yrs." is the lab's determination of the age of the sample, in radioactive years.
- "Standard Deviation" is the lab's estimate of the error in the age, at 1σ confidence interval.
- "BP" is before present, referring to a reference date of 1950, like 500 BP means the year 1450 AD (Stuiver and Polach 1977).

Sample preparation

For AMS C-14 dating two samples LKP-45 and LKP- 1were employed to three cycles of decarbonation using 0.7 N HCl with ultrasonic heating at 80°C, this is because the area is dominated by Eocene limestone and dolomite. Dolomite has a stronger bond, which does not break easily. Hence heating is required. Also, AMS samples were not taken from the extreme top layer to avoid anthropogenic contamination.

(B) The principle of ^{210}Pb dating

^{210}Pb is a natural radioactive form of lead found in small quantities in most soils as a part of the uranium decay series. In the recently deposited materials, it is also produced as natural fallout from the atmosphere by radioactive decay of ^{222}Rn (radon) gas. This ^{210}Pb in ocean or lake bounded by other organics and gets deposited into the sediments (Fig.4.8). This type of ^{210}Pb is known as unsupported ^{210}Pb. The sediments also contain supported ^{210}Pb. It is the unsupported fraction of ^{210}Pb, so-called ^{210}Pb excess which decays exponentially with depth. In a state of radioactive secular equilibrium, ^{210}Pb is derived from ^{226}Ra and is called supported ^{210}Pb (Hewitt W. Jeter 2000).

Detection of ^{210}Pb activity using gamma counter

Most of the radioactive sources produce gamma rays of various energies and intensities, and these emissions are measured by a Gamma counter. Gamma counter counts the activity of a gamma emitting sample, in this study Gamma counter is used for ^{210}Pb dating was made up of high purity Germanium (HPGe) crystals which are mounted in a vacuum chamber to protect from moisture and other condensable contaminants and cooled by liquid nitrogen. The HPGe detector converts gamma rays into electrical impulses which are used for determining their energies and intensities. The efficiency of this instrument ranges from 5–10 %. The activity of all three isotopes ^{226}Ra, ^{210}Pb, and ^{137}Cs are measured in HPGe

gamma detector. The detector gives the counts concerning the channels at a particular energy. The ^{210}Pb activity was detected at energy 46 keV (Zaborska et al. 2007). The gamma-spectrometric method provides a concurrent determination of ^{226}Ra, which allows the activities of supported ^{210}Pb to be estimated (Swarzenski, P.W., 2013).

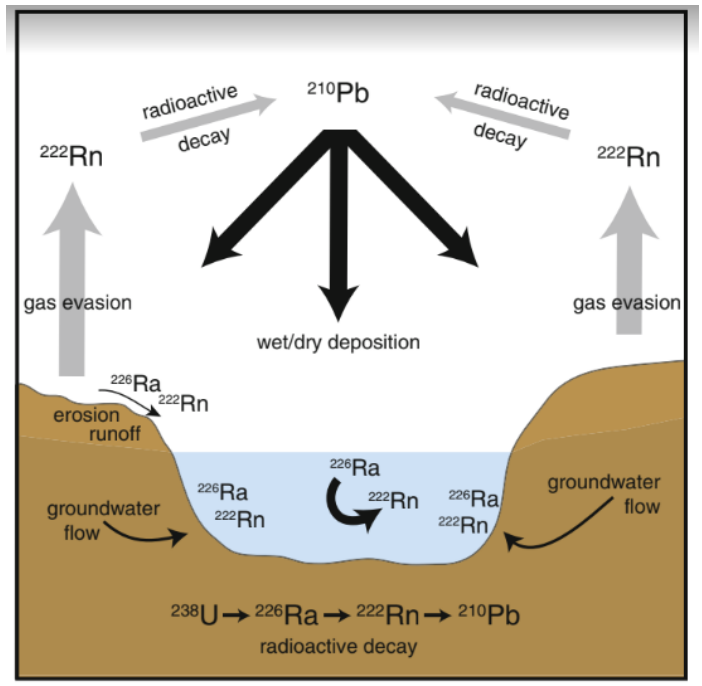

Figure 4.8: Conceptual illustration of the dominant sources and transport pathways for Pb-210 (Peter W. Swarzenski 2013).

^{226}Ra activity is determined by quantifying intermediate daughter radionuclides ^{214}Pb (at 295 and 352 keV) and ^{214}Bi (at 609 keV) after establishing their radioactive equilibrium with ^{222}Rn (Kirchner and Ehlers 1998; Swarzenski et al. 2006). Importantly, the gamma-spectrometric method also provides for the determination of ^{137}Cs ($t_{1/2}$ = 30.17 year; 661 keV), an independent, nuclear bomb-produced geochronometer (Swarzenski, P.W., 2013).

Sedimentation rate and age estimation

From the data, the activity of total ^{210}Pb and ^{226}Ra (= supported ^{210}Pb) can be obtained. After that, the ^{210}Pb excess is calculated using the equation (Hewitt W. Jeter 2000).

$^{210}Pb_{excess} = {}^{210}Pb_{total} - {}^{226}Ra$

Using the radioactive decay equation, age of sediment is estimated by the following relation.

$N = N_0 e^{-\lambda t}$

$\text{Log } N = \log N_0 - \lambda t$

While sedimentation rate is calculated as, $S = x/t$

$\text{Log } N = \log N_0 - \lambda (x/S)$

Where,

x = depth

S = sedimentation rate

λ= decay constant of ^{210}Pb

$$\text{Log } (^{210}Pb_{excess}) = \text{Log } (^{210}Pb_{total}) - \lambda(x/S)$$

The above relation is nothing but the equation of a straight line, i.e., y = mx + c. We plot the log of $^{210}Pb_{excess}$ versus Depth which provides the slope (m). From the above equation slope **= λ/ S.**

Therefore, sedimentation rate (S) = λ / slope and Age (t = X/S). Using the sedimentation rate, the age for the respective depth of the sediment core can be assigned. The slope of the line and the decay constant of ^{210}Pb (0.0311 yr^{-1}) is used to calculate the sedimentation rate.

In this technique of ^{210}Pb, the average accumulation rate over a period of 100—120 years can be obtained, because the half-life of ^{210}Pb is 22.3 years. So we can go up to the maximum five to six half-lives of the originally present ^{210}Pb activity, and after that, the activity would be almost negligible or undecipherable which cannot be measurable due to the overlap of the background signal.

^{137}Cesium dating

In the late 1950s and early 1960s, the concentration of neutrons along with ^{137}Cs was hugely increased in the atmosphere due to above ground nuclear tests. The ^{137}Cs concentration peak was found to be during 1963 in the atmosphere. This ^{137}Cs got deposited along with sediments and showed a peak in the representative year of the chronologically deposited sediments in 1963. The activity of ^{137}Cs is measured by a gamma counter and can be

interpreted to assign the calendar date of sediments, and this is why ^{137}Cs isotope age is supplemented with ^{210}Pb dating (Hewitt W. Jeter 2000).

Sample preparation

For Pb-210 and Cs-137 dating seven decarbonated samples viz. LKP-49, LKP-46, LKP-44, LKP-41, LKP-39, LKP-36 and LKP 31 were packed. For this approximately 3grams of sample were weighted using weighing machine, and the sample was tightly packed in 10 ml tube, and sample was enthrusted inside using rippit and cap was sealed by fevibond, so no radon gas can escape from the tube itself and no external gas can also enter in the tube, further the tubes were left for 15 days to attain the equilibrium of Ur-238 and radon gas.

References

Ishiwatari, R. and Uzaki, M., 1987. Diagenetic changes of lignin compounds in a more than 0.6 million-year-old lacustrine sediment (Lake Biwa, Japan). *Geochimica et Cosmochimica Acta*, *51*(2), pp.321-328.

Brouwer, P., 2006. Theory of XRF. Almelo, Netherlands: PANalytical BV.

Lowe, J.J. and Walker, M.J., 2014. *Reconstructing quaternary environments*. Routledge.

Gray, K.R., 1973. Composting-Process Paramaters. *The Chemical Engineer*, pp.71-76.

Stewart, K., 2006. It'sa Long Road to a Tomato: Tales of an Organic Farmer Who Quit the Big City for the (Not So) Simple Life.

McNichol, A.P., Jull, A.J.T. and Burr, G.S., 2001. Converting AMS data to radiocarbon values: considerations and conventions. *Radiocarbon*, *43*(2A), pp.313-320.

Renfrew, C. 1973. *Before Civilisation: The Radiocarbon Revolution and Prehistoric Europe*. Jonathan Cape, London.

Stuiver, M., Braziunas, T.F., Becker, B. and Kromer, B., 1991. Climatic, solar, oceanic, and geomagnetic influences on late-glacial and Holocene atmospheric 14 C/12 C change. *Quaternary research*, *35*(1), pp.1-24.

H. P. Myers (2002). Introductory Solid State Physics. Taylor & Francis. ISBN 0-7484-0660-3.

van Geel, B., van der Plicht, J. and Renssen, H., 2003. Major Δ14C excursions during the late glacial and early Holocene: changes in ocean ventilation or solar forcing of climate change?. *Quaternary International*, *105*(1), pp.71-76.

Solomon, S., Qin, D., Manning, M., Averyt, K. and Marquis, M. eds., 2007. *Climate change 2007-the physical science basis: Working group I contribution to the fourth assessment report of the IPCC* (Vol. 4). Cambridge university press.

Dutta, K., Bhushan, R. and Somayajulu, B., 2001. ΔR correction values for the northern Indian Ocean. *Radiocarbon*, *43*(2A), pp.483-488.

Bard, E., Arnold, M. and Duplessy, J.C., 1991. Reconciling the sea level record of the last deglaciation with the δ 18 O spectra from deep sea cores. In *Quaternary Proceedings* (pp. 67-73).

Kuzmin, Y.V., Burr, G.S. and Jull, A.T., 2001. Radiocarbon reservoir correction ages in the Peter the Great Gulf, Sea of Japan, and eastern coast of the Kunashir, southern Kuriles (northwestern Pacific). *Radiocarbon*, *43*(2A), pp.477-481.

Christie, M., 2018. Radiocarbon dating. *WikiJournal of Science*, *1*(1), p.1.

Stuiver, M. and Polach, H.A., 1977. Discussion reporting of 14 C data. *Radiocarbon*, *19*(3), pp.355-363.

Jeter, H.W., 2000. Determining the ages of recent sediments using measurements of trace radioactivity. *Terra et Aqua*, *78*, pp.21-28.

Zaborska, A., Carroll, J., Papucci, C. and Pempkowiak, J., 2007. Intercomparison of alpha and gamma spectrometry techniques used in 210Pb geochronology. *Journal of environmental radioactivity*, *93*(1), pp.38-50.

Swarzenski, P.W., 2013. 210 Pb Dating. *Encyclopedia of Scientific Dating Methods*, pp.1-11.

Kirchner, G. and Ehlers, H., 1998. Sediment geochronology in changing coastal environments: potentials and limitations of the 137Cs and 210Pb methods. *Journal of Coastal Research*, pp.483-492.

Swarzenski, P.W., Baskaran, M., Rosenbauer, R.J. and Orem, W.H., 2006. Historical trace element distribution in sediments from the Mississippi River delta. *Estuaries and Coasts*, *29*(6), pp.1094-1107.

Chapter 5
Results

5.1 Geochemical analysis of tidal flat sediments

Major and selected trace element concentrations of 51 samples of the mudflat sediments are provided in Table 5.1. In the analyzed samples, concentrations of major elements vary narrowly. The mudflat sediments are consist of 51.69 to 65.21 wt.% SiO_2; 14.14 to 17.55 wt.% Al_2O_3; 0.08 to 0.95 wt.% TiO_2; 6.23 to 8.56 wt.% Fe_2O_3; 0.06 to 0.1 wt.% MnO; 1.02 to 2.76 wt.% CaO; 2.27 to 4.31 wt.% MgO; 0.00 to 14.36 wt.% Na_2O; 2.25 to 3.27 wt.% K_2O and 0.05 to 0.17 wt.% P_2O_5. Among the analyzed trace elements, Cr varies from 26.0 to 94.0 ppm; Ni, from 57 to 112 ppm; Rb from 151 to 257 ppm; Sr from 148 to 345 ppm; V from 37 to 158 ppm; and Zr from 63 to 150 ppm and statistical data is given in Table 5.4.

To check for the constant sum problem and dilution effect (Rollinson, 1992), the correlation coefficient is calculated after normalizing the concentrations with aluminum concentration (Table 5.3). Numerous studies suggest that if the interpretations rely on the absolute percentage values, it may not be correct. For example, both negative and positive correlation (calculated using an absolute percentage of any two elements) between any two elements might not be true as other than the geological processes, the affinity or repulsion between the two elements is also governed by their inherent nature. On the other hand, the correlation values between the ratios of two elements normalized by a common element (here, aluminum is used) more effectively tell only about the change in the provenance or mode of transport, i.e., of geological processes.

Table 5.1: Major (wt. %) and trace element (ppm) composition of Lakhpat mudflat sediments.

Sample ID	Depth	Al_2O_3	CaO	Fe_2O_3	K_2O	MgO	MnO	Na_2O	P_2O_5	SiO_2	TiO_2	Cr	Ni	Rb	Sr	V	Zr
	cm	%	%	%	%	%	%	%	%	%	%	ppm	ppm	ppm	ppm	ppm	ppm
LKP-51	0	16.32	1.62	8.56	2.97	3.84	0.1	0.2	0.1	58.67	0.62	56	101	238	260	109	109
LKP-50	2	15.94	1.62	7.27	2.79	3.92	0.08	0.36	0.1	59.46	0.74	74	93	234	291	127	95
LKP-49	4	16.86	1.23	7.32	2.92	2.81	0.06	0.19	0.08	61.76	0.59	69	89	239	257	108	100
LKP-48	6	16.74	1.39	7.74	3.05	2.87	0.06	0.15	0.08	60.78	0.57	58	98	227	259	101	118
LKP-47	8	15.68	2.43	7.14	2.75	4.11	0.08	0.14	0.07	56.77	0.85	90	80	202	260	145	150
LKP-46	10	16.97	1.11	7.84	3.19	2.76	0.06	0.08	0.05	61.45	0.49	65	81	170	155	92	136
LKP-45	12	15.79	1.83	7.56	2.8	3.47	0.07	0.05	0.09	56.18	0.77	77	88	195	288	132	124
LKP-44	14	16.05	1.74	7.5	2.83	3.99	0.08	0.15	0.09	57.17	0.75	69	98	225	338	127	114
LKP-43	16	14.14	2.15	7.13	2.28	3.08	0.07	14.36	0.1	51.69	0.95	91	91	236	324	156	115
LKP-42	18	17.32	1.18	8.52	3.27	3.19	0.07	0.07	0.09	60.83	0.49	48	112	256	253	90	111
LKP-41	20	15.59	2.76	7.04	2.56	4.31	0.08	0	0.1	54.84	0.95	94	94	223	307	158	123
LKP-40	22	15.98	2.21	7.33	2.68	3.65	0.07	0	0.1	56.85	0.82	89	73	224	311	142	117
LKP-39	24	15.58	2.6	6.96	2.77	3.92	0.09	0.31	0.09	57.29	0.87	92	73	160	199	148	140
LKP-38	26	16.06	1.82	7.52	2.82	3.85	0.08	0.02	0.09	57.62	0.71	68	100	228	222	124	126
LKP-37	28	16.11	2.24	7.48	2.87	3.85	0.08	0.06	0.08	57.37	0.76	74	100	209	316	132	120
LKP-36	30	15.96	2.38	7.54	2.85	4.3	0.1	0.32	0.09	57.45	0.74	73	100	217	344	126	113
LKP-35	32	16.38	1.15	7.36	2.87	2.64	0.06	0.01	0.06	59.39	0.59	65	86	249	265	107	107
LKP-34	34	16.94	1.04	7.55	3.06	2.66	0.06	0.32	0.05	62.94	0.48	64	89	257	262	89	96
LKP-33	36	16.14	1.47	7.45	2.79	2.9	0.07	0.33	0.1	60.56	0.59	74	73	179	195	106	125

LKP-32	38	16.76	1.09	7.21	2.8	2.6	0.06	0.29	0.06	62.87	0.45	66	76	243	257	86	88
LKP-31	40	15.42	2.75	6.47	2.45	3.25	0.09	0.92	0.12	60.13	0.74	88	83	223	345	131	95
LKP-30	42	15.76	2.35	6.78	2.54	3.19	0.09	0.47	0.13	60.59	0.68	78	88	222	299	118	95
LKP-29	44	16.27	1.14	6.91	2.68	2.4	0.06	0.73	0.06	64.85	0.45	67	86	242	274	89	83
LKP-28	46	15.79	1.62	6.99	2.47	2.71	0.07	0.29	0.14	61.84	0.52	74	78	151	215	99	105
LKP-27	48	16.19	1.24	6.92	2.58	2.44	0.06	0.39	0.07	62.98	0.53	69	82	175	164	98	130
LKP-26	50	15.29	2.22	6.61	2.3	2.89	0.08	0.46	0.14	60.04	0.7	81	80	217	272	125	95
LKP-25	52	15.9	1.3	6.93	2.55	2.46	0.06	0.71	0.11	64.23	0.52	71	70	216	267	99	80
LKP-24	54	15.12	1.91	6.44	2.25	2.62	0.07	0.41	0.17	60.89	0.65	74	78	227	305	117	63
LKP-23	56	15.55	2.3	6.54	2.38	2.92	0.07	0.62	0.15	61.73	0.66	79	57	226	301	116	80
LKP-22	58	15.65	1.61	6.62	2.43	2.59	0.07	0.63	0.11	62.11	0.62	61	88	233	290	110	76
LKP-21	60	15.29	2.3	6.28	2.39	2.76	0.07	0.8	0.11	60.85	0.78	86	73	227	317	133	85
LKP-20	62	15.89	1.53	6.74	2.47	2.87	0.07	0.52	0.15	62.51	0.62	70	91	229	283	109	79
LKP-19	64	16	1.69	6.64	2.5	2.79	0.07	1.06	0.09	62.33	0.68	76	74	234	294	123	87
LKP-18	66	15.98	1.38	7.23	2.66	2.72	0.07	0.58	0.13	62.33	0.6	69	97	190	224	108	101
LKP-17	68	15.17	2.29	6.59	2.36	3.22	0.08	0.37	0.12	59.03	0.88	80	89	226	288	144	104
LKP-16	70	16.05	1.19	6.83	2.68	2.55	0.06	0.71	0.07	63.75	0.68	73	89	242	279	117	92
LKP-15	72	15.96	1.31	6.89	2.61	2.69	0.07	0.85	0.11	62.15	0.72	67	92	232	267	123	98
LKP-14	74	15.08	1.62	6.5	2.31	2.67	0.07	2.37	0.15	60.57	0.8	76	87	235	290	138	88
LKP-13	76	15.35	1.79	6.24	2.35	2.65	0.07	0.79	0.16	62.5	0.86	92	83	228	297	146	91
LKP-12	78	15.56	2.44	6.23	2.44	2.79	0.07	0.69	0.11	61.77	0.83	88	77	199	211	141	122

LKP-11	80	16.09	1.37	6.76	2.56	2.73	0.07	0.59	0.16	63.59	0.59	55	88	236	285	108	72
LKP-10	82	14.49	2.03	6.3	2.37	2.27	0.07	0.33	0.08	58.78	0.82	79	80	232	295	141	87
LKP-09	84	16.41	1.73	7.28	2.82	3.53	0.09	0.5	0.12	61.15	0.68	62	95	244	286	121	94
LKP-08	86	17.08	1.6	7.94	3.17	3.34	0.08	0.54	0.08	61.17	0.59	56	102	256	276	105	101
LKP-07	88	17.03	1.04	7.73	3.14	2.85	0.07	0.27	0.07	62.56	0.52	51	104	224	211	93	106
LKP-06	90	16.56	1.17	8.06	2.85	2.69	0.06	0.3	0.09	59.24	0.44	59	59	164	148	89	144
LKP-05	92	17.1	1.11	8.42	2.89	3	0.07	0	0.1	58.99	0.38	43	101	251	252	78	107
LKP-04	94	17.55	2.63	7.58	3.14	3.86	0.1	0.71	0.1	62.52	0.66	63	95	236	304	116	109
LKP-03	96	17.01	1.14	7.47	2.66	2.69	0.06	0.74	0.11	65.21	0.4	55	81	226	259	82	91
LKP-02	98	16.39	1.93	7.88	2.45	2.93	0.09	0.28	0.12	59.34	0.36	39	98	220	270	75	99
LKP-01	100	16.5	1.02	8.26	2.5	2.36	0.07	0.08	0.08	61.52	0.08	26	85	226	259	37	90

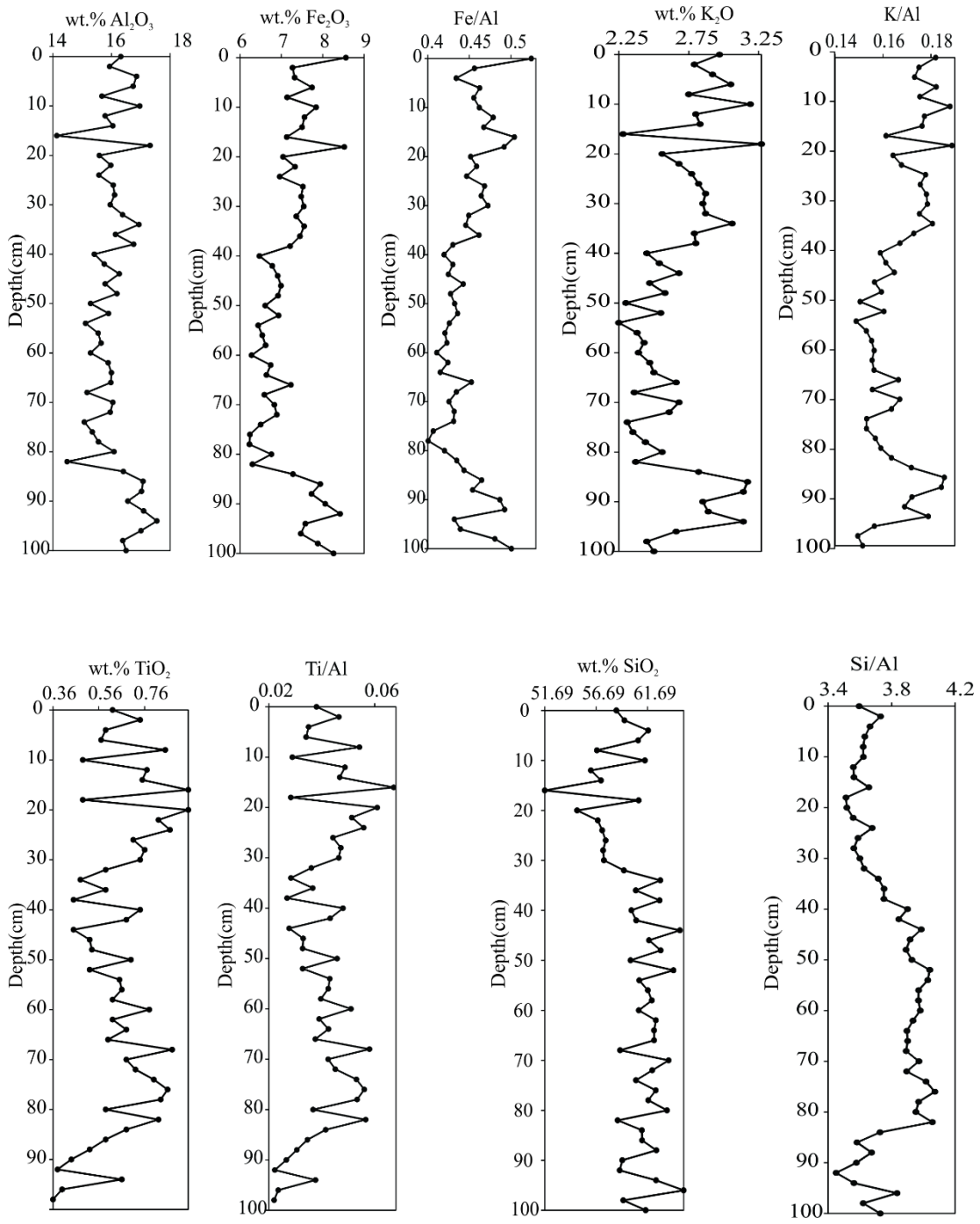

Figure 5.1: Depth wise variation in concentration of major elements oxides (wt. %).

The following proxies are used to infer sea level fluctuations and climate variability.

1. *Silica/Aluminium (Si/Al)*

The ratio of detrital Si/Al provides an estimation of the sediment textural maturity because of the relative enrichment of Al-rich phyllosilicates at the expense of Si-rich phases in fine-grained sediments (Weltje and Eynatten, 2004). As the grain size or the textural maturity decreases, it is reflected in the decreased Si/Al ratio (McLennan et al., 1993; Lo´pez-Gonza´lez et al., 2006).

2. *Aluminum (Al), Iron (Fe) and Potassium (K)*

Changes in concentration of aluminum (Al), potassium (K) and iron (Fe) are used as proxies for detrital contribution (Sarin et al., 1979; Banerjee et al., 2015). In the study area, in absence of any major streams (continental flux) draining into/near the coring site the changes in the Al and Fe concentrations inferred as a proxy for higher inter-tidal sedimentation during high sea-level which is deposited as a suspended fallout from the tidal current (Banerjee et al., 2015).

3. *Iron/Manganese (Fe/Mn)*

The ratio of the redox-sensitive elements Fe and Mn is used to ascertain the dominant zones of oxidation/reduction and hence lower/higher sea level. However, compared to Fe, Mn is more readily mobilized due to its greater solubility. Therefore, the pattern of Fe/Mn ratio is interpreted as a proxy to identify higher sea level/wetter conditions (Bhushan et al., 2018).

4. *Titanium/Aluminium ratio (Ti/Al)*

Both Al and Ti are robust to diagenetic processes and considered well-conserved elements (Spears and Kanaris-Sotiriou, 1976; Chen et al., 2012). In suspended fluvial silts Ti is suggested to be independent of grain size than Al that shows closer affinity with clays (Lisitzin, 1996). Thus, Ti/Al is often used to infer the dynamic conditions where the higher ratio is suggested for more dynamic hydrological conditions and can be used to infer changes in the grain size similar to Si/Al ratio (Lisitzin, 1996).

4. *E/P ratio (Ca/ Al + Fe + Ti)*

The higher deposition of Calcium (Ca) is suggestive of greater evaporation during arid conditions as also indicated by E/P (Ca/Al+Fe+Ti) ratio (Banerjee et al., 2015).

6. *Rubidium/Strontium* (*Rb/Sr) and Chemical index of alteration (CIA)*

CIA was defined by Nesbitt and Young (1982) using the molecular proportions:

$$CIA = [Al_2O_3/(Al_2O_3 + CaO + NaO + K_2O)]*100$$

Where CaO is measured in the silicate fraction of the rock.

CIA measures the ratio of non-labile to labile elements and is used to infer the in situ weathering of feldspar/clay minerals and thus, inferring the climate changes. Under warmer/wetter conditions the ratio tends toward higher values as more labile elements exit the system and vice versa (Roman- Ross et al. 2002; Das and Haake 2003; Roy et al. 2010). The Rb/Sr ratio generally mimics the pattern of CIA with Sr being more mobile under warmer/wetter conditions as the rate of chemical weathering increases (Chen et al., 1999; Bhushan et al., 2018).

5. Carbon / Nitrogen Ratio

The Corg and C/N ratio in tidal flat/estuarine sediment are governed by the autochthonous (indigenous plants) and allochthonous contribution from a river catchment (Sampei et al., 1997; Allen et al., 2007). Higher C/N ratios in tidal flat environment suggest an increased proportion of river-imported detritus and lower C/N suggest proportionately more algae and less organic material from fluvial/terrestrial sources (Allen et al., 2007). Also, the plants, in general, have higher C/N ratios than animals due to their low protein and high cellulose content. Therefore, the autochthonous component contributed by aquatic organisms, algae and phytoplankton have a C/N ratio ranging from 4 to 10. The allochthonous constituent mostly coming from terrestrial plants is more refractory due to their high lignin and cellulose content and has a C/N ratio of >12 (Nazneen and Raju, 2017).

In the present study, 50 samples at the regular interval of 2cm were analyzed to infer the dominant source of carbon and nitrogen in the sediments (Table 5.5). Five samples were repeated to check precession, which is given in Table 5.2 as std. error.

Table 5.2: Statistical values for Total organic carbon (TOC), Total nitrogen (TN) and C/N.

	Mean	Std. error	Stand. dev	Min	Max
TN	0.04	0.0017	0.01	0.02	0.75
TOC	0.37	0.03	0.23	0.12	1.00
C/N	10.75	1.26	9.01	2.64	35.20

Table 5.3: Values of Pearson's coefficient of correlation of Normalised major and trace elements ratios of Lakhpat mudflats.

	Al_2O_3	K-Al	Fe-Al	Fe/Mn	C/N	CIA	Rb/Sr	TOC	Si-Al	Zr- Al	Ti-Al	E/P	Ca/Al
Al_2O_3	1												
K-Al	0.60	1											
Fe-Al	0.25	0.58	1										
Fe/Mn	0.51	0.31	0.22	1									
C/N	-0.30	-0.21	-0.33	-0.72	1								
CIA	0.14	0.23	0.27	0.08	0.12	1							
Rb/Sr	0.58	0.37	0.19	0.65	-0.38	0.12	1						
TOC	-0.10	0.10	-0.05	-0.68	0.92	0.24	-0.33	1					
Si-Al	-0.53	-0.74	-0.78	-0.19	0.21	-0.25	-0.19	-0.11	1				
Zr- Al	-0.06	0.42	0.46	0.01	0.04	0.24	0.11	0.22	-0.55	1			
Ti-Al	-0.80	-0.22	-0.16	-0.62	0.37	-0.15	-0.60	0.31	0.17	0.32	1		
E/P	-0.63	-0.32	-0.21	-0.82	0.74	-0.01	-0.70	0.69	0.10	0.25	0.77	1	
Ca/Al	-0.63	-0.29	-0.16	-0.81	0.72	0.01	-0.70	0.68	0.06	0.29	0.78	1.00	1

Table 5.4: Statistical data of major (wt.%) and trace elements(ppm) along with selected major elements ratio.

	Al_2O_3	CaO	Fe_2O_3	K_2O	MgO	MnO	Na_2O	P_2O_5	SiO_2	TiO_2	Cr	Ni	Rb
Mean	16.05	1.72	7.20	2.68	3.06	0.07	0.71	0.10	60.45	0.64	69.86	86.76	221.57
Std.error	0.10	0.07	0.08	0.04	0.08	0.00	0.28	0.00	0.37	0.02	2.00	1.58	3.48
Std. dev	0.70	0.52	0.60	0.27	0.55	0.01	1.99	0.03	2.65	0.17	14.29	11.30	24.89
Min	14.14	1.02	6.23	2.25	2.27	0.06	0.00	0.05	51.69	0.08	26.00	57.00	151.00
Max	17.55	2.76	8.56	3.27	4.31	0.10	14.36	0.17	65.21	0.95	94.00	112.00	257.00

	Sr	V	Zr	Zr- Al	Mg-Al	Si-Al	Ti-Al	CIA	Rb/Sr	K-Al	Fe-Al	Fe/Mn	E/P
Mean	268.43	114.39	103.45	0.00	0.19	3.77	0.04	82.67	0.84	0.17	0.45	100.47	0.07
Std.error	6.28	3.31	2.67	0.00	0.00	0.03	0.00	0.36	0.02	0.00	0.00	2.31	0.00
Std. dev	44.88	23.66	19.06	0.00	0.04	0.18	0.01	2.53	0.12	0.01	0.03	16.47	0.02
Min	148.00	37.00	63.00	0.00	0.14	3.45	0.02	76.33	0.63	0.15	0.40	71.89	0.04
Max	345.00	158.00	150.00	0.00	0.28	4.07	0.07	87.54	1.11	0.19	0.52	134.33	0.12

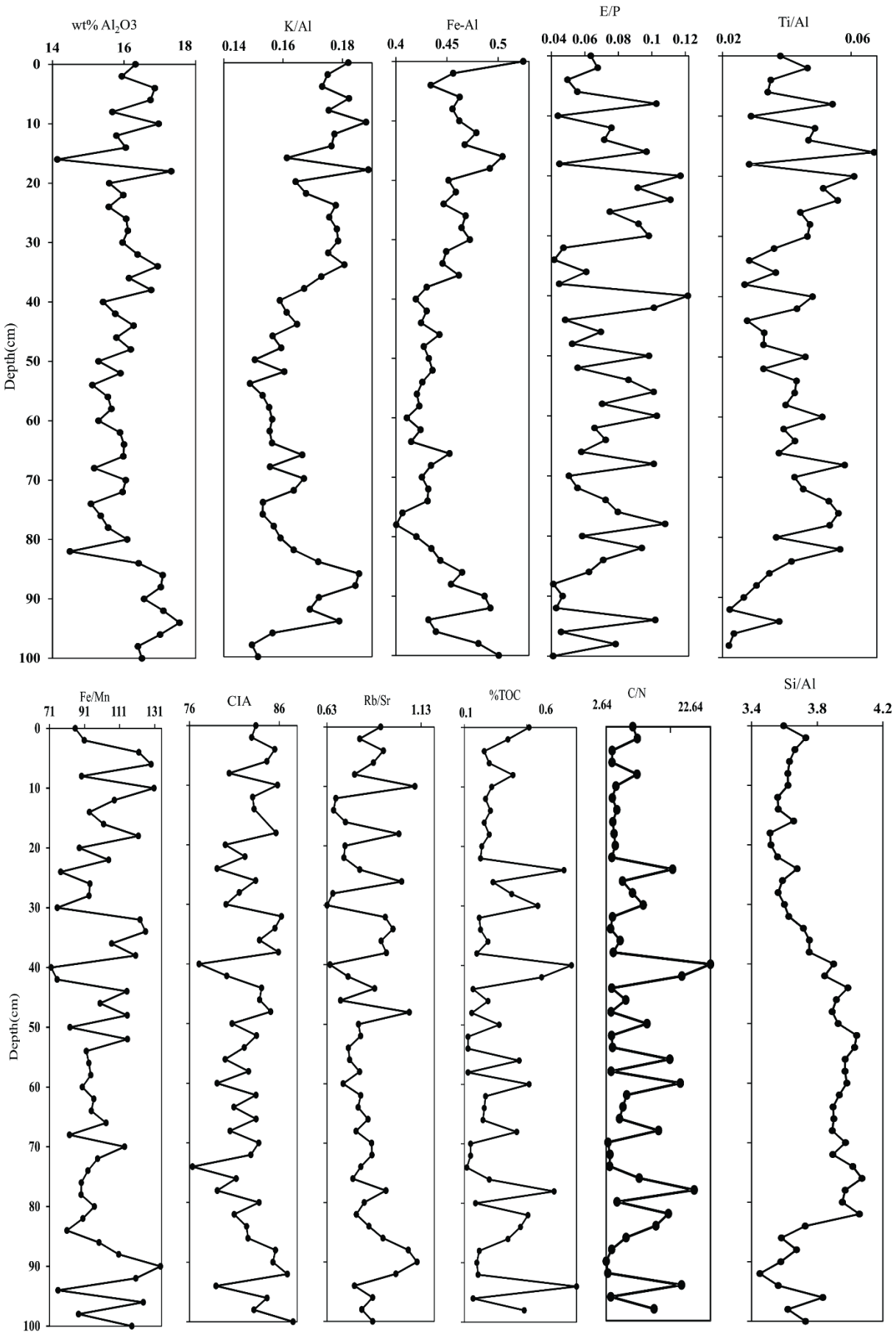

Figure 5.2: Depth wise variation in the normalized ratio.

Table 5.5: Total carbon and nitrogen percentage in Lakhpat mudflat sediments at an interval of 2cm from bottom to the top of the core. Five samples are repeated at regular interval to check precession (e.g., LKP 10R).

Sample ID	%N	%C	C/N	Sample ID	%N	%C	C/N
LKP2	0.033	0.58	17.58	LKP 28	0.033	0.29	8.71
LKP 3	0.041	0.17	4.05	LKP 29	0.04	0.17	4.33
LKP 4	0.038	1	26.19	LKP 30	0.027	0.72	26.25
LKP 5	0.069	0.21	3.13	LKP 30 R	0.031	0.72	23.06
LKP 6	0.075	0.2	2.64	LKP 31	0.027	0.96	35.2
LKP 7	0.05	0.22	4.35	LKP 32	0.041	0.2	4.83
LKP 8	0.051	0.45	8.84	LKP 33	0.041	0.29	6.96
LKP 9	0.03	0.55	18.18	LKP 34	0.059	0.23	3.99
LKP 10	0.028	0.61	22.09	LKP 35	0.047	0.22	4.56
LKP 10 R	0.03	0.61	20.36	LKP 36	0.049	0.69	14.19
LKP 11	0.032	0.19	5.98	LKP 37	0.044	0.48	10.85
LKP 12	0.027	0.82	30.14	LKP 38	0.043	0.33	7.7
LKP 13	0.023	0.3	12.92	LKP 39	0.038	0.9	23.4
LKP 14	0.031	0.12	3.72	LKP 40	0.051	0.23	4.4
LKP 15	0.038	0.15	3.8	LKP 40 R	0.054	0.23	4.21
LKP 16	0.048	0.15	3.16	LKP 41	0.045	0.24	5.44
LKP 17	0.028	0.52	18.99	LKP 42	0.059	0.3	5.06
LKP 18	0.037	0.25	6.8	LKP 43	0.056	0.26	4.69
LKP 19	0.033	0.26	7.87	LKP 44	0.053	0.31	5.95
LKP 20	0.03	0.27	9.05	LKP 45	0.059	0.27	4.52
LKP 20 R	0.033	0.28	8.45	LKP 46	0.056	0.32	5.68
LKP 21	0.024	0.62	25.76	LKP 47	0.04	0.49	12.24
LKP 22	0.032	0.13	4.14	LKP 48	0.067	0.3	4.43
LKP 23	0.024	0.54	22.51	LKP 49	0.058	0.26	4.49
LKP 24	0.029	0.13	4.58	LKP 50	0.036	0.45	12.33
LKP 25	0.032	0.13	4.27	LKP 51	0.056	0.62	10.93
LKP 26	0.025	0.38	15.39	LKP 51 R	0.059	0.65	10.96
LKP 27	0.038	0.16	4.16				

5.2 Chronology

To chronologically restrained the events AMS C-14 and Pb-210 along with Cs-137 dating technique have been employed.

C-14

The core was sampled for AMS C-14 dating. Initially six samples were taken viz. LKP-1, LKP-10, LKP-20, LKP-30, LKP-40 and LKP-45 for AMS C-14 dating and the ages obtained are provided in Table 5.6.

Table 5.6: First run AMS ages for the samples.

Sample ID	**AMS Uncalibrated ages.**
LKP-1	10599±85 BP
LKP-10	13764±111 BP
LKP-20	12563±114 BP
LKP-30	12336±107 BP
LKP-40	10552±62 BP
LKP-45	7255±83 BP

But the ages obtained seemed suspicious for the 1m long core hence the ages obtained is discarded and for second run two samples LKP-45 and LKP-1 are re-processed with ultrasonic heating up to 80° C to ensure any contribution from carbonate fraction is removed.

In the second run the AMS C-14 (mean) date estimated for the sample LKP-45 (at the depth of 12 cm from top) and LKP-1 (bottom) are provided in Table 5.7, and plotted in Fig. 5.4 respectively.

Table 5.7: Second run AMS ages for the samples.

Sample ID	**AMS Uncalibrated ages.**
LKP-1	4014±108 BP.
LKP-45	6584 ± 111 BP.

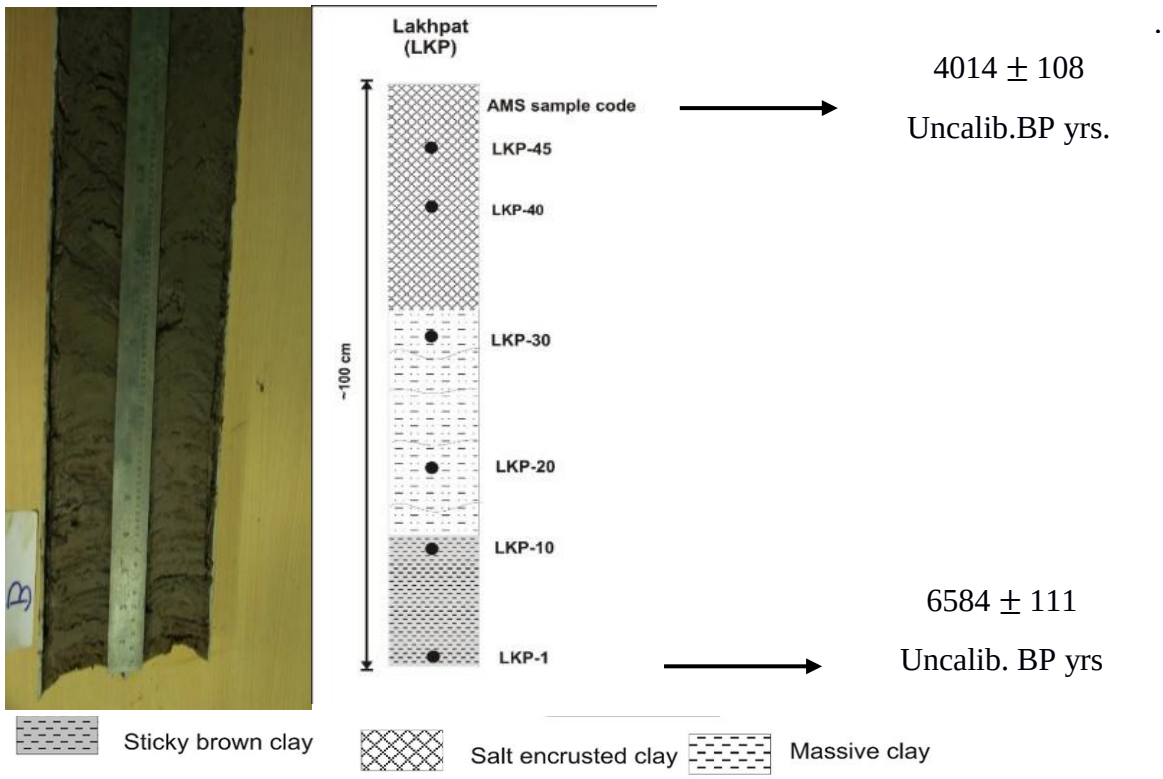

Figure 5.3: Image of Core and its lithology log and AMS C-14 dates.

^{210}Pb and ^{137}Cs

The core is also sampled for Pb-210 and Cs-137 dating and the activity of Pb-210 excess and Cs-137 is provided in Table 5.8.

Table 5.8: The table showing Pb-210 excess and Cs-137 activity in the samples.

Sample ID	**Depth (cm)**	**^{137}Cs (dpm/gm)**	**error**	**^{210}Pb (excess)**
LKP-49	2.5	0.0204	0.0712	0.7481
LKP-46	10	0.0026	0.0626	-0.5985
LKP-44	15	0.0318	0.0656	-0.4204
LKP-41	20	-	-	-
LKP-39	25	0.0048	0.0661	1.20005
LKP-36	30	0.1023	0.0643	-0.1788
LKP-31	40	0.0557	0.0649	-1.2968

The core could not be dated through ^{210}Pb and ^{137}Cs because of none of the sample have appreciable amount of $^{210}Pb_{excess}$ and no ^{137}Cs peak is detected down the core (Fig.5.4)

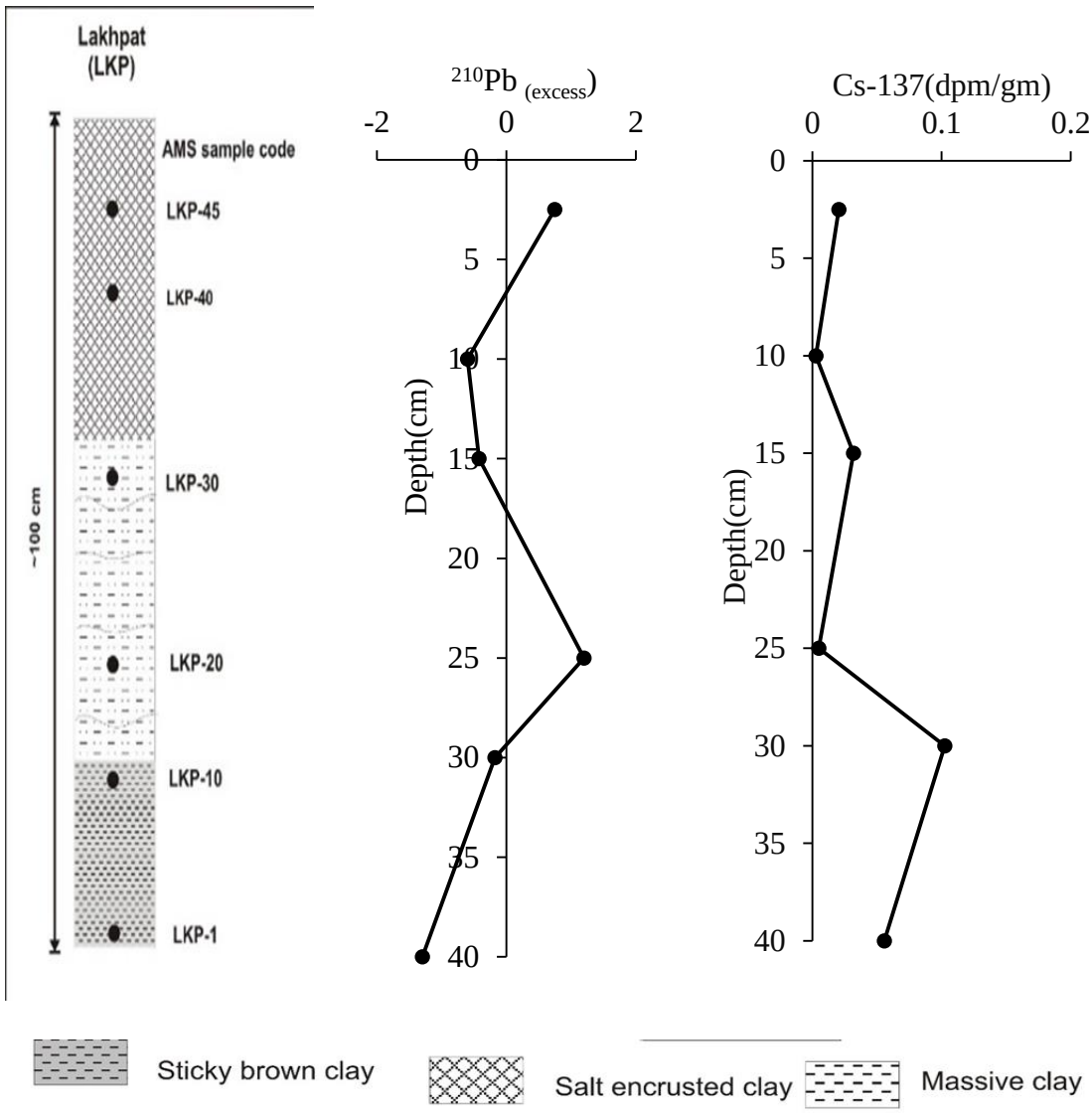

Figure 5.4: Lithology log and plots of ^{210} Pb and ^{137}Cs decay down the core.

References

Allen, J.R., Lamb, A.L. and Dark, P., 2007. Seasonality of δ13C and C/N ratios in modern and mid-Holocene sediments in the Severn Estuary Levels, SW Britain. *The Holocene, 17*(1), pp.139-144.

Banerji, U.S., Pandey, S., Bhushan, R. and Juyal, N., 2015. Mid-Holocene climate and land–sea interaction along the southern coast of Saurashtra, western India. *Journal of Asian Earth Sciences, 111,* pp.428-439.

Bhushan, R., Sati, S.P., Rana, N., Shukla, A.D., Mazumdar, A.S. and Juyal, N., 2018. High-resolution millennial and centennial scale Holocene monsoon variability in the

Higher Central Himalayas. *Palaeogeography, Palaeoclimatology, Palaeoecology*, *489*, pp.95-104.

Chen, H.F., Yeh, P.Y., Song, S.R., Hsu, S.C., Yang, T.N., Wang, Y., Chi, Z., Lee, T.Q., Chen, M.T., Cheng, C.L. and Zou, J., 2013. The Ti/Al molar ratio as a new proxy for tracing sediment transportation processes and its application in aeolian events and sea level change in East Asia. *Journal of Asian Earth Sciences*, *73*, pp.31-38.

Das, B.K. and Haake, B.G., 2003. Geochemistry of Rewalsar Lake sediment, Lesser Himalaya, India: implications for source-area weathering, provenance and tectonic setting. *Geosciences Journal*, *7*(4), pp.299-312.

Deplazes, G., Lückge, A., Stuut, J.B.W., Pätzold, J., Kuhlmann, H., Husson, D., Fant, M. and Haug, G.H., 2014. Weakening and strengthening of the Indian monsoon during Heinrich events and Dansgaard-Oeschger oscillations. *Paleoceanography*, *29*(2), pp.99-114.

Lisitzin, A.P., 1996. The age of terrigenous material as an indicator of its origins (Age and Isotopic Measurements). Oceanic Sedimentation, pp.192-230.

López-González, N., Borrego, J., Ruiz, F., Carro, B., Lozano-Soria, O. and Abad, M., 2006. Geochemical variations in estuarine sediments: provenance and environmental changes (Southern Spain). *Estuarine, Coastal and Shelf Science*, *67*(1-2), pp.313-320.

McLennan, S.M., Hemming, S., McDaniel, D.K. and Hanson, G.N., 1993. Geochemical approaches to sedimentation, provenance, and tectonics. Special Papers-Geological Society of America, pp.21-21.

Nazneen, S. and Raju, N.J., 2017. Distribution and sources of carbon, nitrogen, phosphorus and biogenic silica in the sediments of Chilika lagoon. *Journal of Earth System Science*, *126*(1), p.13.

Nesbitt, H.W. and Young, G.M., 1984. Prediction of some weathering trends of plutonic and volcanic rocks based on thermodynamic and kinetic considerations. *Geochimica et Cosmochimica Acta*, *48*(7), pp.1523-1534.

Rollinson, H.R., 1992. Another look at the constant sum problem in geochemistry. *Mineralogical Magazine*, *56*(385), pp.469-475.

Román-Ross, G., Depetris, P.J., Arribére, M.A., Guevara, S.R. and Cuello, G.J., 2002. Geochemical variability since the Late Pleistocene in Lake Mascardi sediments, northern Patagonia, Argentina. *Journal of South American Earth Sciences*, *15*(6), pp.657-667.

Roy, P.D., Caballero, M., Lozano, R., Ortega, B., Lozano, S., Pi, T., Israde, I. and Morton, O., 2010. Geochemical record of Late Quaternary paleoclimate from lacustrine sediments of paleo-lake San Felipe, western Sonora Desert, Mexico. *Journal of South American Earth Sciences*, *29*(3), pp.586-596.

Sampei, Y., Matsumoto, E., Kamei, T. and Tokuoka, T., 1997. Sulfur and organic carbon relationship in sediments from coastal brackish lakes in the Shimane peninsula district, southwest Japan. *Geochemical Journal*, *31*(4), pp.245-262.

Sarin, M.M., Borole, D.V. and Krishnaswami, S., 1979, January. Geochemistry and geochronology of sediments from the Bay of Bengal and the equatorial Indian Ocean. In Proc. Indian Acad. Sci (Vol. 88, No. 13, pp. l-154).

Spears, D.A. and Kanaris-Sotiriou, R., 1976. Titanium in some Carboniferous sediments from Great Britain. Geochimica et Cosmochimica Acta, 40(3), pp.345-351.

Weltje, G.J. and von Eynatten, H., 2004. Quantitative provenance analysis of sediments: review and outlook. *Sedimentary Geology*, *171*(1-4), pp.1-11.

Chapter 6
Discussion

The objective of the thesis was to reconstruct Holocene sea-level changes and climate variability from the mud flats of Kori Creek. To infer the climate variability and highs in sea-level various geochemical proxies, C/N and TOC have been used. Cumulative responses of geochemical proxies are used to infer high-low sea levels stands. In addition to this, the ratios are also used for tentative inferences about the provenance of the sediments. Below is the response of the proxies inferred and climate variability along with sea level changes are discussed together with provenance.

6.1Climate Variability

The grain size variability can affect the relative concentration of elements which show preference toward finer/coarser grain fraction (Sarin, 1979). Therefore before discussing the geochemical proxies used for climate variability; it is important to understand the effect of grain size on elemental concentration. The Si/Al and Ti/Al ratios together are used to evaluate the sediment maturity and to quantify the variation in grain size that can affect the relative concentration of some elements. There is not much variation in the Si/Al ratio as it varies from 4.1 to 3.4. Where under estuarine environments the ratio is observed to differ up to 20 units in sand and mud dominated horizons (Lo´pez-Gonza´lez et al., 2006). The sediments up to ratio variation of 5 in grain size are suggested to be of uniform particle nature (Teasdale et al., 2010). Further, Ti/Al ratio is very low and shows no correlation with Si/Al (r = 0.17) (Fig.6.2) that dominates the coarser quartz fraction (Spears and Kanaris-Sotiriou, 1976) which is again suggestive of the dominance of silt-clay fraction.)For example, Si content is largely associated with the coarse sediment fraction although alumino-silicate feldspars present do contribute to clay content within the coarser fraction.

However, it is important that biogenic silica supplied by the phytoplankton and planktonic microorganisms residing in the tidal flat or by the surrounding marshy plants should be discounted (Hou et al., 2008; 2010). Being marine-organic in origin and also one of the important nutrients, biogenic silica shows a close positive relationship with carbon and nitrogen (Hou et al., 2008). However, that is not observed in the present study ($r_{Si/Al\ vs.\ TOC}$ = -0.1, Fig 6.1) and thus can be discounted for. The suggestion is further supported by

the low concentration of organic carbon (mean: 0.4%) in the sediments hence suggesting low productivity.

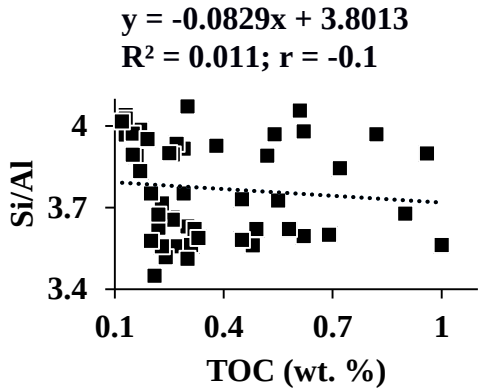

Figure 6.1 Correlation plot of Si/Al vs TOC.

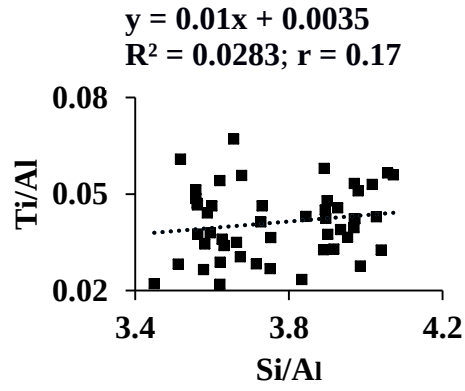

Figure 6.2 Correlation plot of Ti/Al vs Si/Al.

1) *Al, Fe, and K*

The changes in the concentration of Aluminum (Al), Potassium (K) and Iron (Fe) inferred as a proxy for higher inter-tidal sedimentation during high sea-level which is deposited as a suspended fallout from the tidal current (Banerjee et al., 2015). The tidal current carries the clayey continental detritus containing Al, Fe, and K that is supplied to the Arabian sea by the Indus river (Sirocko and Sarnthein, 1989). As the higher flux of finer fraction (inter-tidal clay) is associated with high sea level, the grain size dependency of Al, K, and Fe do not affect our inference.

For using Fe as a proxy for detrital influx (in this study as intertidal sedimentation) Fe concentration is often normalized with total organic carbon (TOC). Fe^{3+} is immobile and having low solubility as $Fe^{3+,}$ and it mobilizes as Fe^{2+} under redox condition which also favors the preservation of organic compounds. Therefore, any post-deposition changes in Fe should directly correlate with the changes in the concentration of organic carbon but no correlation is found between Fe/Al and TOC (-0.04) (Fig.6.2b). Therefore, suggesting a negligible diagenetic alteration in Fe concentration. Similarly, K/Al follows the trend of Fe/Al (Fig.6.2c) and is used as a proxy for enhanced sedimentation.

2) *Ti/Al ratio*

The Ti/Al ratio is used to infer the sea-level changes in enclosed sea margins, mode of transport (aqueous or aeolian) and hence the regional aridity (Chen et al., 2013;

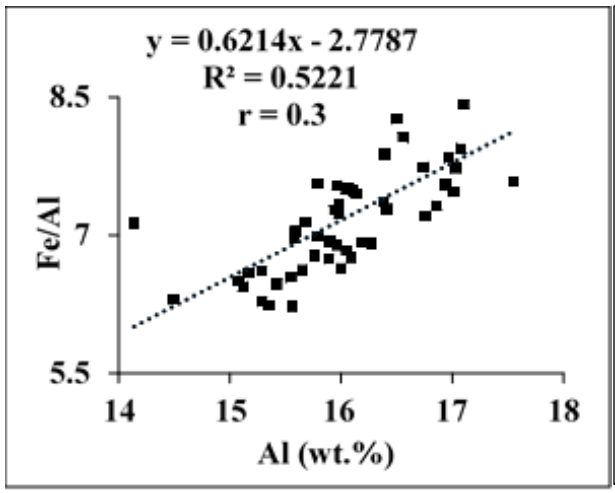

Figure 6.2a: Correlation plots of Fe/Al vs Al (wt. %)

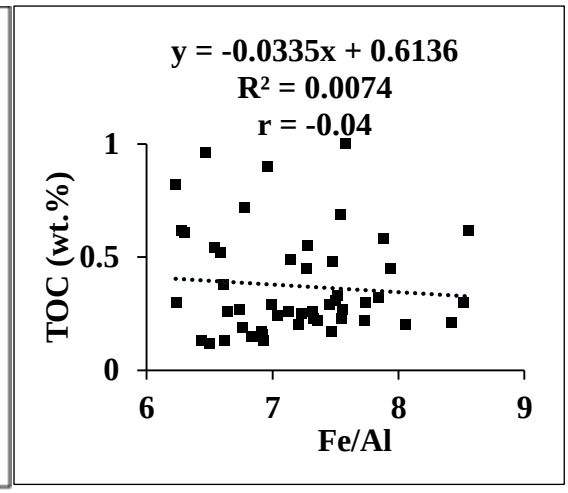

Figure 6.2b: Correlation plot of TOC (wt. %) vs Fe/Al.

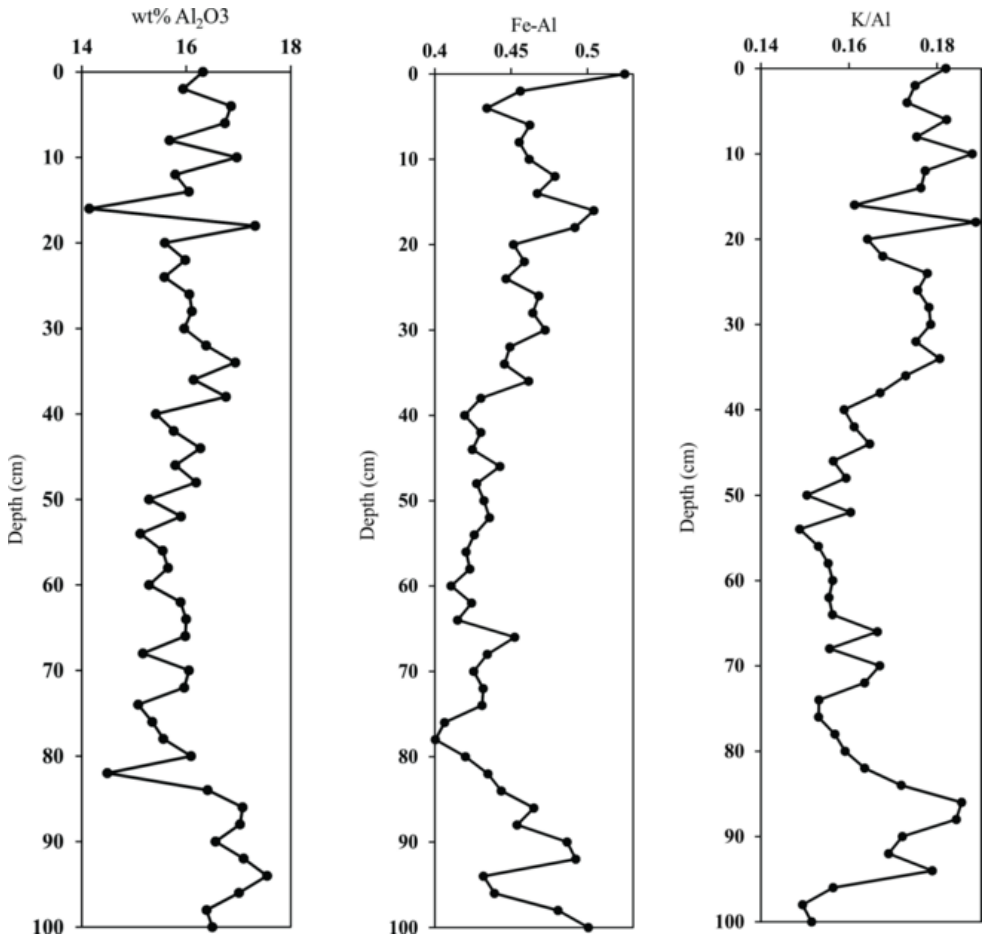

Figure 6.2c: Depth wise variation of Al_2O_3, Fe/Al and K/Al.

Deplazes et al., 2014). Though Ti is associated with coarser grain size but once it is deposited in suspended fluvial silts, it is suggested to be independent of size effect (Lisitzin, 1996; Prins et al., 2000). The enhanced wind strength during the winter dust storms from Arabian Peninsula is more effective in transporting heavy minerals like Ti and Mg to the Arabian Sea/ Indus delta sediments and is hence associated with increased aridity (Prins and Weltje, 1999; Prins et al., 2000; Deplazes et al., 2014). Due to gravitation processes the sink areas are often depleted in Ti than Al, however, during low sea level higher Ti in otherwise depleted sea marginal areas can be transported via continental streams which move more toward the sea or by frequent and stronger dust storms from source proximal regions (Prins et al., 2000; Chen et al., 2013). In the study area, though there is no major stream draining into the creek, the enhanced dust storms are reported to supply additional sediments enriched in Mg, Ca and Ti from the Arabian Peninsula and Thar desert (Prins et al., 2000) and hence are indicative of increased aridity and lower sea-level. Further, the ratio does not show any correlation with Si/Al (Fig.6.2) that dominates the coarser fraction indicating that the fluctuation in Ti/Al is independent of grain size and is indicative of climate processes/change in provenance (Fig.6.4c) (Spears and Kanaris-Sotiriou, 1976).

Together with Ti enrichment of Fe is sometimes also inferred as a signature of enhanced aridity (Yancheva et al., 2007) as both having the same ionic radius are well-correlated in terrigenous sediments. But beyond the detrital influence, these become separated (El-Wakeel, and Riley, 1996). In the present study, there is a low negative correlation (r= -0.16) (Fig.6.3) between the two suggesting different sources and hence Fe is not used as a proxy for aridity here.

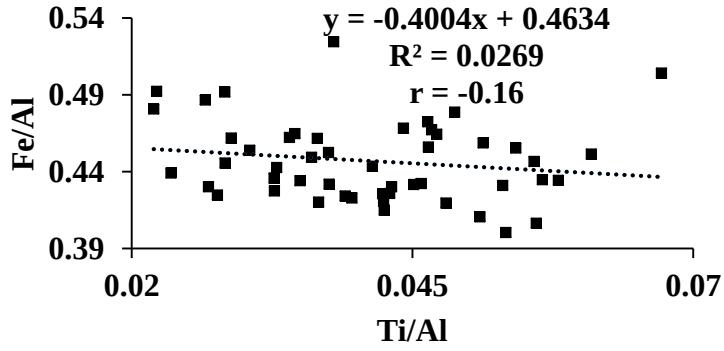

Figure 6.3: Correlation plot of Fe/Al vs Ti/Al.

3) *Fe/Mn ratio*

The ratio of the redox-sensitive elements Fe and Mn used to ascertain the dominant zones of oxidation/reduction and hence lower/higher sea level. Fe and Mn remain in solution under reducing condition which in the study area can result from waterlogging during high sea level. However, compared to Fe, Mn is more readily mobilized due to its greater solubility. Therefore, the pattern of Fe/Mn ratio is interpreted as a proxy to identify higher sea level/wetter conditions (Fig.6.4a) (Engstrom and Wright, 1984; Bhushan et al., 2018).

4) *Carbon / Nitrogen Ratio (C/N)*

In the present study, the carbon is dominantly of marine origin (mean C/N =10.75) which is expected as the core is raised from a mudflat; while there are intermittent horizons showing the higher contribution from terrestrial plants and thus, higher C/N ratio suggesting lowered sea level.

5) *E/P ratio (Ca/Al+Fe+Ti):*

In the study, the calcium (Ca) associated with silicate fraction was measured which if it is associated with the coarser fraction serves as a proxy for increased sediment flux (Teasdale et al., 2010). However no correlation of Ca/Al with Si/Al (r= 0.06) is found (Fig.6.5c). The positive correlation with Ti/Al (0.8) (Fig.6.5b) and no correlation with aqueous proxies Fe/Al (-0.2)(Fig.6.5c) are suggesting the higher deposition of Ca due to greater evaporation during arid conditions which is also indicated by E/P (Ca/Al+Fe+Ti) ratio. The additional Ca, and Mg may also be transported by increased aeolian flux further signifying aridity. Hence the ratio will indicate towards the arid episodes (Fig.6.4b) (Prins et al., 2000; Yancheva et al., 2007).

6) *Rb/Sr and Chemical index of alteration (CIA)*

CIA and Rb/Sr ratio are used to infer the variability in climate and the sea level changes (Fig.6.4d and 6.4 e). The Rb/Sr ratio generally mimics the pattern of CIA with Sr being more mobile under warmer/wetter conditions as the rate of chemical weathering increases (Chen et al., 1999; Bhushan et al., 2018).

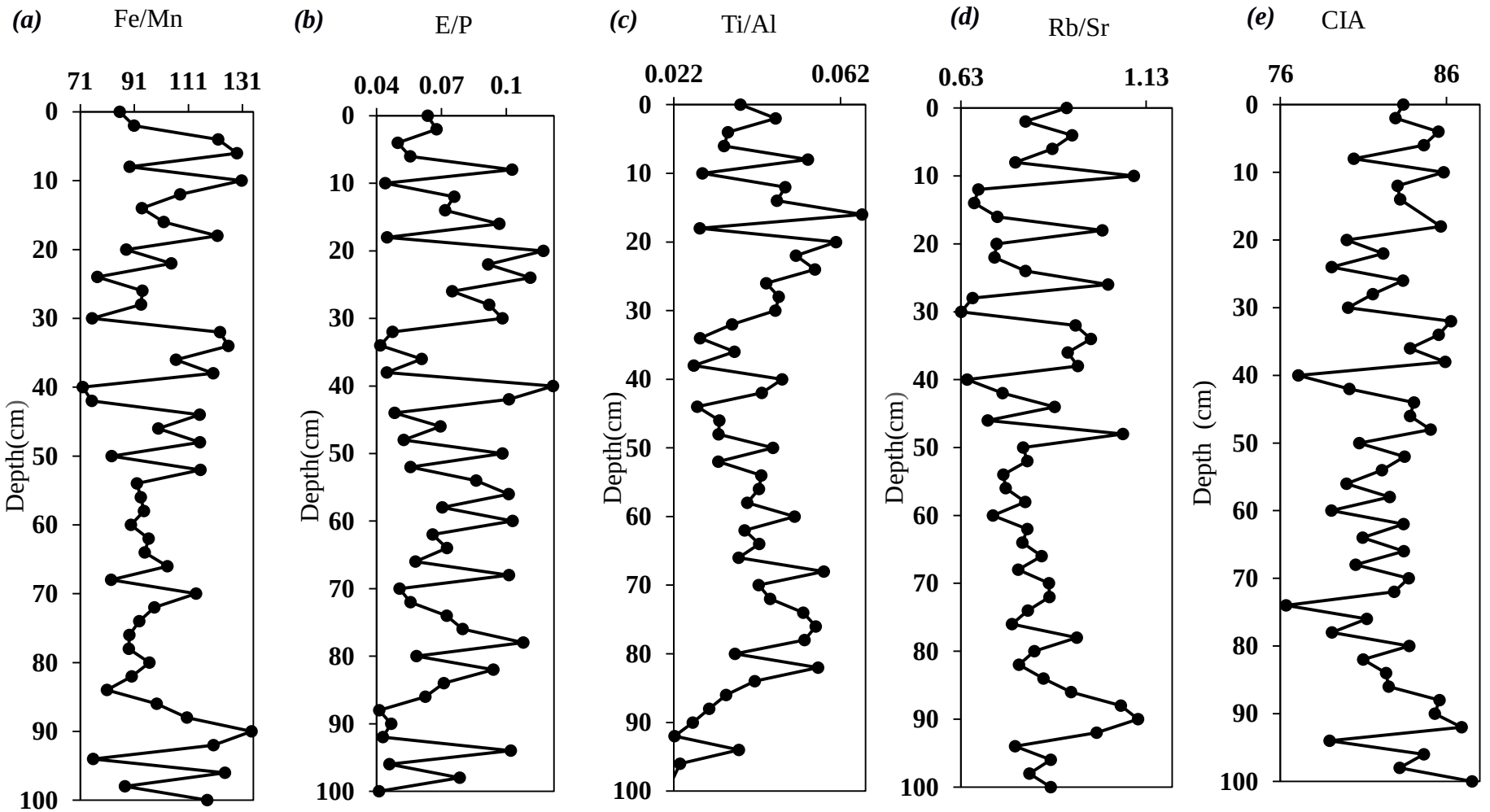

Figure 6.4: Depth wise variation of (a) Fe/Mn, (b) E/P (c) Ti/Al (d) Rb/Sr, and (e) CIA.

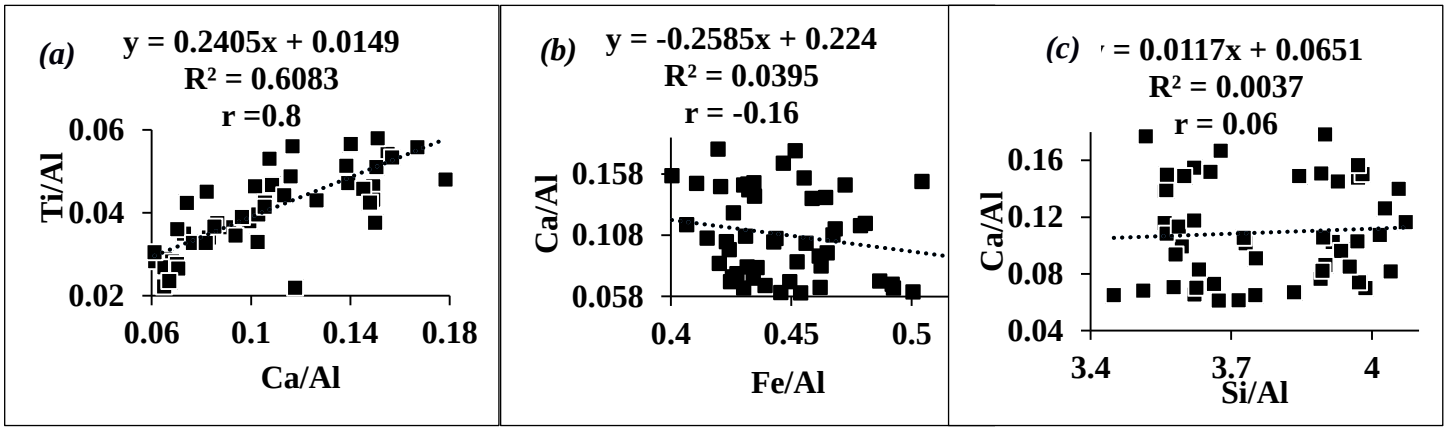

Figure 6.5: Correlation plots of (a) Ti/Al with Ca/Al, (b) Ca/Al with Fe/Al and (c) Ca/Al with Si/Al.

6.2 Provenance

The study area is proximal to Indus, Thar and Arabian sea and is influenced by the monsoon system. During summer season high pressure is created over the Arabian sea while low pressure created over Tibetan plateau and moisture carrying winds blow from sea to land. In winter patterns reversed. In winters NE (Shamal winds) blows very strongly over Arabian peninsula and add dust to the Arabian sea. Similarly, dust is added from the Thar desert by NE monsoon. These monsoon winds also generate longshore currents which bring sediments from Indus Delta to Kori creek (Fig.6.6).

The area is not drained by any major seasonal or perennial fluvial system; if there had been any contribution it should have been reflected by coarser sand particle because the continental flux which is derived from arid to semi-arid dryland fluvial systems are dominated by short distance transport and flashy deposition and hence are represented by coarser sand particles than clay (Tyagi et al., 2012), which is absent in the present case hence the possibilities of this contribution is negated. Thus, sediments at Lakhpat could have a contribution from Indus delta via longshore currents, the Arabian peninsula and Thar desert.

The bivariate plots are plotted to infer the provenance from above mentioned three sources. However robust conclusions would await rare earth element data. The selected elements TiO_2/ Al_2O_3 vs K_2O/Al_2O_3 and K_2O/Al_2O_3 vs SiO_2/ Al_2O_3 are plotted along with

data from Indus delta (Limmer et al., 2012), Thar desert (Ferrat et al., 2011) and Arabian sea (Prakash et al.,2016) (Fig. 6.7a and 6.7b).

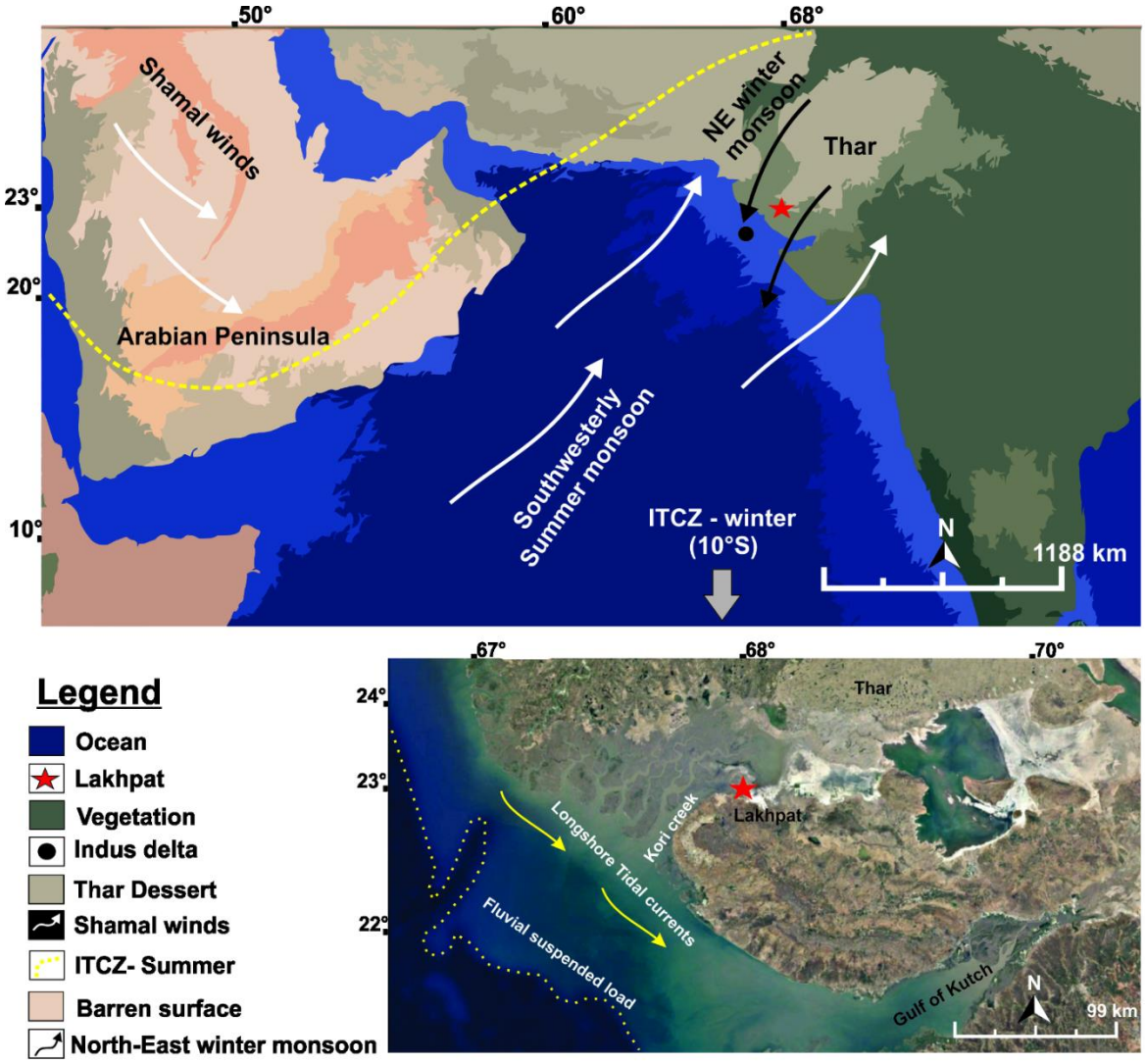

Figure 6.6: Monsson system in the coring site and the surrounding region and; extend of fluvial suspended load is traced from google Earth imagery.

The plots show similarity towards Indus and Thar sediments indicating Indus and Thar being the major sources of sediments' origin.

Further the major oxide data for all the core sediments and for reference some rocks from Indus delta (Limmer et al., 2012), Thar desert (Ferrat et al., 2011) and Arabian sea (Prakash et al., 2016) area have been plotted in Al_2O_3-CaO Na_2O-K_2O (A-CN-K) compositional space (molecular proportions) diagram.

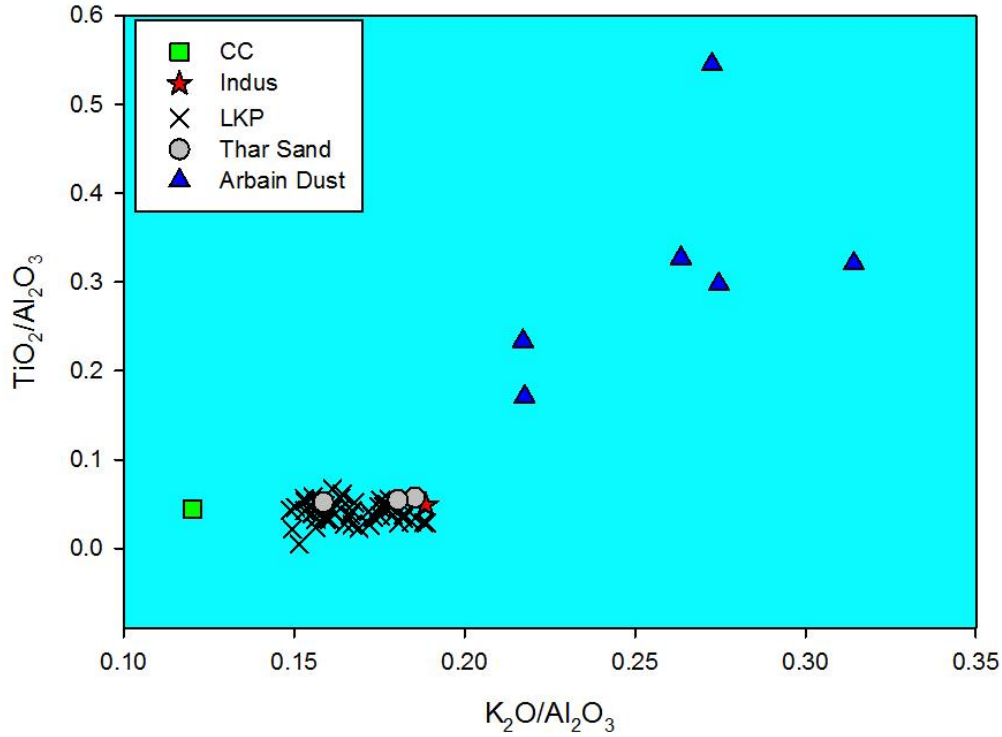

Figure 6.7a: Bivariate plot of TiO_2/Al_2O_3 vs K_2O/ Al_2O_3.

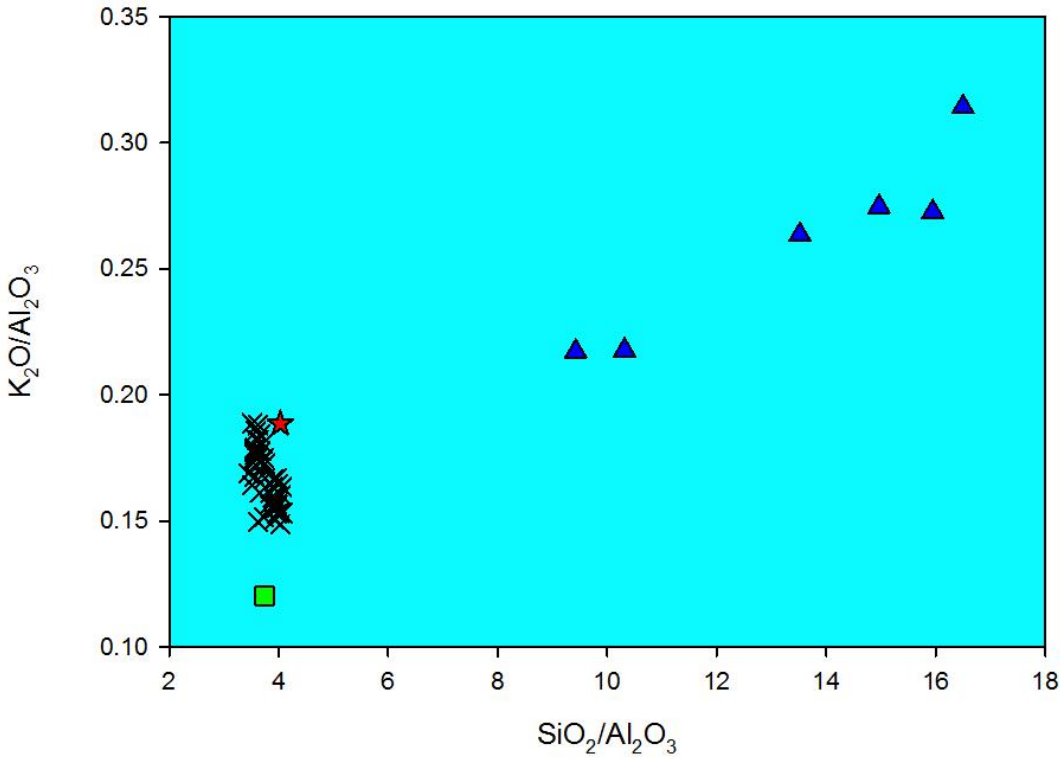

Figure 6.7b: Bivariate plot of K_2O/Al_2O_3 vs SiO_2/ Al_2O_3

In A-CN-K ternary diagram which gives the weathering trend (Nesbitt and Young, 1984; Nesbitt et al., 1996). Lakhpat sediments show similarity with Indus and Thar sediments. The deviation at the top may be due to change in the provenance (Fig.6.7c).

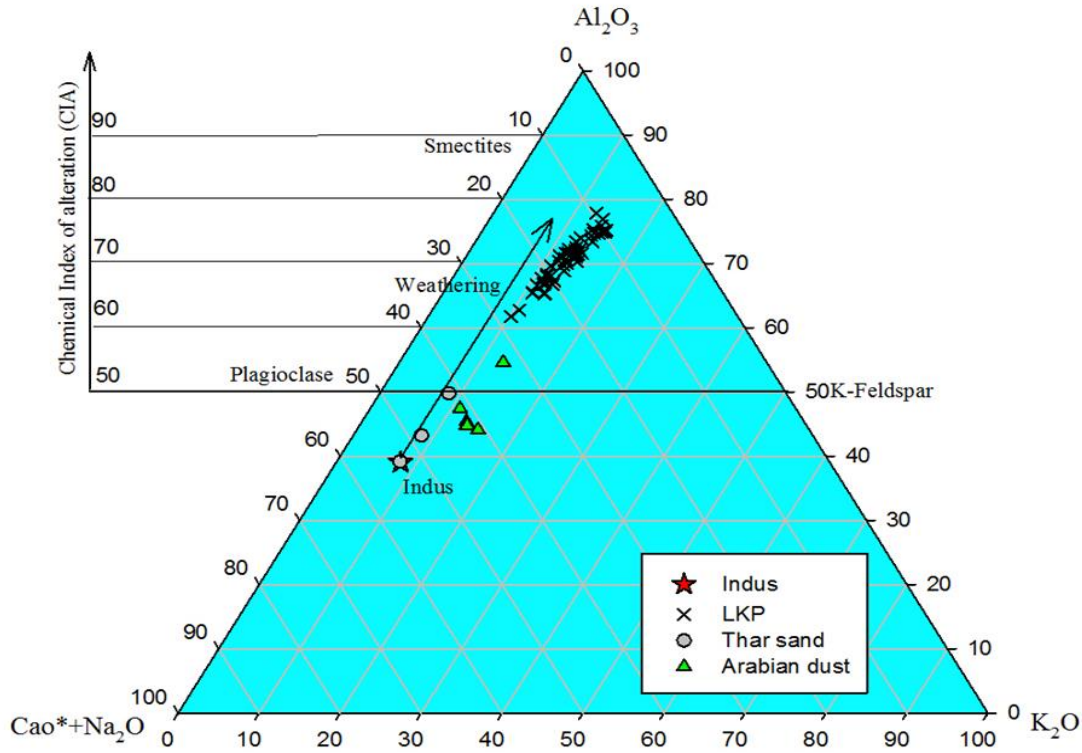

Figure 6.7c: A-CN-K diagram.

6.3Chronology

The sample (LKP-45) (12 cm from the top) and bottom sample (LKP-1) of the Lakhpat core are dated using AMS C-14. In the first run, the top sample (LKP-45) dated to 10599 ± 85 Uncalib. BP, which seemed unreasonable. The samples were reprocessed with ultrasonic heating up to 80° C to ensure any contribution from carbonate fraction is removed. The second run the sample LKP-45 (12 cm from the top) was dated to 4014±108 Uncalib. BP and the bottom sample (LKP-1) was dated to 6584±111 Uncalib. BP.

The ages 6.5 and 4 ka also seem older than expected for a one-meter tidal flat section. The following reasons are suggested for the older ages:

i) Tectonic overprinting as the area lies in the proximity of Sunda high region which was suggested to be uplifted after the 1819 earthquake (Thakkar et al., 2012).

ii) It could be due to the incorporation of dead carbon from the catchment rocks because similar observations are made from the other cores which are raised in the region (under progress).

iii) The ages obtained seems to be unrealistically old as the sedimentation rate calculated using the AMS dates comes out to be ~ 0.3 mm/yr, which is unrealistically low. This argument is supported by another tidal flat section dated north of the Kori creek (Tyagi et al., 2012) who suggested tidal flat sedimentation of 250 cm between 5.5 and 3 ka. This suggested a sedimentation rate of 10 mm/yr. Given that this location is further away of tidal influence (Kori creek) the Lakhpat site ideally should have a higher sedimentation rate than 10 mm/yr.

The inactivity of Pb-210 and Cs-137 down the core suggest that the core is older than 150 years. Hence the unreliability associated with the present ages, the chronology is avoided for regional climate correlation and its impact on relative sea level changes. Nevertheless, the geochemical proxies do indicate a higher sea level with fluctuations during period older than 150-200 years. The study suggests complications involves using AMS C-14 dating in the region and proposes that an alternative technique like OSL (optically stimulated luminescence) dating should be explored.

7 Relative sea level changes

Based on the cumulative response of various geochemical proxies and C/N ratio a schematic diagram of climate variability and sea level change is drawn (Fig.6.8a & Fig. 6.8b)

At the depth of 100 -85 cm the behaviour of geochemical proxies and C/N ratio suggest sea-level was high during wet climate. While during the depth of 85-38 cm sea-level fell during arid climate, thereafter sea level marginally rose with fluctuations (38-0) cm till 4014 $\pm$ 108 Uncalib. BP. Also, the absence of mudflat sedimentation in the last 150-200 years is suggestive of lower sea level in recent times.

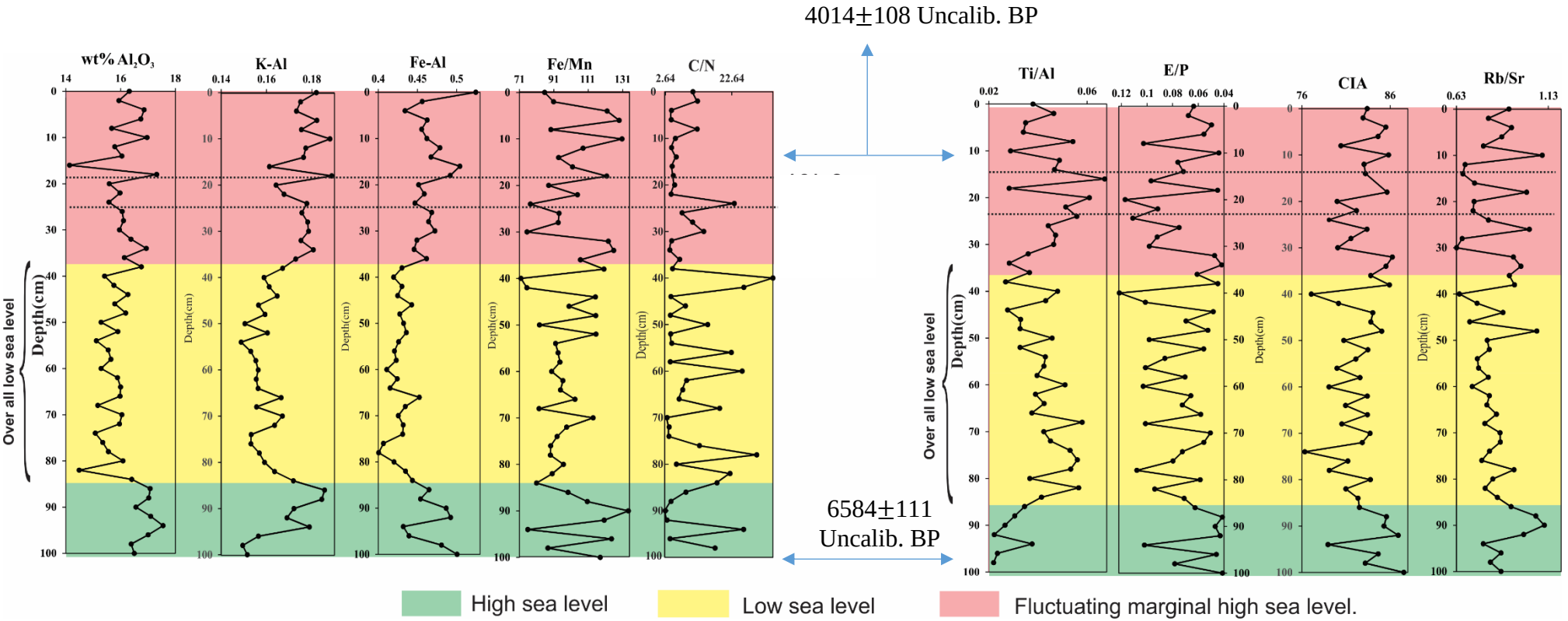

Figure 6.8a: Plot showing sea-level changes.

Figure 6.8b: Plot showing phases of wet and dry climate.

References

Banerji, U.S., Pandey, S., Bhushan, R. and Juyal, N., 2015. Mid-Holocene climate and land–sea interaction along the southern coast of Saurashtra, western India. *Journal of Asian Earth Sciences*, *111*, pp.428-439.

Bhushan, R., Sati, S.P., Rana, N., Shukla, A.D., Mazumdar, A.S. and Juyal, N., 2018. High-resolution millennial and centennial scale Holocene monsoon variability in the Higher Central Himalayas. *Palaeogeography, Palaeoclimatology, Palaeoecology*, *489*, pp.95-104.

Chen, H.F., Yeh, P.Y., Song, S.R., Hsu, S.C., Yang, T.N., Wang, Y., Chi, Z., Lee, T.Q., Chen, M.T., Cheng, C.L. and Zou, J., 2013. The Ti/Al molar ratio as a new proxy for tracing sediment transportation processes and its application in aeolian events and sea level change in East Asia. *Journal of Asian Earth Sciences*, *73*, pp.31-38.

Das, B.K. and Haake, B.G., 2003. Geochemistry of Rewalsar Lake sediment, Lesser Himalaya, India: implications for source-area weathering, provenance and tectonic setting. *Geosciences Journal*, *7*(4), pp.299-312.

Deplazes, G., Lückge, A., Stuut, J.B.W., Pätzold, J., Kuhlmann, H., Husson, D., Fant, M. and Haug, G.H., 2014. Weakening and strengthening of the Indian monsoon during Heinrich events and Dansgaard-Oeschger oscillations. *Paleoceanography*, *29*(2), pp.99-114.

El Wakeel, S.K. and Riley, J.P., 1961. Chemical and mineralogical studies of deep-sea sediments. Geochimica et cosmochimica acta, 25(2), pp.110-146.

Ferrat, M., Weiss, D.J., Strekopytov, S., Dong, S., Chen, H., Najorka, J., Sun, Y., Gupta, S., Tada, R. and Sinha, R., 2011. Improved provenance tracing of Asian dust sources using rare earth elements and selected trace elements for palaeomonsoon studies on the eastern Tibetan Plateau. *Geochimica et Cosmochimica Acta*, *75*(21), pp.6374-6399.

Hou, L., Liu, M., Xu, S., Yan, H., Ou, D., Cheng, S. and Lin, X., 2008. Distribution and accumulation of biogenic silica in the intertidal sediments of the Yangtze Estuary. Journal of Environmental Sciences, 20(5), pp.543-550.

Hou, L., Liu, M., Yang, Y., Ou, D., Lin, X. and Chen, H., 2010. Biogenic silica in intertidal marsh plants and associated sediments of the Yangtze Estuary. *Journal of Environmental Sciences*, *22*(3), pp.374-380.

Jish Prakash, P., Stenchikov, G., Tao, W., Yapici, T., Warsama, B. and Engelbrecht, J.P., 2016. Arabian Red Sea coastal soils as potential mineral dust sources. *Atmospheric Chemistry and Physics*, *16*(18), pp.11991-12004.

Limmer, D.R., Böning, P., Giosan, L., Ponton, C., Köhler, C.M., Cooper, M.J., Tabrez, A.R. and Clift, P.D., 2012. Geochemical record of Holocene to Recent sedimentation on the Western Indus continental shelf, Arabian Sea. *Geochemistry, Geophysics, Geosystems*, *13*(1).

Lisitzin, A.P., 1996. The age of terrigenous material as an indicator of its origins (Age and Isotopic Measurements). Oceanic Sedimentation, pp.192-230.

López-González, N., Borrego, J., Ruiz, F., Carro, B., Lozano-Soria, O. and Abad, M., 2006. Geochemical variations in estuarine sediments: provenance and environmental changes (Southern Spain). *Estuarine, Coastal and Shelf Science*, *67*(1-2), pp.313-320.

McLennan, S.M., Hemming, S., McDaniel, D.K. and Hanson, G.N., 1993. Geochemical approaches to sedimentation, provenance, and tectonics. Special Papers-Geological Society of America, pp.21-21.

Nesbitt, H.W. and Young, G.M., 1984. Prediction of some weathering trends of plutonic and volcanic rocks based on thermodynamic and kinetic considerations. *Geochimica et Cosmochimica Acta*, *48*(7), pp.1523-1534.

Nesbitt, H.W., Young, G.M., McLennan, S.M. and Keays, R.R., 1996. Effects of chemical weathering and sorting on the petrogenesis of siliciclastic sediments, with implications for provenance studies. *The Journal of Geology*, *104*(5), pp.525-542.

Prins, M.A. and Weltje, G.J., 1999. End-member modeling of siliciclastic grain-size distributions: the late Quaternary record of eolian and fluvial sediment supply to the Arabian Sea and its paleoclimatic significance.

Prins, M.A., Postma, G., Cleveringa, J., Cramp, A. and Kenyon, N.H., 2000. Controls on terrigenous sediment supply to the Arabian Sea during the late Quaternary: the Indus Fan. *Marine Geology*, *169*(3-4), pp.327-349.

Rollinson, H.R., 1992. Another look at the constant sum problem in geochemistry. *Mineralogical Magazine*, *56*(385), pp.469-475.

Román-Ross, G., Depetris, P.J., Arribére, M.A., Guevara, S.R. and Cuello, G.J., 2002. Geochemical variability since the Late Pleistocene in Lake Mascardi sediments, northern Patagonia, Argentina. *Journal of South American Earth Sciences*, *15*(6), pp.657-667.

Roy, P.D., Caballero, M., Lozano, R., Ortega, B., Lozano, S., Pi, T., Israde, I. and Morton, O., 2010. Geochemical record of Late Quaternary paleoclimate from lacustrine sediments of paleo-lake San Felipe, western Sonora Desert, Mexico. *Journal of South American Earth Sciences*, *29*(3), pp.586-596.

Sarin, M.M., Borole, D.V. and Krishnaswami, S., 1979, January. Geochemistry and geochronology of sediments from the Bay of Bengal and the equatorial Indian Ocean. In Proc. Indian Acad. Sci (Vol. 88, No. 13, pp. l-154).

Sirocko, F., Sarnthein, M., 1989. Wind-borne deposits in the Northwestern Indian Ocean: record of Holocene sediments versus modern satelitte data. In: Leinen, M., Sarnthein, M. (Eds.), Paleoclimatology and Paleometeorology: Modern and Past Patterns of Glacial Atmospheric Transport. NATO ASI Series CKluwer Academic, Dordrecht, pp. 401±433.

Spears, D.A. and Kanaris-Sotiriou, R., 1976. Titanium in some Carboniferous sediments from Great Britain. Geochimica et Cosmochimica Acta, 40(3), pp.345-351.

Thakkar, M.G., Ngangom, M., Thakker, P.S. and Juyal, N., 2012. Terrain response to the 1819 Allah Bund earthquake in western Great Rann of Kutch, Gujarat, India. *Current Science*, pp.208-212.

Tyagi, A.K., Shukla, A.D., Bhushan, R., Thakker, P.S., Thakkar, M.G. and Juyal, N., 2012. Mid-Holocene sedimentation and landscape evolution in the western Great Rann of Kachchh, India. *Geomorphology*, *151*, pp.89-98.

Weltje, G.J. and von Eynatten, H., 2004. Quantitative provenance analysis of sediments: review and outlook. *Sedimentary Geology*, *171*(1-4), pp.1-11.

Yancheva, G., Nowaczyk, N.R., Mingram, J., Dulski, P., Schettler, G., Negendank, J.F., Liu, J., Sigman, D.M., Peterson, L.C. and Haug, G.H., 2007. Influence of the intertropical convergence zone on the East Asian monsoon. Nature, 445(7123), p.74.

Chapter 7

Conclusions

1. The sea-level was relatively higher at 100-85 cm depth as suggested by the geochemical proxies, and C/N data. The proxies also indicate wetter climate conditions during the same time period which could be the dominant cause for higher sea level. At 85-38 cm depth relatively lower sea-level is suggested during arid climatic conditions after which the sea level rose marginally although with fluctuations under slightly improved climatic conditions at 38-0 cm.

2. The core could not be dated through Pb-210 and Cs-137 dating technique due to absence of Pb-210 (excess) and Cs-137 indicating that the core is older than ~150-200 yrs. Absence of mud-flat sedimentation in last 150-200 years indicates that sea-level has been consistently low since then.

The AMS dating was employed to date the bottom and the top (12 cm depth) of the core and yielded ages as 6584 $\pm$ 111 Uncalib. BP yrs and 4014$\pm$108 Uncalib. BP respectively.

3. The ages seem to be older than anticipated for 1 m core as the sedimentation rate calculated using the AMS dates is only ~ 0.3 mm/yr. Another 250 cm thick tidal flat section dated between 5.5 and 3 ka in the north of the Kori creek (Tyagi et al., 2012) suggests tidal flat sedimentation rate of 10 mm/yr during late Holocene. This location is further away from the tidal influence (Kori creek) than a more proximal Lakhpat site which ideally should have a higher sedimentation rate than 10 mm/yr.

Further, the core is in the proximity of Sunda high region and therefore sediments seem to have been tectonically uplifted due to flexural buckling caused by oblique compression (Thakkar et al., 2012).

It is also speculated that there could be incorporation of dead carbon from the catchment rocks leading to older ages. Similar observations are made by other studies (currently under progress) from the region.

4. Ternary and bivariate plots suggest dominance of Indus sediments brought by longshore current along with contribution from Thar desert in the Lakhpat mudflat sediments. The desert dust is suggested to be dominantly added during the arid climatic conditions.

5. The regional climate and sea-level change correlation could not be established at the current stage due to problems encountered in C-14 samples which awaits more robust data on chronology. Nevertheless the various proxies do indicate fluctuating sea-level changes in the speculatively assigned late-mid Holocene period in response to the climatic variability. We hypothesize for future research that the sea-level changes in the region are dominantly controlled by the climate with tectonic over printing which needs to be corrected for.

References

Thakkar, M.G., Ngangom, M., Thakker, P.S. and Juyal, N., 2012. Terrain response to the 1819 Allah Bund earthquake in western Great Rann of Kutch, Gujarat, India. *Current Science*, pp.208-212.

Tyagi, A.K., Shukla, A.D., Bhushan, R., Thakker, P.S., Thakkar, M.G. and Juyal, N., 2012. Mid-Holocene sedimentation and landscape evolution in the western Great Rann of Kachchh, India. *Geomorphology*, *151*, pp.89-98.